

Regge Limit of R -Current Correlators in the AdS/CFT-Correspondence

Dissertation
zur Erlangung des Doktorgrades
des Departments Physik
der Universität Hamburg

vorgelegt von
Anna-Maria Mischler
aus Unna

Hamburg
2009

Gutachter der Dissertation:

Prof. Dr. Jochen Bartels
Prof. Dr. Volker Schomerus

Gutachter der Disputation:

Prof. Dr. Jochen Bartels
Prof. Dr. Bernd A. Kniehl

Datum der Disputation:

27. November 2009

Vorsitzender des Prüfungsausschusses:
Vorsitzender des Promotionsausschusses:

Prof. Dr. Günter Sigl
Prof. Dr. Robert Klanner

Leiter des Departments Physik:
Dekan der Fakultät für Mathematik,
Informatik und Naturwissenschaften:

Prof. Dr. Jochen Bartels
Prof. Dr. Heinrich Graener

Abstract

The scattering of highly virtual photons offers a reliable environment to investigate the BFKL Pomeron in perturbative quantum chromodynamics. Correlators of conserved R -currents in $\mathcal{N} = 4$ supersymmetric Yang-Mills theory are close analogs of electromagnetic current correlation functions. In the leading logarithmic approximation, the BFKL Pomeron of R -current scattering in $\mathcal{N} = 4$ supersymmetric Yang-Mills theory is the same as in perturbative quantum chromodynamics.

The AdS/CFT-correspondence provides one opportunity to study the strong coupling limit of R -current correlation functions. The correspondence connects $\mathcal{N} = 4$ supersymmetric Yang-Mills theory and type IIB string theory on a five-dimensional Anti-de Sitter background. The strong coupling regime of the conformal field theory is related to the weakly coupled string theory and vice versa. In particular, the strong coupling limit of $\mathcal{N} = 4$ supersymmetric Yang-Mills theory in the large N_c -limit is equivalent to classical type IIB supergravity.

We consider the scattering of R -currents in the Regge limit at weak and strong coupling using the AdS/CFT-correspondence. First, we compute the four and six point function of R -currents in $\mathcal{N} = 4$ supersymmetric Yang-Mills theory at weak coupling in the leading logarithmic approximation. We study the influence of the supersymmetry, especially of the new scalar degrees of freedom, on the scattering process. The main results for the four point function of R -currents are the Regge factorization of the amplitude and the explicit computations of the R -current impact factors. Subsequently, we investigate the six point function of R -currents at weak coupling for arbitrary N_c and in the large N_c -limit. We observe a new direct coupling of t -channel gluons to the R -current impact factor, which is not known from quantum chromodynamics.

In the second part of our work, we study the strong coupling limit of the four and six point R -current correlator in the corresponding classical supergravity theory. The leading contribution in the center-of-mass energy of the four point function in the Regge limit is given by a Witten diagram with one graviton exchange. We observe a factorization of the amplitude similar to the factorization of the four point amplitude at weak coupling. The six point function of R -currents leads to Witten diagrams with a triple graviton vertex and with two graviton exchange, respectively. We analyze the high energy behavior of the triple graviton vertex diagram and find a suppression of the diagram in the triple Regge limit.

The investigation of the reggeization of the graviton on the string theory side is an interesting task for future work. As a first step, we have computed tree diagrams, which are lowest order diagrams, on the string theory side. In order to study the reggeization of the graviton, further computations beyond the classical supergravity limit are necessary.

Zusammenfassung

Die Streuung hoch virtueller Photonen ist ein bewährter Prozess, um das BFKL-Pomeron in perturbativer Quantenchromodynamik zu studieren. Die Korrelatoren erhaltener R -Ströme in der $\mathcal{N} = 4$ supersymmetrischen Yang-Mills-Theorie sind ähnlich zu Korrelationsfunktionen elektromagnetischer Ströme. In der Näherung führender Logarithmen ist das BFKL-Pomeron der R -Ströme-Streuung in der $\mathcal{N} = 4$ supersymmetrischen Yang-Mills-Theorie das gleiche wie in perturbativer Quantenchromodynamik.

Die AdS/CFT-Korrespondenz bietet eine Möglichkeit, den starken Kopplungslimes der R -Ströme-Korrelationsfunktionen zu untersuchen. Die Korrespondenz stellt eine Verbindung her zwischen der $\mathcal{N} = 4$ supersymmetrischen Yang-Mills-Theorie und der Typ-IIB-Stringtheorie auf einem fünfdimensionalen Anti-de-Sitter-Hintergrund. Der Bereich starker Kopplung der konformen Feldtheorie steht in Beziehung zur schwach gekoppelten Stringtheorie und umgekehrt. Insbesondere ist der starke Kopplungslimes der $\mathcal{N} = 4$ supersymmetrischen Yang-Mills-Theorie im Limes des großen N_c äquivalent zur klassischen Typ-IIB-Supergravitation.

Wir nutzen die AdS/CFT-Korrespondenz und betrachten die R -Ströme-Streuung im Regge-Limes bei schwacher und starker Kopplung. Zuerst berechnen wir die Vier- und Sechspunktfunktion der R -Ströme in der $\mathcal{N} = 4$ supersymmetrischen Yang-Mills-Theorie bei schwacher Kopplung in der Näherung führender Logarithmen. Zu untersuchen ist der Einfluss der Supersymmetrie, insbesondere der neuen skalaren Freiheitsgrade, auf den Streuprozess. Die Hauptresultate für die R -Ströme-Vierpunktfunktion sind die Regge-Faktorisierung der Amplitude und die explizite Berechnung der R -Ströme-Impaktfaktoren. Anschließend studieren wir die Sechspunktfunktion der R -Ströme bei schwacher Kopplung für beliebiges N_c sowie im Limes des großen N_c . Beobachten können wir eine neue direkte Kopplung der t -Kanalgluonen an die R -Ströme-Impaktfaktoren, die nicht aus der Quantenchromodynamik bekannt ist.

Im zweiten Teil dieser Arbeit wird der starke Kopplungslimes des Vier- und Sechspunktkorrelators der R -Ströme in der schwach gekoppelten Supergravitationstheorie analysiert. Der führende Beitrag in der Schwerpunktenergie der Vierpunktfunktion im Regge-Limes ist durch ein Witten-Diagramm gegeben, in dem ein Graviton ausgetauscht wird. Wir erkennen eine Faktorisierung der Amplitude ähnlich zur Faktorisierung der Vierpunktfunktion bei schwacher Kopplung. Die Sechspunktfunktion der R -Ströme führt zu Witten-Diagrammen mit einem Dreifachgravitonvertex bzw. mit Zweigravitonenaustausch. Wir analysieren das Hochenergieverhalten des Diagramms mit Dreifachgravitonvertex und stellen eine Unterdrückung des Diagramms im dreifachen Regge-Limes fest.

Die Untersuchung der Reggesierung des Gravitons auf der Stringtheorieseite ist eine interessante Aufgabe für die Zukunft. Als einen ersten Schritt haben wir Baumdiagramme, das heißt Diagramme niedrigster Ordnung, auf der Stringtheorieseite berechnet. Um die Reggesierung des Gravitons zu studieren, sind weitere Rechnungen jenseits des klassischen Supergravitationslimes notwendig.

Contents

Introduction	vii
1 Theoretical Background	1
1.1 The AdS/CFT-Correspondence	1
1.1.1 Mapping Symmetries	2
1.1.2 Mapping Type IIB Fields and CFT Operators	2
1.1.3 Mapping Correlation Functions	3
1.2 The Process	4
1.2.1 $\gamma^*\gamma^*$ -Scattering in QCD	4
1.2.2 An Analog Process in $\mathcal{N} = 4$ SYM	6
2 The Four Point Function in $\mathcal{N} = 4$ SYM	9
2.1 Supersymmetry	9
2.2 $\mathcal{N} = 4$ Supersymmetric Yang-Mills Theory	10
2.2.1 The Lagrangian of $\mathcal{N} = 4$ SYM	10
2.2.2 Feynman Rules	13
2.3 Setup of the Computation	15
2.4 One-Loop Diagrams	18
2.4.1 UV Poles	18
2.4.2 High Energy Behavior	20
2.5 Impact Factors	23
2.5.1 Explicit Computation of the Impact Factors	26
2.5.2 Full Impact Factors	33
3 The Six Point Function in $\mathcal{N} = 4$ SYM	35
3.1 Setup of the Computation	35
3.2 Impact Factors	37
3.2.1 Fermion Impact Factors	38
3.2.2 Scalar Impact Factors	40
3.3 The Six Point Amplitude	42
3.4 The Large N_c -Limit in a Topological Approach	47
3.4.1 Diagrams on a Deformed Pair-of-Pants	50
3.4.2 Analytic Expressions	53
4 The Four Point Function in Supergravity	55
4.1 Setup of the Computation	55
4.1.1 Bulk-to-Bulk Propagator of the Gauge Boson	58

4.1.2	Bulk-to-Boundary Propagator of the Gauge Boson	65
4.1.3	Bulk-to-Bulk Propagator of the Graviton	66
4.2	Graviton Exchange	68
4.2.1	Stress-Energy Tensor	69
4.2.2	Graviton Exchange Amplitude	72
4.3	Gauge Boson Exchange	76
5	The Six Point Function in Supergravity	83
5.1	Setup of the Computation	83
5.2	Graviton Exchange with the Triple Graviton Vertex	85
5.2.1	The Triple Graviton Vertex	85
5.2.2	High Energy Behavior	90
6	Summary	93
	Danksagung	101

Introduction

Quantum chromodynamics (QCD) is the fundamental theory describing the strong interactions of the standard model particles. Its basic degrees of freedom are quarks and gluons. QCD is a non-Abelian gauge theory with the gauge group $SU(N_c)$; N_c is the number of colors in the theory. The strong interaction of the particles is characterized by the strong coupling constant α_s . Due to the asymptotic freedom of QCD [1, 2], the coupling constant α_s is small at large momentum transfers. In this case, a perturbative investigation of QCD is reasonable, and an expansion in Feynman diagrams is applicable. On the other hand, if α_s is large, a perturbative treatment of the theory is not justified. One possibility to explore the strong coupling regime of QCD is given by lattice computations.

Before the introduction of QCD, Regge theory [3] has been used to describe the strong interactions of particles at high center-of-mass energies. The basic ideas of Regge theory are the following: The partial wave amplitude of a scattering process analytically continued to complex values of the angular momentum contains singularities in the complex angular momentum plane. In the Regge limit, when the center-of-mass energy s is much larger than the momentum transfer t and all other mass scales, the leading Regge pole $\alpha(t)$ in the t -channel, the one with the largest real part, determines the asymptotic behavior of the amplitude in the s -channel. Consequently, a scattering process in the s -channel is described by the exchange of an object with angular momentum equal to $\alpha(t)$. This object can be understood as a superposition of amplitudes for the exchange of all possible particles in the t -channel. It is called a Regge trajectory or a Reggeon. Furthermore, to explain the slow rise of total cross-sections with the energy s , a Reggeon with vacuum quantum numbers, that means isospin zero and even under charge conjugation, has been introduced: the Pomeron. Besides Regge poles the partial wave amplitude contains further singularities in the complex angular momentum plane, namely Regge cuts. They represent the exchange of two or more Reggeons in the t -channel.

Another line of interest has been the connection between Regge theory and string theory. For real and positive t , Regge poles correspond to resonances and bound states of increasing spin. In the 1960s, the remarkable relation between the mass m and the spin $J = \alpha(t)$ of particles exchanged in the t -channel has been observed [4]: $J = \alpha_0 + \alpha' t$ with the so-called Regge slope α' and the intercept α_0 . The particles with square mass m^2 are said to lie on the leading Regge trajectory. This trajectory holds for a wide range of t and is true for mesonic and baryonic trajectories. String theory has seemed to provide an interesting explanation for this relation. Scattering of open strings in flat space leads to crossing-symmetric scattering amplitudes proposed by Veneziano [5]. The Veneziano amplitude expanded for small energies s indeed includes

the desired Regge trajectory of resonances.

The amplitude can be examined not only for small s , but also for large values of s . In the Regge region, the region of large energy s and small scattering angles, the Veneziano amplitude for a linear Regge trajectory is proportional to $s^{\alpha(t)}$ and in quite good agreement with the actual high energy behavior. Unfortunately, in the region of high energy scattering at fixed angles the Veneziano amplitude falls off exponentially with s while experiments show that scattering amplitudes only fall off according to a power law. Therefore, the early attempts of string theory to describe the high energy behavior of strong interactions failed.

After the establishment of QCD as the theory of strong interactions, there has been the need to clarify, in particular the meaning of the Pomeron in QCD. In perturbative QCD, a possibility to investigate the Pomeron is given by the scattering of two highly virtual photons [6, 7]. The high virtualities of the photons provide hard scales, that is the strong coupling constant α_s is small, and a perturbative treatment of the process is possible. However, in some cases the smallness of the coupling constant is compensated by large logarithms of the energy s , so that $\alpha_s \ln s \sim 1$. Then a resummation of diagrams, which lead to large logarithms, becomes necessary. This resummation is called leading logarithmic approximation (LLA) and collects all terms of the form $(\alpha_s \ln s)^n$ to all orders in the strong coupling constant α_s .

In leading order, the scattering of two virtual photons corresponds to the exchange of two gluons in the t -channel. Generalizing to all orders of the strong coupling constant the gluons are replaced by the Green's function of the BFKL (Balitsky-Fadin-Kuraev-Lipatov) equation [8, 9, 10]. The BFKL equation describes the evolution of a gluon ladder in the LLA. In a gluon ladder, the vertical lines are reggeized gluons, and the couplings to the horizontal lines are given by effective vertices. In a color singlet state, the BFKL equation determines the behavior of the BFKL Pomeron in perturbative QCD. The BFKL Pomeron is a state of two interacting reggeized gluons that is related to a cut instead to a pole in the complex angular momentum plane. The BFKL equation is also known in the next-to-leading logarithmic approximation (NLLA) [11, 12].

The BFKL Pomeron in the LLA predicts a power-like rise of the total cross section with s that would violate unitarity at very high energies. Higher order corrections, so-called unitarity corrections, are believed to restore unitarity. The BFKL equation describes the evolution of two reggeized gluons in the t -channel. First higher order corrections are given by the BKP (Bartels-Kwieciński-Praszałowicz) equations [13, 14]; they describe the evolution of n reggeized gluons in the t -channel. The gluons interact pairwise mediated by the BFKL equation. Further elements that emerge in the context of generalizing the BFKL equation are a transition vertex from two to four reggeized gluons, the triple Pomeron vertex, [15, 16, 17] and a transition vertex from two to six reggeized gluons [18]. The BKP equations and the triple Pomeron vertex appear in $3 \rightarrow 3$ scattering processes the first time, an example is the scattering of highly virtual photons again.

The BFKL and BKP equations as well as the transition vertices have remarkable properties: In the LLA, they are integrable in the large N_c -limit [19, 20, 21] and

conformal invariant in the two-dimensional transverse coordinate space [22, 23].

All elements describing the exchange of reggeized gluons have been introduced in perturbative QCD. Their connection to the strong coupling regime of QCD is not clear.

A new connection between gauge theories and string theories is the AdS/CFT-correspondence [24, 25]. The correspondence offers a promising possibility to study gauge theories at strong coupling. It relates conformal field theories (CFT) to string theories in an Anti-de Sitter (AdS) background. The AdS/CFT-correspondence is a weak-strong coupling duality since it relates the strong coupling limit of a conformal field theory to the weak coupling limit of string theory and vice versa. Thus, the duality suggests to study strong coupling effects of the gauge theory on the string theory side. One of the best understood examples of the AdS/CFT-correspondence is the connection between $\mathcal{N} = 4$ supersymmetric Yang-Mills theory (SYM) and type IIB string theory on an $AdS_5 \times S_5$ background.

$\mathcal{N} = 4$ SYM is a maximal supersymmetric version of QCD. Certainly, QCD and $\mathcal{N} = 4$ SYM differ in several points, nevertheless the AdS/CFT-correspondence offers an excellent opportunity to study the Pomeron at strong coupling: The Regge asymptotics in the LLA are the same in $\mathcal{N} = 4$ SYM and in QCD since the gluons involved in the scattering process are not influenced by the supersymmetry. Therefore, it is interesting to investigate the Regge limit of the supersymmetric theory; the chance is given to analyze the Regge behavior of $\mathcal{N} = 4$ SYM at weak and strong coupling.

$\mathcal{N} = 4$ SYM is conformal invariant and believed to be integrable [26]-[31]. It exhibits similar remarkable features as the BFKL Pomeron in QCD. The correspondence connects the BFKL Pomeron in $\mathcal{N} = 4$ SYM and graviton exchange on the string side. Such as in $\mathcal{N} = 4$ SYM the two gluon exchange is replaced by the BFKL Green's function in the LLA, the graviton on the string side is believed to reggeize [32, 29, 33].

The strong coupling regime of $\mathcal{N} = 4$ SYM is addressed on the string side, but since string theory on a curved manifold as $AdS_5 \times S_5$ has not been solved completely yet, computations on the string side are performed in the classical supergravity limit. In this limit, the type IIB string theory is well approximated by classical supergravity and provides the environment for efficient calculations. Witten proposed [34] a precise matching between the observables of classical supergravity and a CFT. This matching allows the computation of correlation functions of observables on both sides of the correspondence. We are interested in the correlation functions of virtual photons in the Regge limit since the scattering of electromagnetic currents enables the analysis of the Pomeron in a perturbative regime. However, in $\mathcal{N} = 4$ SYM we need a substitute for the virtual photons. In Ref. [35] it has been suggested to use R -currents instead of electromagnetic currents. R -currents belong to a global $SU(4)_R$ group of $\mathcal{N} = 4$ SYM, and we pick up one of the $U(1)$ subgroups.

Beyond Witten's proposal, other approaches exist that address the high energy behavior of amplitudes at strong coupling within the framework of the AdS/CFT-correspondence. In Ref. [33], the BFKL regime and the classical Regge regime are described simultaneously within string theory on a curved background and corrections to the graviton trajectory are derived. Deep inelastic scattering in $\mathcal{N} = 4$ SYM at

strong coupling is analyzed in Refs. [36] and [37]. A description of scalar correlators that could allow to interpolate between weak and strong coupling results has been introduced in Refs. [38] and [39].

Two and three point correlators of R -currents have already been studied on the gauge theory side as well as on the string theory side [40], whereas higher correlation functions have not been considered yet. In this work, we compute four and six point functions of R -currents on the gauge theory side as well as on the string theory side. That is, we obtain analytic expressions for R -current correlation functions in $\mathcal{N} = 4$ SYM at weak and strong coupling.

First, we investigate the elastic scattering of two R -currents in the Regge limit in $\mathcal{N} = 4$ SYM and analyze the influence of the supersymmetry on the scattering amplitude. We verify that the fermionic and scalar one-loop diagrams are finite and subleading compared to diagrams with two gluon exchange in the t -channel. Since these requirements are fulfilled, the factorization of the amplitude in the LLA stays the same as in QCD. The leading diagrams factorize into two impact factors and two exchanged gluons in the t -channel. In $\mathcal{N} = 4$ SYM, the impact factors in the amplitude consist of a sum of fermion and, in addition to QCD, scalar loops. The fermions and scalars are in the adjoint representation of the gauge group $SU(N_c)$. We compute the impact factors and compare them with the QCD impact factors [41].

Next, we consider the six point function of R -currents in $\mathcal{N} = 4$ SYM in the LLA in the triple Regge limit, first for arbitrary N_c [42]. Six point functions provide the first unitarity corrections to the BFKL Pomeron. The impact factors of the amplitude again consist of fermion and scalar loops. We show that the scalar impact factors can be written as a superposition of two gluon impact factors in the same way as the fermion impact factors. Since more than two gluons are exchanged in the t -channel during the scattering process, the BKP equations and the triple Pomeron vertex appear in the scattering amplitude. These pieces are the same as in QCD because they are independent of the coupling to the external particles. In contrast, a new coupling of the gluons to the impact factor, called direct coupling, appears in the supersymmetric theory. The exchanged gluons in the t -channel couple directly to the impact factor without any transition by a triple gluon vertex. This coupling does not exist in QCD. The direct coupling of two noninteracting BFKL Pomerons to the upper R -currents is given by the unintegrated impact factor. We compute this impact factor for fermions and scalars.

We study the large N_c -limit of the six point function in a topological approach, that is the color structure of the diagrams is projected onto surfaces, for example onto pairs-of-pants. In the large N_c -limit, the direct coupling of the gluons is preserved, but the BKP states with more than two gluons are suppressed [43].

Then we compute the four and six point functions of R -currents in the Regge limit on the string theory side in the classical supergravity limit. These computations are meant as a first step in analyzing the reggeization of the graviton on the string theory side. We study a sort of Feynman diagrams in an AdS_5 background, the so-called Witten diagrams. In the classical supergravity limit, we only have to consider tree Witten diagrams.

In case of the four point function of R -currents, we find one diagram with a graviton exchange in the t -channel and one diagram with a gauge boson exchange in the t -channel. The leading contribution in the Regge limit is given by the Witten diagram with one graviton exchange. The graviton exchange amplitude exhibits similar properties as the four point amplitude with gluon exchange at weak coupling. It factorizes into two impact factors and an exchange propagator, which are convoluted by a two-dimensional integration [44].

The six point function of R -currents in the Regge limit in classical supergravity also leads to two different types of Witten diagrams: one diagram with a triple graviton vertex exchange and two diagrams with two graviton exchange. We start with the computation of the triple graviton vertex diagram. For that purpose we derive the triple graviton vertex in an AdS_5 background and determine the high energy behavior of the triple graviton vertex diagram in the triple Regge limit. The diagram decouples in the high energy limit, and the two graviton exchange diagrams give the leading contribution [45].

My thesis has the following structure: A short survey of the AdS/CFT-correspondence and its mapping between $\mathcal{N} = 4$ SYM and type IIB superstring theory is given in chapter 1. Furthermore, we overview scattering of virtual photons in QCD and R -current scattering in $\mathcal{N} = 4$ SYM. In the following four chapters, we discuss the four and six point function of R -currents in the Regge limit on the gauge theory side as well as on the string theory side. The gauge theory side of the AdS/CFT-correspondence is considered in chapters 2 and 3: The four point correlator of R -currents in the Regge limit is computed in chapter 2. The six point correlator of R -currents is discussed in chapter 3. The next two chapters, chapters 4 and 5, deal with correlation functions of R -currents on the supergravity side of the correspondence. We compute Witten diagrams with graviton and gauge boson exchange in the t -channel in the Regge limit in chapter 4. In chapter 5, we start with the investigation of the six point correlation function of R -currents in classical supergravity. In particular, we study the Witten diagram with the triple graviton vertex. Finally, we conclude with a summary in chapter 6.

1 Theoretical Background

1.1 The AdS/CFT-Correspondence

The AdS/CFT-correspondence conjectures a duality between conformal field theories in d dimensions and string theory on a $d + 1$ -dimensional Anti-de Sitter background [24, 25]. If the dimension d is 4, the conformal field theory is $\mathcal{N} = 4$ supersymmetric Yang-Mills theory with the gauge group $SU(N_c)$ and the Yang-Mills coupling g_{YM} , and the dual string theory is type IIB string theory on an $AdS_5 \times S_5$ background with the string coupling g_s . The metric of $AdS_5 \times S_5$ is

$$ds^2 = \frac{R^2}{z_0^2}(dz_0^2 + d\vec{x}^2) + R^2 d\Omega_5^2 \quad (1.1)$$

with $z_0 > 0$ and $\vec{x} = (x_1, \dots, x_4)$. That is the Euclidean continuation of a five-dimensional Anti-de Sitter space in Poincaré coordinates times a five-sphere both with the same radius R . Sometimes the radius R is expressed in units of the string length l_s .

The AdS/CFT-correspondence states the duality of the two theories if

$$g_s = g_{YM}^2 \quad \text{and} \quad R^4 = l_s^4 g_s N_c. \quad (1.2)$$

This is the strongest version of the correspondence, it is to hold at any value of N_c and for all values of the coupling $g_s = g_{YM}^2$. The string theory lives in $AdS_5 \times S_5$, and the gauge theory lives at $z_0 \rightarrow 0$, that is on the four-dimensional boundary S_4 of the AdS_5 space. String theory on a general curved background is hardly tractable, but certain limits of the strongest version of the correspondence exist in which computations are much simpler.

The first limit is the t'Hooft limit: The t'Hooft coupling $\lambda \equiv g_{YM}^2 N_c$ is kept fixed while $N_c \rightarrow \infty$. λ is the effective coupling in an $SU(N_c)$ gauge theory at large N_c . If $\lambda \ll 1$, a perturbative treatment of $\mathcal{N} = 4$ SYM is possible, and the theory can be expanded in Feynman diagrams. On the other hand, the t'Hooft limit leads to a weakly coupled string theory since $g_s = \frac{\lambda}{N_c}$. The type IIB string theory reduces to classical string theory on $AdS_5 \times S_5$, and string loops can be neglected. In the t'Hooft limit, the AdS/CFT-correspondence is a duality between classical string theory and the large N_c -limit of gauge theories.

An even weaker version of the correspondence is achieved by the second limit, sending the radius R expressed in units of the string length l_s to infinity, $R/l_s \rightarrow \infty$, after taking the t'Hooft limit. This is the strong coupling limit on the SYM side, since

$(R/l_s)^4 = \lambda = g_{YM}^2 N_c \gg 1$, but the curvature of the string background is small, and the massive string excitations decouple from the low energy ones. Consequently, the classical string theory can be approximated by classical type IIB supergravity in ten dimensions. After performing a Kaluza-Klein compactification on S_5 , one ends with a classical theory in five dimensions that is $\mathcal{N} = 8$, $D = 5$ supergravity with $SO(6)$ Yang-Mills gauge group. Summarizing, the strong coupling limit of $\mathcal{N} = 4$ SYM in the large N_c -limit is equivalent to classical type IIB supergravity.

The AdS/CFT-correspondence is a weak-strong coupling duality. It relates the strong coupling limit of one side with the weak coupling limit on the other side. This fact can be used to study aspects of the gauge theory at strong coupling. The duality comes with a precise matching of symmetries, fields and operators as well as correlations functions of both theories. We explain these mappings in the next sections.

1.1.1 Mapping Symmetries

A strong indication for the correctness of the AdS/CFT-correspondence is the matching of the global unbroken symmetries of the two theories.

$\mathcal{N} = 4$ SYM is invariant under $\mathcal{N} = 4$ Poincaré supersymmetry and under special conformal transformations. Moreover, the theory is classically scale invariant. In a relativistic field theory, Poincaré invariance, scale invariance and special conformal transformations combine to a larger conformal symmetry group, the group $SU(2, 2) \sim SO(2, 4)$. In addition, SYM is invariant under R -symmetry forming the group $SU(4)_R \sim SO(6)_R$. An R -symmetry is by definition a symmetry that does not commute with the supersymmetries. Thus, the maximal bosonic subgroup of SYM is $SU(2, 2) \times SU(4)_R \sim SO(2, 4) \times SO(6)_R$. Furthermore, $\mathcal{N} = 4$ Poincaré supersymmetry and conformal invariance produce the even larger superconformal symmetry, the supergroup $SU(2, 2|4)$, which is the global continuous symmetry group of $\mathcal{N} = 4$ SYM.

The bosonic subgroup $SO(2, 4) \times SO(6)_R$ can be identified on the AdS side with the isometry group of AdS_5 that is $SO(2, 4)$ and the isometry group of S_5 that is $SO(6)$. The matching of the full supergroup arises on the AdS side because type IIB string theory has 32 supersymmetries just as $\mathcal{N} = 4$ SYM. The supercharges combine with the isometries to the group $SU(2, 2|4)$, and the global symmetry group matches on both sides of the correspondence.

1.1.2 Mapping Type IIB Fields and CFT Operators

The duality includes a precise matching between states and fields on the string theory side and local gauge invariant operators on the SYM side. The gauge invariant operators \mathcal{O} are characterized by a conformal dimension Δ and a representation index I_n for the $SO(6)_R \sim SU(4)_R$ symmetry. All type IIB massless supergravity and massive string degrees of freedom are described by fields ϕ living in $AdS_5 \times S_5$. S_5 is a compact space, and thus the Kaluza-Klein procedure of compactification can be applied. The

fields ϕ are expanded in spherical harmonics on the sphere S_5 , for example for scalars fields:

$$\phi(x, y) = \sum_n \sum_{I_n} \phi_{(n)}^{I_n}(x) Y_{(n)}^{I_n}(y). \quad (1.3)$$

x^μ is a coordinate for AdS_5 with $\mu = 0, 1, \dots, 4$ and y^ν with $\nu = 1, \dots, 5$ for S_5 . $Y_{(n)}^{I_n}$ is a basis of spherical harmonics on S_5 . Here, n is the level, and I_n is an index in a representation of the symmetry group. The fields $\phi_{(n)}^{I_n}(x)$ compactified on S_5 receive a contribution to the mass m , and fields of mass m living in AdS_5 correspond to operators $\mathcal{O}_{(n)}^{I_n}$ with conformal dimension Δ in $\mathcal{N} = 4$ SYM. The relation between mass m and conformal dimension Δ is for example for scalar fields

$$\Delta = \frac{d}{2} + \sqrt{\frac{d^2}{4} + m^2 R^2}. \quad (1.4)$$

1.1.3 Mapping Correlation Functions

In a conformal field theory, the only physical observables are correlation functions of gauge invariant operators. If we want to apply the AdS/CFT-correspondence, we need a prescription how to compute these correlation functions in the classical supergravity theory. Ref. [34] provides such an instruction. As explained in the last section, an operator \mathcal{O} with conformal dimension Δ in $\mathcal{N} = 4$ SYM corresponds to a field ϕ with mass m living on AdS_5 in the supergravity theory. The field ϕ has a value at the boundary of AdS_5 , that is at $z_0 = 0$, where the $\mathcal{N} = 4$ SYM theory lives. The boundary value is denoted ϕ_0 . The meaning of ϕ_0 in the gauge theory is the following: It couples to the operator \mathcal{O} via $\int_{S_4} \mathcal{O} \phi_0$. S_4 is the boundary of AdS_5 and can be interpreted as a source for the operator \mathcal{O} . Then the partition function of the gauge theory is defined as

$$Z_{\mathcal{O}}[\phi_0] = \int \mathcal{D}[\text{SYM fields}] \exp \left(-S_{\mathcal{N}=4\text{SYM}} + \int_{S_4} d^4x \mathcal{O}(x) \phi_0(x) \right). \quad (1.5)$$

$S_{\mathcal{N}=4\text{SYM}}$ is the action of $\mathcal{N} = 4$ SYM. The partition function is a generating functional for n -point correlation functions of operators \mathcal{O} at distinct points x_1, \dots, x_n , and the correlation functions are computed by

$$\langle \mathcal{O}(x_1) \mathcal{O}(x_2) \dots \mathcal{O}(x_n) \rangle = \frac{\delta^n}{\delta \phi_0(x_1) \dots \delta \phi_0(x_n)} Z_{\mathcal{O}}[\phi_0] |_{\phi_0=0}. \quad (1.6)$$

Now, the partition function $Z_{\mathcal{O}}[\phi_0]$ has to be related to a quantity on the string side. It should be a partition function of string theory for the field ϕ with a boundary value ϕ_0 . In the classical supergravity limit, the classical supergravity partition function is a good approximation. It is given by

$$Z[\phi_0]_{\text{sugra}} = \exp(-S_{\text{sugra}}[\phi[\phi_0]]) \quad (1.7)$$

with the classical supergravity action S_{sugra} . The AdS/CFT-correspondence states that

$$Z_{\mathcal{O}}[\phi_0]_{\text{CFT}} = Z[\phi_0]_{\text{sugra}}. \quad (1.8)$$

Consequently, n -point correlation functions are computed on both sides of the correspondence by

$$\begin{aligned} \frac{\delta^n}{\delta\phi_0(x_1)\dots\delta\phi_0(x_n)} Z_{\mathcal{O}}[\phi_0]_{\text{CFT}}|_{\phi_0=0} &= \langle \mathcal{O}(x_1), \dots, \mathcal{O}(x_n) \rangle \\ &= \frac{\delta^n}{\delta\phi_0(x_1)\dots\delta\phi_0(x_n)} Z[\phi_0]_{\text{sugra}}|_{\phi_0=0}. \end{aligned} \quad (1.9)$$

This prescription enables to evaluate correlation functions of $\mathcal{N} = 4$ SYM at weak and at strong coupling perturbatively. First, the correlators can be studied at weak coupling on the SYM side, and then, using the correspondence, the strong coupling behavior can be addressed on the supergravity side where it corresponds to the weak coupling regime. We use this possibility to investigate a certain class of correlation functions that we present in the next section.

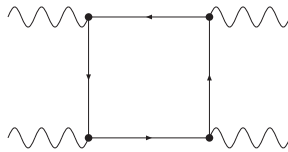
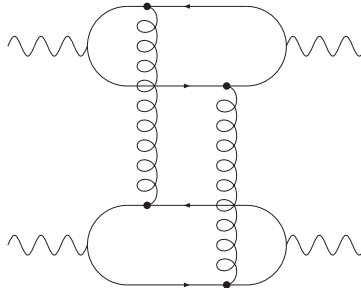
1.2 The Process

1.2.1 $\gamma^*\gamma^*$ -Scattering in QCD

The scattering of two highly virtual photons offers the most convenient way of studying Regge dynamics in perturbative QCD [6, 7]. The scattering provides an IR-finite and gauge invariant amplitude. Processes that are mediated by the exchange of a virtual photon are for example e^+e^- -annihilation and deep inelastic scattering. If the momentum transfer Q in the scattering process is large, the strong coupling constant $\alpha_s(Q^2)$ is reasonably small, and the use of perturbation theory is allowed. The decay of the photon is mediated by the electromagnetic current j_μ associated with the $U(1)$ gauge symmetry of QED. Thus, the $\gamma^*\gamma^*$ -scattering process is described by the four point function of electromagnetic currents in momentum space

$$\begin{aligned} &i(2\pi)^4 \delta^{(4)}(p_A + p_B - p_{A'} - p_{B'}) A^{\mu_A \mu_B \mu_{A'} \mu_{B'}}(s, t) \\ &= \int \prod_i d^4 x_i e^{-ip_A \cdot x_A - ip_B \cdot x_B + ip_{A'} \cdot x_{A'} + ip_{B'} \cdot x_{B'}} \langle j^{\mu_A}(x_A) j^{\mu_B}(x_B) j^{\mu_{A'}}(x_{A'}) j^{\mu_{B'}}(x_{B'}) \rangle. \end{aligned} \quad (1.10)$$

The amplitude A depends on the usual Mandelstam variables s and t . p_A and p_B are the incoming momenta whereas $p_{A'}$ and $p_{B'}$ are the outgoing momenta of the photons. We only consider the lowest order in the electric charge α , but the order of the strong coupling constant α_s can be arbitrary high. An example of a lowest order diagram is shown in Fig. 1.1. In the high energy limit, these boxdiagrams behave as $\log^2 s$ [46]. In higher order α_s , radiative gluonic corrections to the boxdiagrams do not modify the power of the energy dependence.

Figure 1.1: A lowest order diagram for $\gamma^*\gamma^*$ -scatteringFigure 1.2: A three-loop diagram for $\gamma^*\gamma^*$ -scattering in QCD

New diagrams with two exchanged t -channel gluons, Fig. 1.2, become available at three-loop level. The photons split into the quark-antiquark pairs, and the two t -channel gluons couple to the two loops. The three-loop diagrams behave as $\alpha_s^2 s$ at high energies [47] and dominate with respect to the box diagrams. In general, the high energy behavior of scattering amplitudes in the Regge limit is determined by the exchange of highest spin particles, which are gluons with spin one in QCD.

In arbitrary high orders of the strong coupling constant, the smallness of α_s is potentially compensated by a large logarithm of the energy s , and a resummation of terms enhanced by a large logarithm becomes necessary. In the LLA, we collect all these terms proportional to $(\alpha_s \ln s)^m$ and sum them up to all orders in α_s . Then the four point amplitude of electromagnetic currents in Eq. (1.10) factorizes into two fermion impact factors D of the virtual photons [47] and the BFKL Green's function $G(s)$,

$$A(s, t) = is D_A \otimes G(s) \otimes D_B. \quad (1.11)$$

The symbol \otimes denotes the convolution of transverse gluon momenta and contraction of color indices.

The BFKL Pomeron predicts a rise of the total cross section with some power of s . At very high energies this rise would violate unitarity. Higher order corrections to the BFKL equation, so-called unitarity corrections, are believed to restore unitarity at high energies. Such corrections are for example the BKP equations, which describe the evolution of n gluons in the t -channel, and the triple Pomeron vertex. They appear in $3 \rightarrow 3$ scattering processes the first time. These processes naturally arise in the context of deep inelastic scattering on a weakly bound nucleus, Fig. 1.3. An example is deep inelastic scattering on a nucleus consisting of two weakly bound nucleons. To obtain a completely perturbative process, we replace the nucleons by virtual photons.

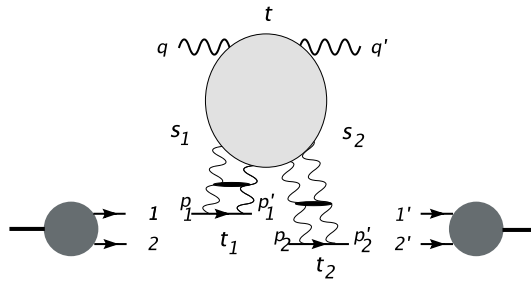


Figure 1.3: Scattering of a virtual photon on a weakly bound nucleus in QCD

We arrive at a six point correlator of electromagnetic currents j_μ , the generalization of Eq. (1.10). The leading diagrams are those with the exchange of highest spin particles in the t -channel, that means diagrams with four t -channel gluons. The coupling between the external photons and the exchanged gluons is mediated by three fermion impact factors. In higher order α_s in the LLA, the structure of the diagrams is more complex than those of a four point function. We explain the structure in chapter 3, there is still a factorization of the amplitude into impact factors and exchanged gluon structures.

1.2.2 An Analog Process in $\mathcal{N} = 4$ SYM

The AdS/CFT-correspondence offers a comfortable possibility to study scattering amplitudes at strong coupling. It relates the weak coupling limit of correlation functions on the string theory side to the strong coupling limit of correlation functions on the gauge theory side. Eq. (1.9) gives a concrete connection between correlators on both sides of the correspondence.

In QCD, the scattering process of interest is $\gamma^*\gamma^*$ -scattering. Since the duality connects classical supergravity with conformal field theories and not with QCD, we have to look for an analog process to $\gamma^*\gamma^*$ -scattering in $\mathcal{N} = 4$ SYM. In particular, we need a substitute for the electromagnetic current j^μ in the correlation function (1.10).

$\mathcal{N} = 4$ SYM has a global $SU(4)_R$ R -symmetry. This symmetry allows to introduce an analog of the electromagnetic current. Namely, we choose as a replacement the conserved R -current J_R [35], see the next chapter for a detailed description. Therefore, we compute the correlation function of R -currents according to

$$\begin{aligned} \frac{\delta^n}{\delta\phi_0(x_1)\dots\delta\phi_0(x_n)} Z_{J_R}[\phi_0]_{\text{CFT}}|_{\phi_0=0} &= \langle J_R(x_1), \dots, J_R(x_n) \rangle \\ &= \frac{\delta^n}{\delta\phi_0(x_1)\dots\delta\phi_0(x_n)} Z[\phi_0]_{\text{sugra}}|_{\phi_0=0}. \end{aligned} \tag{1.12}$$

We introduce the explicit expression for the field ϕ_0 , which is the source of the operator J_R , in chapter 4.

The resulting diagrams for four and six point functions of R -currents in $\mathcal{N} = 4$ SYM are similar to the QCD diagrams with the external photons replaced by R -currents. Of course, $\mathcal{N} = 4$ SYM has differences compared with QCD. For example, the $\mathcal{N} = 4$ SYM diagrams contain besides fermion loops also scalar loops. Additionally, in $\mathcal{N} = 4$ SYM all particles, fermions and scalars, are in the adjoint representation of the gauge group $SU(N_c)$, see section 2.2.1, whereas in QCD, the fermions are in the fundamental representation of the gauge group. This difference leads to different color factors for the diagrams in QCD and $\mathcal{N} = 4$ SYM.

Nevertheless, the factorization of the four point amplitudes stays the same in $\mathcal{N} = 4$ SYM in the LLA. The reason is the following: First, a requirement is that the one-loop diagrams in $\mathcal{N} = 4$ SYM, including scalar contributions, are finite and subleading. We verify this in the next chapter. Then we can turn to the three-loop diagrams. We have two parts in the factorized amplitude (1.11), the impact factors and the BFKL Green's function. In $\mathcal{N} = 4$ SYM, the impact factors include fermions and scalars and change compared to the QCD impact factors. But the impact factors do not influence the BFKL Green's function. It stays the same in both theories since the BFKL Green's function contains only gluonic contributions in the LLA. Fermionic corrections, which could change in $\mathcal{N} = 4$ SYM, and new scalar corrections first appear in the NLLA. Consequently, in the LLA the factorization is the same in both theories. The new scalar degrees of freedom are only apparent in the impact factors and in the one-loop diagrams. A similar argument holds in the case of a six point function, see chapter 3. Since Regge factorization works the same for R -current scattering in $\mathcal{N} = 4$ SYM and virtual photon scattering in QCD a promising opportunity is provided to study Regge behavior at strong coupling using the AdS/CFT-correspondence.

2 The Four Point Function in $\mathcal{N} = 4$ SYM

In this chapter, we compute correlation functions of R -currents in $\mathcal{N} = 4$ SYM at weak coupling in the Regge limit, that is on the CFT side of the correspondence, see our publication [41]. Before we begin with the concrete computation of correlation functions, we present some facts about supersymmetry and $\mathcal{N} = 4$ SYM theory.

2.1 Supersymmetry

Supersymmetry is a symmetry that relates fermions and bosons. A supersymmetry transformation turns a fermionic into a bosonic state and a bosonic one into a fermionic. The corresponding operator is a complex anticommuting spinor Q_α^a ,

$$Q_\alpha^a |\text{boson}\rangle = |\text{fermion}\rangle, \quad Q_\alpha^a |\text{fermion}\rangle = |\text{boson}\rangle. \quad (2.1)$$

Since Q_α^a is complex, also $(Q_\alpha^a)^\dagger$ is a symmetry generator. Q_α^a with $\alpha = 1, 2$ is a left-handed Weyl spinor and $(Q_\alpha^a)^\dagger =: \bar{Q}_{\dot{\alpha}a}$ with $\dot{\alpha} = 1, 2$ a right-handed Weyl spinor. a runs from 1 to \mathcal{N} ; \mathcal{N} is the number of independent supersymmetries of the algebra. Q_α^a and $\bar{Q}_{\dot{\alpha}a}$ commute with translations P_μ ,

$$[Q_\alpha^a, P_\mu] = [\bar{Q}_{\dot{\alpha}a}, P_\mu] = 0, \quad (2.2)$$

transform as Weyl spinors under $SO(1, 3)$,

$$\begin{aligned} [Q_\alpha^a, M_{\mu\nu}] &= (\sigma_{\mu\nu})_\alpha{}^\beta Q_\beta^a, \\ [\bar{Q}_{\dot{\alpha}a}, M_{\mu\nu}] &= (\bar{\sigma}_{\mu\nu})^{\dot{\alpha}}{}_{\dot{\beta}} \bar{Q}_{\dot{\beta}a}, \end{aligned} \quad (2.3)$$

and satisfy the supersymmetry algebra,

$$\begin{aligned} \{Q_\alpha^a, \bar{Q}_{\dot{\beta}b}\} &= 2\sigma_{\alpha\dot{\beta}}^\mu P_\mu \delta_b^a, \\ \{Q_\alpha^a, Q_\beta^b\} &= 2\epsilon_{\alpha\beta} Z^{ab}, \\ \{\bar{Q}_{\dot{\alpha}a}, \bar{Q}_{\dot{\beta}b}\} &= 2\epsilon_{\dot{\alpha}\dot{\beta}} (Z^{ab})^*. \end{aligned} \quad (2.4)$$

Z^{ab} are central charges that are antisymmetric in the indices a and b and commute with all generators of the supersymmetry algebra. In the case $\mathcal{N} = 1$, the antisymmetry implies that there are no central charges. This is called unextended supersymmetry. For $\mathcal{N} > 1$ we have an extended supersymmetry.

The Weyl spinors are connected to the four-component Dirac spinors by

$$Q^a = \begin{pmatrix} Q_\alpha^a \\ \bar{Q}_{\dot{a}}^a \end{pmatrix} \quad (2.5)$$

and the four-dimensional gamma matrix is

$$\gamma^\mu = \begin{pmatrix} 0 & \sigma^\mu \\ \bar{\sigma}^\mu & 0 \end{pmatrix}. \quad (2.6)$$

Furthermore, we have

$$P_L Q^a = \begin{pmatrix} Q_\alpha^a \\ 0 \end{pmatrix} \quad \text{and} \quad P_R Q^a = \begin{pmatrix} 0 \\ \bar{Q}_{\dot{a}}^a \end{pmatrix} \quad (2.7)$$

with

$$P_L = (1 - \gamma_5)/2, \quad P_R = (1 + \gamma_5)/2, \quad \text{and} \quad \gamma_5 = \begin{pmatrix} -1 & 0 \\ 0 & 1 \end{pmatrix}. \quad (2.8)$$

The particles of supersymmetric theories fall into irreducible representations of the supersymmetry algebra, which are called supermultiplets. Each multiplet contains an equal number of degrees of freedom of fermions and bosons. All particles belonging to one supermultiplet have got the same mass. The simplest multiplets are the $\mathcal{N} = 1$ massless supermultiplets, that are a chiral supermultiplet with one Weyl fermion and a complex scalar, a gauge supermultiplet with one gauge boson and one Weyl fermion, the gravitino supermultiplet with one gravitino and a gauge boson, and the graviton supermultiplet with one graviton and one gravitino.

2.2 $\mathcal{N} = 4$ Supersymmetric Yang-Mills Theory

2.2.1 The Lagrangian of $\mathcal{N} = 4$ SYM

The gauge multiplet of $\mathcal{N} = 4$ SYM consists of one vector field A_μ , four chiral spinors λ_I , and six real scalars X_M . The gauge multiplet transforms under the adjoint representation of the gauge group $SU(N_c)$. The Lagrangian for $\mathcal{N} = 4$ SYM in $d = 4$ dimensions can be obtained by dimensional reduction of the $d = 10$ supersymmetric Yang-Mills theory [48]. It is

$$\begin{aligned} \mathcal{L}_{\text{SYM}} = & \text{Tr} \left(-\frac{1}{4} F_{\mu\nu} F^{\mu\nu} + \frac{1}{2} D_\mu X_M D^\mu X_M + i \lambda_I \sigma^\mu D_\mu \bar{\lambda}^I \right. \\ & \left. - ig \lambda_I [\lambda_J, X^{IJ}] - ig \bar{\lambda}^I [\bar{\lambda}^J, X_{IJ}] + \frac{1}{4} g^2 [X_M, X_N] [X_M, X_N] \right). \quad (2.9) \end{aligned}$$

The covariant derivative and the gauge field strength tensor are defined as usual

$$D_\mu \Phi = \partial_\mu \Phi - ig [A_\mu, \Phi], \quad (2.10)$$

$$F_{\mu\nu} = \partial_\mu A_\nu - \partial_\nu A_\mu - ig [A_\mu, A_\nu]. \quad (2.11)$$

Φ stands for the fields X or λ . X_M and X_{IJ} are related by the $SU(4)_R \sim SO(6)_R$ sigma symbols,

$$X_{IJ} = -\frac{1}{2}(\Sigma_M)_{IJ}X_M, \quad X^{IJ} = \frac{1}{2}(\Sigma_M^{-1})^{IJ}X_M \quad (2.12)$$

with

$$\text{Tr}(\Sigma_M \Sigma_N^{-1}) = 4\delta_{MN} \quad \text{and} \quad X_M X_M = X_{IJ} X^{IJ}. \quad (2.13)$$

Then we get

$$\begin{aligned} \mathcal{L}_{\text{SYM}} = & -\frac{1}{4}(\partial_\mu A_\nu^a - \partial_\nu A_\mu^a)^2 + \frac{1}{2}\partial_\mu X_M^a \partial^\mu X_M^a + i\lambda_I^a \sigma^\mu \partial_\mu \bar{\lambda}^{Ia} \\ & -gf_{abc}\partial_\mu A_\nu^a A^{\mu b} A^{\nu c} - \frac{1}{4}g^2 f_{abe} f_{cde} A_\mu^a A_\nu^b A^{\mu c} A^{\nu d} \\ & +gf_{abc}A^{\mu a} X_M^b \partial_\mu X_M^c + \frac{1}{2}g^2 f_{abe} f_{cde} A_\mu^a X_M^b A^{\mu c} X_M^d \\ & -igf_{abc}A_\mu^a \lambda_I^b \sigma^\mu \bar{\lambda}^{cI} - \frac{1}{4}g^2 f_{abe} f_{cde} X_M^a X_N^b X_M^c X_N^d \\ & +gf_{abc}X^{aIJ}\lambda_I^b \lambda_J^c + gf_{abc}X_{IJ}^a \bar{\lambda}^{bI} \bar{\lambda}^{cJ}. \end{aligned} \quad (2.14)$$

Small indices $a, b, c, \dots = 1, \dots, N_c^2 - 1$ are adjoint representation indices for the gauge group $SU(N_c)$. We can write $\Phi = \Phi_{ab} = \Phi^c(T^c)_{ab}$ with $(T^c)_{ab} = -if^{abc}$. f^{abc} are the $SU(N_c)$ structure constants with $[T^a, T^b] = if^{abc}T^c$. The normalization of the generators T^a is $\text{Tr}(T^a T^b) = N_c \delta^{ab}$.

The Lagrangian \mathcal{L}_{SYM} is invariant under global $SU(4)_R$ transformations, see section 1.1.1. Capital indices in the Lagrangian transform under this R -symmetry group. In particular, $I, J, \dots = 1, \dots, 4$ transform under the fundamental and $M, N, \dots = 1, \dots, 6$ under the vector representation of $SU(4)_R$. A_μ is a scalar of $SU(4)_R$, the chiral spinors λ_I are in the fundamental representation and the scalars X_M in the vector representation of $SU(4)_R$. The $SU(4)_R$ transformations are given by

$$\begin{aligned} \delta\lambda^{a\alpha I} &= i\varepsilon_A \lambda^{a\alpha J} (T^A)_{JI}, \\ \delta\bar{\lambda}^{a\dot{\alpha}I} &= -i\varepsilon_A (T^A)_{IJ} \bar{\lambda}^{a\dot{\alpha}J}, \\ \delta X_M^a &= i\varepsilon_A (T^A)_{MN} X_N^a. \end{aligned} \quad (2.15)$$

ε_A are small parameters, and T^A are the $SU(4)_R$ generators in the appropriate representation.

We introduce the R -current here, which we use as a substitute of the electromagnetic current in our computations of correlation functions within the AdS/CFT-correspondence. The $SU(4)_R$ symmetry provides a conserved Noether current, named $J_R^{\mu A}$, our R -current,

$$J_R^{A\mu} = i \frac{\partial \mathcal{L}}{\partial(\partial_\mu \Phi)} \Delta^A \Phi = \text{Tr}(-\lambda \sigma^\mu T^A \bar{\lambda} - i X T^A D^\mu X). \quad (2.16)$$

$\Delta^A \Phi$ is defined by $\delta\Phi = i\varepsilon_A \Delta^A \Phi$ for an infinitesimal transformation.

One subtlety concerning R -currents are their associated Ward identities. $J_R^{A\mu}$ is a conserved current. The time-ordered product of a conserved current J^μ and some operators \mathcal{O}_i gives rise to Ward identities. It is given by

$$\partial_\mu T J^\mu(x) \mathcal{O}_1(x_1) \dots \mathcal{O}_n(x_n) = \sum_{i=1}^n \delta(x^0 - x_i^0) T \mathcal{O}_1(x_1) \dots [j^0(x), \mathcal{O}_i(x_i)] \dots \mathcal{O}_n(x_n). \quad (2.17)$$

On the right-hand side of Eq. (2.17), the equal-time commutator of the zero-component of the current and the operator is

$$[j^0(\vec{x}, t), \mathcal{O}(\vec{y}, t)] = \delta^{(3)}(\vec{x} - \vec{y}) q_{\mathcal{O}} \mathcal{O}(\vec{x}, t). \quad (2.18)$$

$q_{\mathcal{O}}$ is the charge of the operator \mathcal{O} in units of the electric charge e . Inserting (2.18) in (2.17) gives an explicit expression for the so-called contact terms on the right-hand side of (2.17),

$$\partial_\mu T J^\mu(x) \mathcal{O}_1(x_1) \dots \mathcal{O}_n(x_n) = \sum_{i=1}^n \delta^{(4)}(x - x_i) q_{\mathcal{O}_i} T \mathcal{O}_1(x_1) \dots \mathcal{O}_n(x_n). \quad (2.19)$$

In an Abelian theory, the conserved currents are neutral, and the contact terms vanish,

$$\partial_\mu T J^\mu(x) \mathcal{O}_1(x_1) \dots \mathcal{O}_n(x_n) = 0. \quad (2.20)$$

We get the well-known Ward identities. Going to momentum space and taking the vacuum expectation value we arrive at

$$p_\mu \langle j^\mu(p) j^{\mu_1}(p_1) \dots j^{\mu_n}(p_n) \rangle = 0. \quad (2.21)$$

Since $\mathcal{N} = 4$ SYM is a non-Abelian theory, the conserved currents are charged and the contact terms do not vanish. The equal-time commutator (2.18) with the operator \mathcal{O} replaced by an R -current is now

$$[J_R^{A0}(\vec{x}, t), J_R^{B\mu}(\vec{y}, t)] = \delta^{(3)}(\vec{x} - \vec{y}) (T^A)_C^B J_R^{C\mu}(\vec{x}, t), \quad (2.22)$$

and the time-ordered product of R -currents respects

$$\begin{aligned} & \partial_\mu T J_R^{A\mu}(x) J_R^{A_1\mu_1}(x_1) \dots J_R^{A_n\mu_n}(x_n) \\ &= \sum_{i=1}^n \delta^{(4)}(x - x_i) T J_R^{A_1\mu_1}(x_1) \dots (T^A)_C^{A_i} J_R^{C\mu_i}(x) \dots J_R^{A_n\mu_n}(x_n). \end{aligned} \quad (2.23)$$

The non-vanishing of the contact terms introduces some complications in the following computations. Nevertheless, there is a possibility to get back to the simple Ward identities (2.20) of Abelian theories. The full R -symmetry group is $SU(4)_R$. If we restrict ourselves to a subgroup $U(1)$, we reach a situation with vanishing contact terms. The restriction means to pick up one of the 15 R -currents of the global $SU(4)_R$ group. To go to a $U(1)$ subgroup, we choose a particular linear combination of the three diagonal $SU(4)_R$ generators [35]. Since the diagonal generators commute, all $(T^A)_C^{A_i} = -if^{AA_iC}$ vanish, and we get, omitting the $SU(4)_R$ labels A_i for the $U(1)$ current,

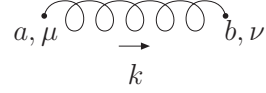
$$\partial_\mu T J_R^\mu(x) J_R^{\mu_1}(x_1) \dots J_R^{\mu_n}(x_n) = 0. \quad (2.24)$$

At some point, we will use this restriction in the next chapters.

2.2.2 Feynman Rules

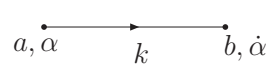
From the Lagrangian (2.9) we derive the Feynman rules of $\mathcal{N} = 4$ SYM. The propagators of the theory have the following form:

the gluon propagator is given by



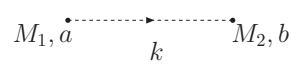
$$\frac{i}{k^2 + i\epsilon} \left(-g_{\mu\nu} + (1 - \xi) \frac{k_\mu k_\nu}{k^2} \right), \quad (2.25)$$

the fermion propagator looks like



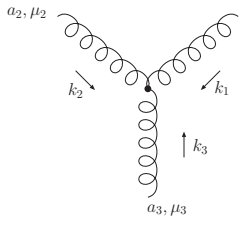
$$\frac{ik_\mu (\sigma^\mu)_{\alpha\dot{\alpha}} \delta_{ab}}{k^2 + i\epsilon}, \quad (2.26)$$

and the scalar propagator is



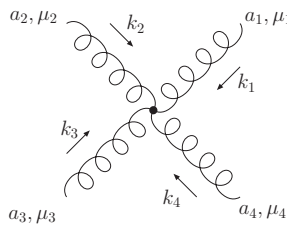
$$\frac{i}{k^2 + i\epsilon} \delta_{M_1 M_2} \delta_{ab}. \quad (2.27)$$

The vertices of $\mathcal{N} = 4$ SYM are the three gluon vertex



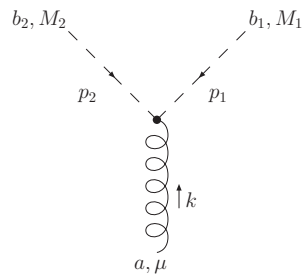
$$gf_{a_1 a_2 a_3} [g^{\mu_2 \mu_3} (k_2 - k_3)^{\mu_1} + g^{\mu_3 \mu_1} (k_3 - k_1)^{\mu_2} + g^{\mu_1 \mu_2} (k_1 - k_2)^{\mu_3}], \quad (2.28)$$

the four gluon vertex



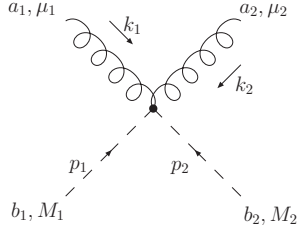
$$-ig^2 [f_{a_1 a_2 b} f_{a_3 a_4 b} (g^{\mu_1 \mu_3} g^{\mu_2 \mu_4} - g^{\mu_1 \mu_4} g^{\mu_2 \mu_3}) + f_{a_1 a_3 b} f_{a_2 a_1 b} (g^{\mu_1 \mu_2} g^{\mu_3 \mu_4} - g^{\mu_1 \mu_4} g^{\mu_2 \mu_3}) + f_{a_1 a_4 b} f_{a_2 a_3 b} (g^{\mu_1 \mu_2} g^{\mu_3 \mu_4} - g^{\mu_1 \mu_3} g^{\mu_2 \mu_4})], \quad (2.29)$$

the one gluon-two scalar vertex



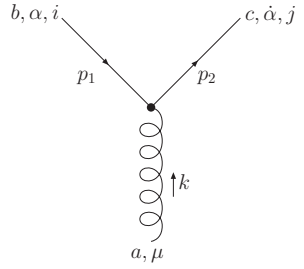
$$gf_{ab_1 b_2} (p_2 - p_1)^\mu \delta_{M_1 M_2}, \quad (2.30)$$

the two gluon-two scalar vertex



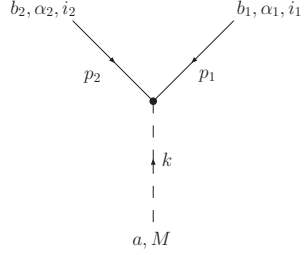
$$ig^2 g^{\mu_1 \mu_2} \delta_{M_1 M_2} (f^{a_1 b_1 c} f^{a_2 b_2 c} + f^{a_1 b_2 c} f^{a_2 b_1 c}), \quad (2.31)$$

the one gluon-two fermion vertex

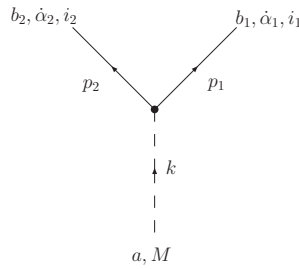


$$- g f_{abc} (\bar{\sigma}^\mu)^{\dot{\alpha} \alpha} \delta^{ij}, \quad (2.32)$$

the one scalar-two fermion vertices

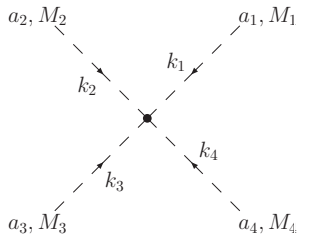


$$- ig f_{ab_1 b_2} \varepsilon^{\alpha_1 \alpha_2} (\Sigma_M^{-1})^{i_1 i_2}, \quad (2.33)$$



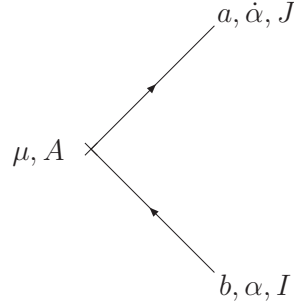
$$ig f_{ab_1 b_2} \varepsilon^{\dot{\alpha}_1 \dot{\alpha}_2} (\Sigma_M)_{i_1 i_2}, \quad (2.34)$$

and the four scalar vertex



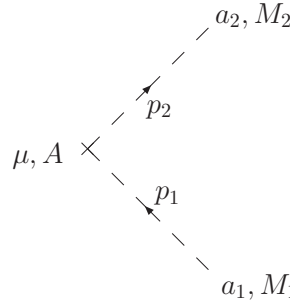
$$-ig^2 [f_{a_1 a_2 b} f_{a_3 a_4 b} (\delta_{M_1 M_3} \delta_{M_2 M_4} - \delta_{M_2 M_3} \delta_{M_1 M_4}) + f_{a_1 a_3 b} f_{a_2 a_4 b} (\delta_{M_1 M_2} \delta_{M_3 M_4} - \delta_{M_2 M_3} \delta_{M_1 M_4}) + f_{a_1 a_4 b} f_{a_2 a_3 b} (\delta_{M_1 M_3} \delta_{M_2 M_4} - \delta_{M_1 M_2} \delta_{M_3 M_4})]. \quad (2.35)$$

We deduce further Feynman rules from the R -current (2.16): the coupling of an external R -current, symbolized by the cross, to fermions



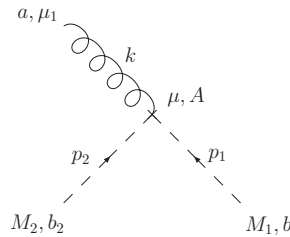
$$(\bar{\sigma}^\mu)^{\dot{\alpha}\alpha} (T^A)_J^I \delta^{ab}, \quad (2.36)$$

to scalars



$$(p_1 + p_2)^\mu (T^A)_{M_1 M_2} \delta^{ab}, \quad (2.37)$$

and to two scalars and one gluon



$$2igg^{\mu\mu_1} f_{ab_1b_2} (T^A)_{M_1 M_2}. \quad (2.38)$$

2.3 Setup of the Computation

We start with the definition of a four point amplitude of R -currents in momentum space:

$$\begin{aligned} & i(2\pi)^4 \delta(p_A + p_B - p_{A'} - p_{B'}) A_R(s, t)^{\mu_A \mu_B \mu_{A'} \mu_{B'}} \\ &= \int \prod_i d^4 x_i e^{-ip_A \cdot x_A - ip_B \cdot x_B - ip_{A'} \cdot x_{A'} - ip_{B'} \cdot x_{B'}} \\ & \quad \times \langle J_R^{A\mu_A}(x_A) J_R^{B\mu_B}(x_B) J_R^{A'\mu_{A'}}(x_{A'}) J_R^{B'\mu_{B'}}(x_{B'}) \rangle. \end{aligned} \quad (2.39)$$

p_A and p_B denote the momenta of the incoming R -currents, $p_{A'}$ and $p_{B'}$ the momenta of the outgoing. A_R depends on the Mandelstam variables $s = (p_A + p_B)^2$ and $t = q^2 =$

$(p_A - p_{A'})^2 \simeq -\mathbf{q}^2 < 0$ and on the virtualities of the R -current momenta $Q_i^2 = -p_i^2 > 0$. We study the amplitude in the Regge limit defined as

$$s \gg |t|, Q_i^2. \quad (2.40)$$

In the Regge limit, the high energy behavior of the four point function (2.39) is expected to be fixed by the so-called spin argument. This argument states that the exchange of two particles of spin s in the t -channel leads to a high energy behavior of the amplitude $\sim s^{2s-1}$. Therefore, we anticipate that the R -current scattering amplitude is dominated by gluon exchange since gluons are the particles with highest spin in $\mathcal{N} = 4$ SYM. A necessary condition is the finiteness of the one-loop diagrams in $\mathcal{N} = 4$ SYM, the analogs of the QCD diagrams in Fig. 1.1. If this condition is fulfilled, three-loop diagrams give the leading contribution in the Regge limit. Since the factorization of the three-loop amplitude works the same as in QCD, see section 1.2.2, we only have to determine the influence of the scalar particles on the impact factors.

In our computations, we use a Sudakov decomposition of the momenta. We introduce two lightlike vectors p_1 and p_2 with $p_1^2 = p_2^2 = 0$ and $p_1 \cdot p_2 = s/2$. An arbitrary four vector can be decomposed in longitudinal and transverse parts as

$$k = \alpha p_1 + \beta p_2 + k_\perp \quad (2.41)$$

with $\alpha = 2p_2 \cdot k/s$, $\beta = 2p_1 \cdot k/s$, and $k_\perp^2 = -\mathbf{k}^2$. The bold vector denotes the transverse components of k . The Jacobian is

$$d^4k = s/2 d\alpha d\beta d^2\mathbf{k}. \quad (2.42)$$

Then the incoming current momenta can be written as

$$\begin{aligned} p_A &= p_1 - \frac{Q_A^2}{s} p_2 = p_1 + \gamma_A p_2, \\ p_B &= p_2 - \frac{Q_B^2}{s} p_1 = p_2 + \gamma_B p_1. \end{aligned} \quad (2.43)$$

Here we define

$$-\frac{Q_{A,B}^2}{s} =: \gamma_{A,B}. \quad (2.44)$$

The outgoing current momenta are

$$\begin{aligned} p_{A'} &= p_1 - \frac{Q_{A'}^2 + q_\perp^2}{s} p_2 - q_\perp, \\ p_{B'} &= p_2 - \frac{Q_{B'}^2 + q_\perp^2}{s} p_1 + q_\perp. \end{aligned} \quad (2.45)$$

The conditions $p_{A'}^2 = (p_A - q)^2$ and $p_{B'}^2 = (p_B + q)^2$ for the outgoing momenta fix the longitudinal components of the transferred momentum q ,

$$\alpha_q = -\frac{Q_{B'}^2 - Q_B^2 + q_\perp^2}{s} \quad \text{and} \quad \beta_q = \frac{Q_{A'}^2 - Q_A^2 + q_\perp^2}{s}. \quad (2.46)$$

For convenience we will contract the amplitude (2.39) with polarization vectors of the R -currents later. There are three polarization vectors $\epsilon^{L,\pm}(p)$, one with longitudinal polarization, denoted by L , and two with transverse polarization denoted by $h = \pm$. A second longitudinal polarization is absent if the simpler Ward identities (2.24) are fulfilled. The polarization vectors are orthonormal

$$\epsilon_\mu^{(i)}(p)\epsilon^{(j)\mu}(p)^* = \delta^{ij} \quad (2.47)$$

and satisfy the completeness relation

$$g^{\mu\nu} - \frac{p^\mu p^\nu}{p^2} = \sum_{i=L,\pm} \epsilon^{(i)\mu}(p)\epsilon^{(i)\nu}(p)^*. \quad (2.48)$$

We choose $\epsilon_\mu^L(p)$ in such a way that the three-dimensional part is proportional to \vec{p} . $\epsilon_\mu^{(\pm)}(p)$ is chosen to be transverse. The leading order terms in s for each component are

$$\begin{aligned} \epsilon^{(L)}(p) &= \frac{i}{Q} \left[\left(\alpha + \frac{2Q^2}{s(\alpha + \beta)^2} \beta \right) p_1 + \left(\beta + \frac{2Q^2}{s(\alpha + \beta)^2} \alpha \right) p_2 + \left(1 - \frac{2Q^2}{s(\alpha + \beta)^2} \right) p_\perp \right], \\ \epsilon^{(h)}(p) &= \epsilon_\perp^{(h)} + \frac{2\epsilon_\perp^{(h)} \cdot p}{s(\alpha - \beta)} \left(p_1 - p_2 + \frac{p_\perp}{\alpha - \beta} \right) \end{aligned} \quad (2.49)$$

with

$$\epsilon_\perp^{(\pm)} = \frac{1}{\sqrt{2}}(0, 1, \pm i, 0). \quad (2.50)$$

With Eqs. (2.43) and (2.45) the polarization vectors for $p = p_A, p_B, p_{A'}, p_{B'}$ have the following explicit form

$$\epsilon^{(L)}(p_A) = \frac{i}{Q_A} \left(p_1 + \frac{Q_A^2}{s} p_2 \right), \quad (2.51)$$

$$\epsilon^{(L)}(p_B) = \frac{i}{Q_B} \left(\frac{Q_B^2}{s} p_1 + p_2 \right), \quad (2.52)$$

$$\epsilon^{(L)}(p_{A'}) = \frac{i}{Q_{A'}} \left(p_1 + \frac{Q_{A'}^2 - q_\perp^2}{s} p_2 - q_\perp \right), \quad (2.53)$$

$$\epsilon^{(L)}(p_{B'}) = \frac{i}{Q_{B'}} \left(\frac{Q_{B'}^2 - q_\perp^2}{s} p_1 + p_2 + q_\perp \right), \quad (2.54)$$

$$\epsilon^{(h)}(p_{A,B}) = \epsilon_\perp^{(h)}, \quad (2.55)$$

$$\epsilon^{(h)}(p_{A',B'}) = \epsilon_\perp^{(h)} - \frac{2\epsilon_\perp^{(h)} \cdot q}{s} (p_1 - p_2 - q_\perp). \quad (2.56)$$

To simplify the expressions, we shift the polarization vectors by a four vector proportional to p . This shift is allowed if the Ward identities (2.24) are fulfilled. We arrive

at

$$\epsilon^{(L)}(p_{A,A'}) = \frac{2Q_{A,A'}}{s} p_2, \quad (2.57)$$

$$\epsilon^{(L)}(p_{B,B'}) = \frac{2Q_{B,B'}}{s} p_1, \quad (2.58)$$

$$\epsilon^{(h)}(p_{A,B}) = \epsilon_{\perp}^{(h)}, \quad (2.59)$$

$$\epsilon^{(h)}(p_{A'}) = \epsilon_{\perp}^{(h)} + \frac{2\epsilon_{\perp}^{(h)} \cdot q}{s} p_2, \quad (2.60)$$

$$\epsilon^{(h)}(p_{B'}) = \epsilon_{\perp}^{(h)} - \frac{2\epsilon_{\perp}^{(h)} \cdot q}{s} p_1. \quad (2.61)$$

2.4 One-Loop Diagrams

Now we start with the explicit computation of the correlation function of four R -currents defined in (2.39). Since we are in $\mathcal{N} = 4$ SYM, the required Feynman diagrams include in addition to fermions also scalars, and all particles are in the adjoint representation of the gauge group $SU(N_c)$. The lowest order diagrams, which are one-loop diagrams, are shown in Figs. 2.1 and 2.2.

We have fermionic boxes as in QCD and the new scalar boxes. The gray dots symbolize the attached R -currents, which are not shown. Additionally, we have scalar triangles and bubbles. The crosses denote counterterm vertices; the triangle and bubble diagrams are counterterm diagrams. In the next sections, we investigate the UV poles and the high energy behavior of the one-loop diagrams.

2.4.1 UV Poles

In this section, we show that the lowest order diagrams are UV finite. The one-loop fermionic diagrams, which are depicted in Fig. 2.1, are the same boxes as in QCD. Their IR region is regularized by giving the fermions a small mass m . Since we are only interested in the UV behavior, we are allowed to set the external momenta to zero, and the UV singularities can be computed easily. We use the Feynman rules given in section 2.2.2. In d dimensions, the amplitude of the first diagram $BF1$ is

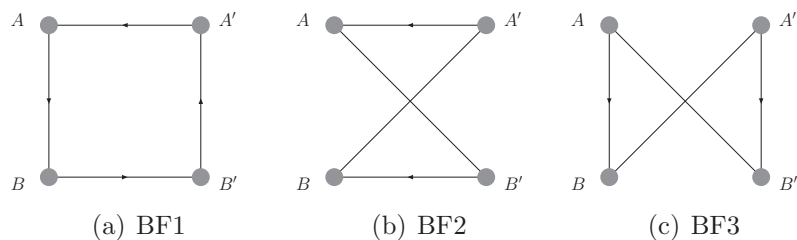


Figure 2.1: One-loop diagrams with fermions

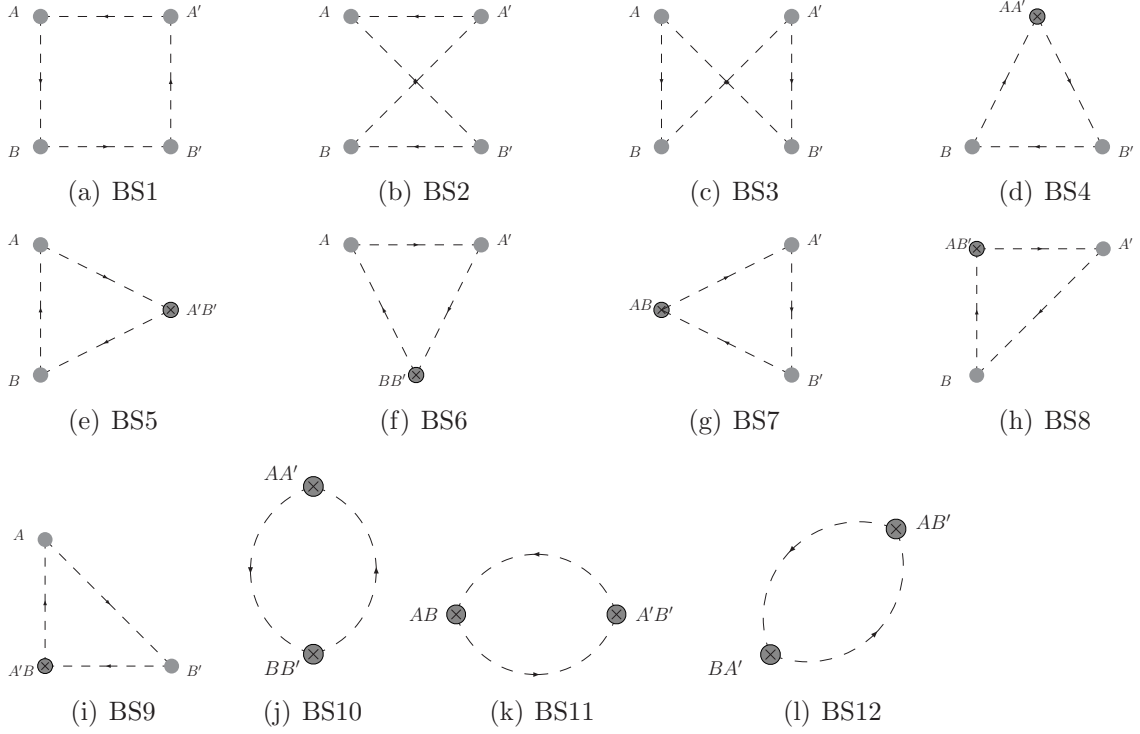


Figure 2.2: One-loop diagrams with scalars

given by

$$\begin{aligned}
 BF1^{\mu_A \mu_B \mu_{B'} \mu_{A'}} &= - \int \frac{d^d k}{(2\pi)^4} T_{M_2 M_1}^A T_{M_3 M_2}^B T_{M_4 M_3}^{B'} T_{M_1 M_4}^{A'} \\
 &\times \frac{\text{Tr}[i(k+m)_\mu \sigma^\mu \bar{\sigma}^{\mu_A} i(k+m)_\nu \sigma^\nu \bar{\sigma}^{\mu_B} i(k+m)_{\mu'} \sigma^{\mu'} \bar{\sigma}^{\mu_{B'}} i(k+m)_{\nu'} \sigma^{\nu'} \bar{\sigma}^{\mu_{A'}}]}{(k^2 - m^2)(k^2 - m^2)(k^2 - m^2)(k^2 - m^2)}. \quad (2.62)
 \end{aligned}$$

The UV divergent part of the amplitude $BF1$ in $d = 4 - 2\epsilon$ dimensions reads

$$\begin{aligned}
 BF1_{UV}^{\mu_A \mu_B \mu_{B'} \mu_{A'}} &= \frac{2 i \pi^{2-\epsilon} m^{-2\epsilon}}{3 (2\pi)^4} \Gamma(\epsilon) \text{Tr} \left(T^A T^{A'} T^{B'} T^B \right) \\
 &\times \left(g_{\mu_A \mu_{A'}} g_{\mu_B \mu_{B'}} + g_{\mu_A \mu_B} g_{\mu_{A'} \mu_{B'}} - 2 g_{\mu_A \mu_{B'}} g_{\mu_{A'} \mu_B} \right). \quad (2.63)
 \end{aligned}$$

The UV poles of the diagrams $BF2$ and $BF3$ can be obtained by permuting indices in Eq. (2.63). The sum of all three UV singularities does not vanish unless we restrict ourselves to the $U(1)$ subgroup of $SU(4)_R$. Then all traces over $SU(4)_R$ generators are the same, and the cancellation of the UV poles precisely works as in QCD.

There are 12 scalar diagrams, see Fig. 2.2. The amplitude of the first scalar boxdi-

agram $BS1$ is given by

$$BS1 = \int \frac{d^d k}{(2\pi)^4} T_{M_2 M_1}^A T_{M_3 M_2}^B T_{M_4 M_3}^{B'} T_{M_1 M_4}^{A'} \\ \times \frac{2ik^{\mu_A} 2ik^{\mu_B} 2ik^{\mu_{B'}} 2ik^{\mu_{A'}}}{(k^2 - m^2)(k^2 - m^2)(k^2 - m^2)(k^2 - m^2)}. \quad (2.64)$$

The UV divergent part in $d = 4 - 2\epsilon$ dimensions looks like

$$BS1_{UV}^{\mu_A \mu_B \mu_{B'} \mu_{A'}} = \frac{2i\pi^{2-\epsilon} m^{-2\epsilon}}{3(2\pi)^4} \Gamma(\epsilon) \text{Tr} \left(T^A T^{A'} T^{B'} T^B \right) \\ \times \left(g_{\mu_A \mu_{A'}} g_{\mu_B \mu_{B'}} + g_{\mu_A \mu_B} g_{\mu_{A'} \mu_{B'}} + g_{\mu_A \mu_{B'}} g_{\mu_{A'} \mu_B} \right). \quad (2.65)$$

The UV divergent parts of diagrams $BS2$ and $BS3$ are obtained by permutation of the indices in Eq. (2.65). The UV divergent contributions of the triangle diagram $BS4$ and of the bubble diagram $BS10$ in Fig. 2.2 read

$$BS4_{UV} = -2 \frac{i\pi^{2-\epsilon} m^{-2\epsilon}}{(2\pi)^4} \Gamma(\epsilon) \text{Tr} \left(\frac{T^A T^{A'} + T^{A'} T^A}{2} T^{B'} T^B \right) g_{\mu_A \mu_{A'}} g_{\mu_B \mu_{B'}} \quad (2.66)$$

and

$$BS10_{UV} = 2 \frac{i\pi^{2-\epsilon} m^{-2\epsilon}}{(2\pi)^4} \Gamma(\epsilon) \text{Tr} \left(\frac{T^A T^{A'} + T^{A'} T^A}{2} \frac{T^B T^{B'} + T^{B'} T^B}{2} \right) g_{\mu_A \mu_{A'}} g_{\mu_B \mu_{B'}}. \quad (2.67)$$

The UV poles of all other triangle and bubble diagrams are obtained by permuting the indices in Eqs. (2.66) and (2.67). If we restrict ourselves to the $U(1)$ subgroup, once again all traces are the same, and the sum of all scalar UV contributions vanishes.

In the case of the full $SU(4)_R$ group, the UV poles do not cancel separately in the fermionic and scalar sector. Nevertheless, a computation shows that the sum of the fermionic divergencies $BF1_{UV} - BF3_{UV}$ and the scalar divergencies $BS1_{UV} - BS12_{UV}$ is zero. We have kept in mind that the scalars are in the vector representation and the fermions are in the fundamental representation of the $SU(4)_R$ group. This fact leads to different results for the traces, see also Eqs. (2.86) and (2.87). The UV finiteness of the amplitude is due to the supersymmetry of the theory.

2.4.2 High Energy Behavior

Since the one-loop diagrams are UV finite, as shown in the last section, we are allowed to apply the spin argument to the scattering amplitude. Therefore, the R -current scattering amplitude is dominated by gluon exchange in the t -channel.

The leading terms of the one-loop diagrams in the Regge limit are doubly logarithmic terms of the form $\ln^2 s$ [49]. Resummation of the doubly logarithmic terms provides the correct asymptotic behavior of the amplitude. The one-loop diagrams

provide subleading corrections compared to the diagrams with t -channel gluon exchange. Also dressed one-loop diagrams, for example with gluon rungs, are included in this argument [46].

From now on, we restrict the R -currents to a $U(1)$ subgroup of the $SU(4)_R$ group, and we drop the trace over the $SU(4)_R$ generators. The computation of the high energy behavior of the fermion box is the same as in QCD. We briefly recall the computation [46, 49] and start with diagram $BF1$ in Fig. 2.1. In the high energy limit, the fermion numerator is proportional to $sk^2 + (k^2)^2$, and the leading term of the amplitude with Sudakov decomposition of the momenta (2.41) is

$$\begin{aligned}
BF1_L &= -\frac{s}{2} \frac{1}{(2\pi)^4} \int d\alpha \int d\beta \int d^2\mathbf{k} \\
&\quad \times \frac{sk^2}{(s\alpha\beta - \mathbf{k}^2 + i\varepsilon)(s(\alpha - \alpha_q)(\beta - \beta_q) - (\mathbf{k} - \mathbf{q})^2 + i\varepsilon)} \\
&\quad \times \frac{1}{(s(\alpha - 1)(\beta + x_A) - \mathbf{k}^2 + i\varepsilon)(s(\alpha - x_B)(\beta + 1) - \mathbf{k}^2 + i\varepsilon)}. \quad (2.68)
\end{aligned}$$

The subscript L means that we are keeping only the leading term in the energy. The region of integration, in which a double logarithm arises, is $Q_i^2, \mathbf{q}^2 \ll \mathbf{k}^2 \ll \alpha s, \beta s$ and $x_i \ll \alpha, \beta \ll 1$ with $x_i = Q_i^2/s$. We close the β -contour below, pick up the pole in the second propagator, and get

$$BF1_L = -\frac{1}{2} \frac{2\pi i}{(2\pi)^4} \int_x^1 \frac{d\alpha}{\alpha} \int_x^1 \frac{d\beta}{\beta} \int d^2\mathbf{k} \delta(s\alpha\beta - (\mathbf{k} - \mathbf{q})^2) \quad (2.69)$$

with $x = Q^2/s \sim x_i$. After a shift in the momentum, $\mathbf{k} \rightarrow \mathbf{k} + \mathbf{q}$, we perform the angular integration. Then the \mathbf{k}^2 integral is carried out via the delta function. We arrive at

$$BF1_L = \frac{1}{2} \frac{i}{2(2\pi)^2} \int_x^1 \frac{d\alpha}{\alpha} \int_{\frac{x}{\alpha}}^1 \frac{d\beta}{\beta} = -\frac{1}{8} \frac{i}{(2\pi)^2} \log^2 \frac{s}{Q^2}. \quad (2.70)$$

In the high energy limit, a double logarithm emerges for the fermion box.

Now, we consider the first scalar box $BS1$ in Fig. 2.2. The amplitude is

$$\begin{aligned}
BS1 &= \frac{s}{2} \frac{1}{(2\pi)^4} \int d\alpha \int d\beta \int d^2\mathbf{k} \\
&\quad \times \frac{(2k - p_A)^{\mu_A} (2k + p_B)^{\mu_B} (2k + p_B - q)^{\mu_{B'}} (2k - p_A - q)^{\mu_{A'}}}{(k - p_A)^2 k^2 (k + p_B)^2 (k - q)^2}. \quad (2.71)
\end{aligned}$$

First, we contract with longitudinal polarization vectors, (2.57) and (2.58), and keep only the leading terms in the numerator in region of integration $x_i \ll \alpha, \beta \ll 1$. We get

$$BS1_L^{LLLL} = Q_A Q_{A'} Q_B Q_{B'} \int \frac{d^4 k}{(2\pi)^4} \frac{1}{k^2 (k - q)^2 (k - p_A)^2 (k + p_B)^2}. \quad (2.72)$$

The superscript $LLLL$ denotes the longitudinal polarization of the R -currents. This integral corresponds to a standard integral in a massless ϕ^3 theory. Here, a double logarithm arises in the infrared region $\mathbf{k} \simeq 0$ due to the vanishing mass of the fields. Therefore, we consider the region of integration $\mathbf{k}^2 \ll Q_i^2, \mathbf{q}^2$, and (2.72) turns into

$$BS1_L^{LLLL} = \frac{sQ_A Q_{A'} Q_B Q_{B'}}{2(2\pi)^4} \int d\alpha \int d\beta \int d^2\mathbf{k} \frac{1}{(s\alpha\beta - \mathbf{k}^2 + i\epsilon)(-\mathbf{q}^2)(-s\beta + i\epsilon)(s\alpha)}. \quad (2.73)$$

We close the β -contour below and pick up the pole from the first propagator

$$BS1_L^{LLLL} = -\frac{iQ_A Q_{A'} Q_B Q_{B'}}{2(2\pi)^3 s \mathbf{q}^2} \int_x^1 \frac{d\alpha}{\alpha} \int_x^1 \frac{d\beta}{\beta} \int_{\mathbf{k}^2 \ll Q^2} d^2\mathbf{k} \delta(s\alpha\beta - \mathbf{k}^2). \quad (2.74)$$

Performing the integral over \mathbf{k} leads to

$$BS1^{LLLL} = -\frac{iQ_A Q_{A'} Q_B Q_{B'}}{4(2\pi)^2 s \mathbf{q}^2} \int_x^1 \frac{d\alpha}{\alpha} \int_x^{x/\alpha} \frac{d\beta}{\beta} \quad (2.75)$$

and over α and β to the expected double logarithm

$$BS1^{LLLL} \simeq \frac{i}{8(2\pi)^2} \frac{Q^2}{s} \log^2 \frac{s}{Q^2}. \quad (2.76)$$

Now, we contract the amplitude with transverse polarization vectors, (2.59)-(2.61), and only keep the leading terms in the energy. h and h' denote the possible transverse polarizations of the incoming and outgoing R -currents, respectively, and we arrive at

$$\begin{aligned} BS1_L^{hh'h'} &= \frac{16}{(2\pi)^4} \int d^4k \frac{k \cdot \epsilon^{h_A} k \cdot \epsilon^{h_{A'}} k \cdot \epsilon^{h_B} k \cdot \epsilon^{h_{B'}}}{k^2(k-q)^2(k-p_A)^2(k+p_B)^2} \\ &= (\delta^{h_A h_{A'}} \delta^{h_B h_{B'}} + \delta^{h_A h_B} \delta^{h_{A'} h_{B'}} + \delta^{h_A h_{B'}} \delta^{h_{A'} h_B}) \\ &\quad \times \frac{s}{3(2\pi)^4} \int d\alpha \int d\beta \int d^2\mathbf{k} \frac{s\alpha\beta - \mathbf{k}^2}{(s\alpha\beta - (\mathbf{k} - \mathbf{q})^2 + i\epsilon)(-s\beta + i\epsilon)(s\alpha)}. \end{aligned} \quad (2.77)$$

We close the contour below and pick up the pole from the first propagator. After a shift in \mathbf{k} we obtain

$$\begin{aligned} BS1_L^{hh'h'} &= (\delta^{h_A h_{A'}} \delta^{h_B h_{B'}} + \delta^{h_A h_B} \delta^{h_{A'} h_{B'}} + \delta^{h_A h_{B'}} \delta^{h_{A'} h_B}) \\ &\quad \times \frac{2\pi i}{3(2\pi)^4 s} \int_x^1 \frac{d\alpha}{\alpha} \int_x^1 \frac{d\beta}{\beta} \int d^2\mathbf{k} (s\alpha\beta - (\mathbf{k} - \mathbf{q})^2) \delta(s\alpha\beta - \mathbf{k}^2). \end{aligned} \quad (2.78)$$

The scalar product vanishes after angular integration, and $s\alpha\beta - \mathbf{k}^2$ is set to zero by the delta function. We get

$$\begin{aligned} BS1_L^{hh'h'} &= (\delta^{h_A h_{A'}} \delta^{h_B h_{B'}} + \delta^{h_A h_B} \delta^{h_{A'} h_{B'}} + \delta^{h_A h_{B'}} \delta^{h_{A'} h_B}) \\ &\quad \times \frac{i}{6(2\pi)^2 s} \int_x^1 \frac{d\alpha}{\alpha} \int_x^{x/\alpha} \frac{d\beta}{\beta} (-\mathbf{q}^2). \end{aligned} \quad (2.79)$$

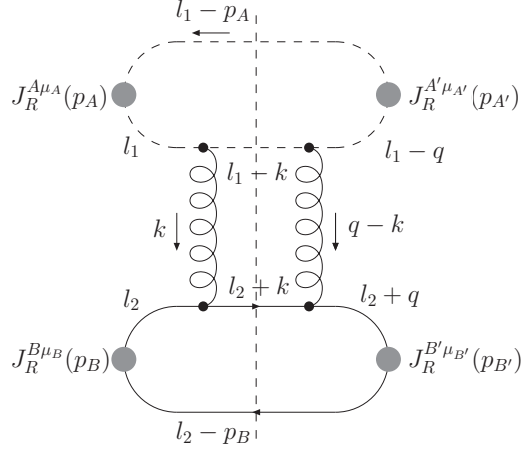


Figure 2.3: One of the lowest order diagrams contributing to the two gluon exchange in $\mathcal{N} = 4$ SYM

The only term left gives

$$\begin{aligned}
 BS1_L^{hh'h'} &\simeq -(\delta^{h_A h_{A'}} \delta^{h_B h_{B'}} + \delta^{h_A h_B} \delta^{h_{A'} h_{B'}} + \delta^{h_A h_{B'}} \delta^{h_{A'} h_B}) \\
 &\times \frac{i}{12(2\pi)^2} \frac{Q^2}{s} \log^2 \frac{s}{Q^2},
 \end{aligned} \tag{2.80}$$

which is once again a double logarithm. Similar computations can be performed for all other diagrams in Fig. 2.2 and give results analog to the ones just presented.

In the above computations, we have considered the region $Q_i^2, \mathbf{q}^2 \ll \mathbf{k}^2 \ll \alpha s, \beta s$ and $\mathbf{k}^2 \ll Q_i^2, \mathbf{q}^2$, respectively. For $\mathbf{k}^2 \sim s$ the numerators in (2.68) and (2.73) seem to lead to an even stronger behavior. But the limit of large \mathbf{k}^2 corresponds to the UV region, which we have computed in the previous section. These terms cancel when we sum over all diagrams.

In this section, we have computed the high energy behavior of fermionic and scalar one-loop diagrams in $\mathcal{N} = 4$ SYM in the Regge limit. All one-loop diagrams are proportional to a double logarithm.

2.5 Impact Factors

The following sections confirm that the high energy behavior of the four point function of R -currents is indeed dominated by two gluon exchange. Due to the spin argument, we expect a dominating gluon exchange amplitude with a high energy behavior $\sim s$. Gluon exchange in the t -channel starts at three-loop level. In Fig. 2.3, we show one possible lowest order diagram with our choice of momenta. In the other three-loop diagrams, which are not shown, the gluons couple to the upper and lower loop in all possible ways. The loops consist of a fermion or a scalar particle. The momenta are decomposed as in Eq. (2.41).

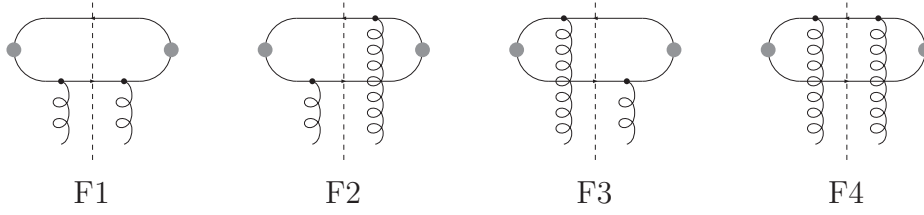


Figure 2.4: The fermion diagrams for the impact factor

In our computation, we consider the imaginary part of the amplitude that is the discontinuity in s symbolized by the dashed line in Fig. 2.3. Taking the discontinuity sets the four intermediate particles on-shell. Two of the resulting delta functions are used to fix the integrations over the longitudinal components, α and β , of loop momentum k . The other two fix one longitudinal integration of each loop momentum l_1 and l_2 , that is β_1 and α_2 . In the Regge limit, the leading logarithmic (LL) contribution arises when $\alpha \ll \alpha_1$ and $\beta \ll \beta_2$. In this regime, the upper loop is independent of α and the lower loop independent of β . The amplitude of the three-loop diagram, $A^{(0)}$, factorizes into two impact factors and two transverse gluon propagators

$$A^{(0)}(s, t) = is \int \frac{d^2\mathbf{k}}{(2\pi)^2 \mathbf{k}^2 (\mathbf{q} - \mathbf{k})^2} \mathbb{D}_A^{a_1 a_2}(\mathbf{k}, \mathbf{q} - \mathbf{k}) \mathbb{D}_B^{a_1 a_2}(\mathbf{k}, \mathbf{q} - \mathbf{k}). \quad (2.81)$$

$\mathbb{D}_{A,B}$ are the impact factors in $\mathcal{N} = 4$ SYM that represent the coupling of the R -currents to the two t -channel gluons. The definition of the impact factor \mathbb{D}_A is

$$\mathbb{D}_A^{\lambda_A \lambda_{A'} a a'}(\mathbf{k}, \mathbf{k}') = \frac{1}{s^2} \epsilon_{\mu_A}^{\lambda_A}(p_A)^* \epsilon_{\mu_{A'}}^{\lambda_{A'}}(p_{A'}) p_{2\rho} p_{2\rho'} \int \frac{ds_1}{2\pi} \text{Im} A^{\mu_A \mu_{A'} \rho \rho'}(s_1, t). \quad (2.82)$$

A similar definition is given for \mathbb{D}_B . The amplitude $A^{\mu_A \mu_{A'} \rho \rho'}(s_1, t)$ describes the scattering of an R -current with polarization λ_A and a gluon with momentum $-k$, Lorentz index ρ and color label a into an R -current with polarization $\lambda_{A'}$ and a gluon with momentum k , Lorentz index ρ' and color label a' . s_1 is the energy squared of the R -current-gluon system, $s_1 = (p_A - k)^2 \simeq -Q_A^2 - \mathbf{k}^2 - s\beta \approx -s\beta$. $\epsilon_{\mu_A}^{\lambda_A}(p_A)^*$ and $\epsilon_{\mu_{A'}}^{\lambda_{A'}}(p_{A'})$ are the polarization vectors of the incoming and outgoing R -currents defined in Eqs. (2.57)-(2.61).

Due to the factorization of the amplitude (2.81) the subdiagrams belonging to the upper impact factor are independent from the lower subdiagrams. Furthermore, fermion and scalar impact factors can be computed separately. The fermion diagrams are shown in Fig. 2.4 and the scalar diagrams in Fig. 2.5. Here, the gluons couple to the fermion and scalar loops in all possible ways. We introduce the convenient notation for the impact factors

$$\mathbb{D}^{\lambda \lambda' a a'} = N_c \alpha_s \delta^{a a'} \int_0^1 d\alpha_l \int \frac{d^2\mathbf{l}}{(2\pi)^2} \sum_i \phi_i^{\lambda \lambda'}(\alpha_l, \mathbf{l}, \mathbf{q}). \quad (2.83)$$

$\phi_i^{\lambda \lambda'}$ is the analytic expression of the i th diagram in Figs. 2.4 and 2.5. The sum runs over $i = F1, \dots, F4$ for fermions and over $i = S1, \dots, S9$ for scalars. α_l is

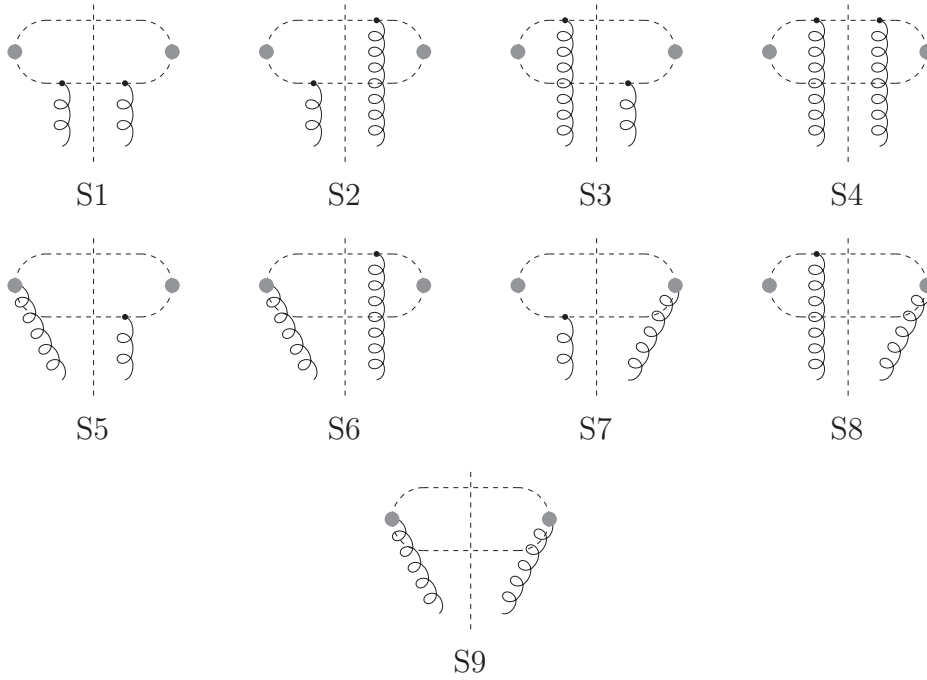


Figure 2.5: The scalar diagrams for the impact factor

the longitudinal component of the loop momentum. Scalars and fermions are in the adjoint representation of the gauge group and provide a factor

$$f^{ac_1c_2} f^{bc_2c_1} = -N_c \delta^{ab}. \quad (2.84)$$

An overall factor of $1/2$ arises from the cutting rule

$$2i\text{Im}(A) = \sum \mathcal{A}. \quad (2.85)$$

\mathcal{A} symbolizes the discontinuity of the amplitude. The computation of the fermion and scalar diagrams is alike, nevertheless there are some differences. The trace over two generators of the $SU(4)_R$ group is for fermions, which are in the fundamental representation,

$$\text{Tr}_4(T^A T^A) = \frac{1}{2}, \quad (2.86)$$

and for scalars in the vector representation

$$\text{Tr}_4(T^A T^A) = 1. \quad (2.87)$$

Furthermore, there is a symmetry factor of $1/2$ for scalar diagrams since the particles crossing the cut are identical. An important difference appears concerning the t -channel gluon propagator. Written in Sudakov decomposition, it is

$$g_{\mu\nu} = \frac{2}{s}(p_{2\mu}p_{1\nu} + p_{1\mu}p_{2\nu}) + g_{\perp\mu\nu}. \quad (2.88)$$

In the fermionic case as well as for the scalar diagrams S1-S4, it is the first term of the gluon propagator, $p_{2\mu}p_{1\nu}$, which contributes to the leading power in s in the Regge limit. But the situation is different for diagrams S6-S9. For example, in diagram S5 the gluon polarization tensor is contracted with the polarization vector of the incoming current, which is proportional to p_2^μ . But the contraction $p_2^\mu g_{\perp\mu\nu}$ does not give a leading contribution and $p_2^2 = 0$. Thus, only the second part of the propagator $p_{1\mu}p_{2\nu}$ contributes. This contraction provides one power of s less than the leading terms of diagrams S1-S4. A similar argument applies for the contraction of the polarization vector proportional to p_1^ν with the lower loop. The argument also holds for diagrams S6-S8. For diagram S9 the suppression is even stronger because the effect takes place at both vertices. Altogether, in the Regge limit, the leading behavior of the scalar impact factors is only given by diagrams S1-S4, which look the same as the fermionic ones.

2.5.1 Explicit Computation of the Impact Factors

Now we give a sample computation of a leading three-loop diagram with a scalar loop above and a fermion loop below as depicted in Fig. 2.3. Considering a scalar and a fermion loop in one diagram allows us to show results for both impact factors in one computation. Since the amplitude factorizes, the two parts of the diagram do not influence one another. The amplitude is given by

$$\begin{aligned}
A^{(0)\mu_A\mu_{A'}\mu_B\mu_{B'}} &= - \int \frac{d^4 l_1}{(2\pi)^4} \int \frac{d^4 l_2}{(2\pi)^4} \int \frac{d^4 k}{(2\pi)^4} g^4 (-2\pi i)^4 \\
&\times f_{a_1 b_1 b_2} f_{a_2 b_2 b_1} (T^A)_{M_1 M_2} (T^{A'})_{M_2 M_1} f_{a_1 c_1 c_2} f_{a_2 c_2 c_1} (T^B)_J^I (T^{B'})_I^J \\
&\times \frac{(2l_1 - p_A)^{\mu_A} (2l_1 - k)^{\mu_1} (2l_1 - k - q)^{\mu_2} (2l_1 - p_A - q)^{\mu_{A'}}}{l_1^2 (l_1 - q)^2} \\
&\times \frac{\text{Tr}[\bar{\sigma}^{\mu_B} i l_{2\mu} \sigma^\mu \bar{\sigma}^{\nu_1} (l_2 + k)_\sigma \sigma^\sigma \bar{\sigma}^{\nu_2} (-i) (l_2 + q)_\rho \sigma^\rho \bar{\sigma}^{\mu_{B'}} (l_2 - p_B)_\nu \sigma^\nu]}{l_2^2 (l_2 + q)^2} \\
&\times \frac{g_{\mu_1 \nu_1}}{k^2} \frac{g_{\mu_2 \nu_2}}{(k - q)^2} \delta((l_1 - p_A)^2) \delta((l_1 - k)^2) \delta((l_2 + k)^2) \delta((l_2 - p_B)^2).
\end{aligned} \tag{2.89}$$

We use a Sudakov decomposition (2.41) for the momenta and the relation $\text{Tr}[\bar{\sigma}^{\mu_1} \sigma^{\mu_2} \dots \sigma^{\mu_{2n}}] = \text{Tr}[P_R \gamma^{\mu_1} \gamma^{\mu_2} \dots \gamma^{\mu_{2n}}]$ with $P_R = \frac{1+\gamma_5}{2}$. We get

$$\begin{aligned}
A^{(0)\mu_A\mu_{A'}\mu_B\mu_{B'}} &= -g^4 \left(\frac{s}{2}\right)^3 \frac{1}{(2\pi)^8} \int d\alpha \int d\beta \int d\alpha_1 \int d\beta_1 \int d\alpha_2 \int d\beta_2 \\
&\times \int d^2 \mathbf{k} \int d^2 \mathbf{1}_1 \int d^2 \mathbf{1}_2 \\
&\times f_{a_1 b_1 b_2} f_{a_2 b_2 b_1} f_{a_1 c_1 c_2} f_{a_2 c_2 c_1} \text{Tr}(T^A T^{A'}) \text{Tr}(T^B T^{B'}) \frac{g_{\mu_1 \nu_1}}{k^2} \frac{g_{\mu_2 \nu_2}}{(k - q)^2}
\end{aligned}$$

$$\begin{aligned}
& \times \frac{(2l_1 - p_A)^{\mu_A} (2l_1 - k)^{\mu_1} (2l_1 - k - q)^{\mu_2} (2l_1 - p_A - q)^{\mu_{A'}}}{(s\alpha_1\beta_1 - \mathbf{l}_1^2)(s(\alpha_1 - \alpha_q)(\beta_1 - \beta_q) - (\mathbf{l}_1 - \mathbf{q})^2)} \\
& \times \frac{\text{Tr}[P_R \gamma^{\mu_B} \not{l}_2 \gamma^{\nu_1} (\not{l}_2 + \not{k}) \gamma^{\mu_2} (\not{l}_2 + \not{q}) \gamma^{\mu'_B} (\not{l}_2 - \not{p}_B)]}{(s\alpha_2\beta_2 - \mathbf{l}_2^2)(s(\alpha_2 + \alpha)(\beta_2 + \beta) - (\mathbf{l}_2 + \mathbf{q})^2)} \\
& \times \delta(s(\alpha_1 - 1)(\beta_1 - \gamma_A) - \mathbf{l}_1^2) \delta(s(\alpha_1 - \alpha)(\beta_1 - \beta) - (\mathbf{l}_1 - \mathbf{k})^2) \\
& \times \delta(s(\alpha_2 + \alpha)(\beta_2 + \beta) - (\mathbf{l}_2 + \mathbf{k})^2) \delta(s(\alpha_2 - \gamma_B)(\beta_2 - 1) - \mathbf{l}_2^2).
\end{aligned} \tag{2.90}$$

In the Regge limit, we have $k^2 \approx \mathbf{k}^2$ and $(k - q)^2 \approx (\mathbf{k} - \mathbf{q})^2$. We perform four integrations with the help of the delta functions. The integrations over α and β fix the longitudinal components of k , the integrations over β_1 and α_2 fix one longitudinal component of each loop momentum l_1 and l_2 . From the first delta function we get

$$\beta_1 = \gamma_A - \frac{\mathbf{l}_1^2}{s(1 - \alpha_1)} \approx \mathcal{O}\left(\frac{1}{s}\right), \tag{2.91}$$

from the second

$$\beta \approx -\frac{(\mathbf{l}_1 - \mathbf{k})^2}{s\alpha_1} + \beta_1 \approx \mathcal{O}\left(\frac{1}{s}\right), \tag{2.92}$$

from the third

$$\alpha \approx -\alpha_2 + \frac{(\mathbf{l}_2 + \mathbf{k})^2}{s\beta_2} \approx \mathcal{O}\left(\frac{1}{s}\right), \tag{2.93}$$

and from the last

$$\alpha_2 = \gamma_B - \frac{\mathbf{l}_2^2}{s(1 - \beta_2)} \approx \mathcal{O}\left(\frac{1}{s}\right). \tag{2.94}$$

Inserting the results into the amplitude gives

$$\begin{aligned}
A^{(0)\mu_A \mu_{A'} \mu_B \mu_{B'}} &= -g^4 \left(\frac{s}{2}\right)^3 \frac{1}{(2\pi)^8} \int d\alpha_1 \int d\beta_2 \int d^2\mathbf{k} \int d^2\mathbf{l}_1 \int d^2\mathbf{l}_2 \\
& \times N_c^2 \delta^{a_1 a_2} \delta^{a_1 a_2} \text{Tr}(T^A T^{A'}) \text{Tr}(T^B T^{B'}) \frac{g_{\mu_1 \nu_1}}{\mathbf{k}^2} \frac{g_{\mu_2 \nu_2}}{(\mathbf{k} - \mathbf{q})^2} \\
& \times \frac{1}{s|1 - \alpha_1|} \frac{1}{s|\alpha_1 - \alpha|} \frac{1}{s|\beta_2 + \beta|} \frac{1}{s|1 - \beta_2|} (1 - \alpha_1)^2 (1 - \beta_2)^2 \\
& \times \frac{(2l_1 - p_A)^{\mu_A} (2l_1 - k)^{\mu_1} (2l_1 - k - q)^{\mu_2} (2l_1 - p_A - q)^{\mu_{A'}}}{((1 - \alpha_1)s\alpha_1\gamma_A - \mathbf{l}_1^2)((1 - \alpha_1)s\alpha_1\gamma_A - \alpha_1\mathbf{l}_1^2 - s\alpha_1\beta_q(1 - \alpha_1) - (1 - \alpha_1)(\mathbf{l}_1 - \mathbf{q})^2)} \\
& \times \frac{\text{Tr}[P_R \gamma^{\mu_B} \not{l}_2 \gamma^{\nu_1} (\not{l}_2 + \not{k}) \gamma^{\nu_2} (\not{l}_2 + \not{q}) \gamma^{\mu'_B} (\not{l}_2 - \not{p}_B)]}{((1 - \beta_2)s\beta_2\gamma_B - \mathbf{l}_2^2)((1 - \beta_2)s\beta_2\gamma_B - \beta_2\mathbf{l}_2^2 + s\beta_2\alpha_q(1 - \beta_2) - (1 - \beta_2)(\mathbf{l}_2 + \mathbf{q})^2)}.
\end{aligned} \tag{2.95}$$

Next, we contract the gluon propagators $g_{\mu_1 \nu_1}$ and $g_{\mu_2 \nu_2}$ with the upper and lower loop using the expression in Eq. (2.88). We keep only the leading terms in s , which

are proportional to α_1 . Additionally, we use $\alpha \ll \alpha_1$ and $\beta \ll \beta_1$ in the Regge limit,

$$\begin{aligned}
A^{(0)\mu_A\mu_{A'}\mu_B\mu_{B'}} &= -g^4 \left(\frac{s}{2}\right)^3 \frac{1}{(2\pi)^8} \int d\alpha_1 \int d\beta_2 \int d^2\mathbf{k} \int d^2\mathbf{l}_1 \int d^2\mathbf{l}_2 \\
&\times N_c^2 \delta^{a_1 a_2} \delta^{a_1 a_2} \text{Tr}(T^A T^{A'}) \text{Tr}(T^B T^{B'}) \frac{1}{\mathbf{k}^2} \frac{1}{(\mathbf{k} - \mathbf{q})^2} \\
&\times (2\alpha_1)^2 \frac{1}{s^4} \frac{1 - \alpha_1}{\alpha_1} \frac{1 - \beta_2}{\beta_2} \\
&\times \frac{(2l_1 - p_A)^{\mu_A} (2l_1 - p_A - q)^{\mu_{A'}}}{((1 - \alpha_1)s\alpha_1\gamma_A - \mathbf{l}_1^2)((1 - \alpha_1)s\alpha_1\gamma_A - \alpha_1\mathbf{l}_1^2 - s\alpha_1\beta_q(1 - \alpha_1) - (1 - \alpha_1)(\mathbf{l}_1 - \mathbf{q})^2)} \\
&\times \frac{\text{Tr}[P_R \gamma^{\mu_B} \not{l}_2 \not{p}_1 (\not{l}_2 + \not{k}) \not{p}_1 (\not{l}_2 + \not{q}) \gamma^{\mu_{B'}} (\not{l}_2 - \not{p}_B)]}{((1 - \beta_2)s\beta_2\gamma_B - \mathbf{l}_2^2)((1 - \beta_2)s\beta_2\gamma_B - \beta_2\mathbf{l}_2^2 + s\beta_2\alpha_q(1 - \beta_2) - (1 - \beta_2)(\mathbf{l}_2 + \mathbf{q})^2)}. \tag{2.96}
\end{aligned}$$

In the last step, we contract the amplitude with the polarization vectors introduced in Eqs. (2.57)-(2.61). First, we choose longitudinal polarization vectors, (2.57) and (2.58), for all R -currents. We will make use of transverse polarization vectors later. The contraction gives

$$\begin{aligned}
A^{(0)} &= - \left(\frac{2}{s}\right)^4 Q_A Q_{A'} Q_B Q_{B'} g^4 \left(\frac{s}{2}\right)^3 \frac{1}{(2\pi)^8} \int d\alpha_1 \int d\beta_2 \int d^2\mathbf{k} \int d^2\mathbf{l}_1 \int d^2\mathbf{l}_2 \\
&\times N_c^2 \delta^{a_1 a_2} \delta^{a_1 a_2} \text{Tr}(T^A T^{A'}) \text{Tr}(T^B T^{B'}) \frac{1}{\mathbf{k}^2} \frac{1}{(\mathbf{k} - \mathbf{q})^2} \\
&\times (2\alpha_1)^2 \frac{1}{s^4} \frac{1 - \alpha_1}{\alpha_1} \frac{1 - \beta_2}{\beta_2} \\
&\times \frac{(2\alpha_1 - 1)^{\frac{s}{2}} (2\alpha_1 - 1)^{\frac{s}{2}}}{((1 - \alpha_1)s\alpha_1\gamma_A - \mathbf{l}_1^2)((1 - \alpha_1)s\alpha_1\gamma_A - \alpha_1\mathbf{l}_1^2 - s\alpha_1\beta_q(1 - \alpha_1) - (1 - \alpha_1)(\mathbf{l}_1 - \mathbf{q})^2)} \\
&\times \frac{\text{Tr}[P_R \not{p}_1 \not{l}_2 \not{p}_1 (\not{l}_2 + \not{k}) \not{p}_1 (\not{l}_2 + \not{q}) \not{p}_1 (\not{l}_2 - \not{p}_B)]}{((1 - \beta_2)s\beta_2\gamma_B - \mathbf{l}_2^2)((1 - \beta_2)s\beta_2\gamma_B - \beta_2\mathbf{l}_2^2 + s\beta_2\alpha_q(1 - \beta_2) - (1 - \beta_2)(\mathbf{l}_2 + \mathbf{q})^2)}. \tag{2.97}
\end{aligned}$$

The result of the trace is $s^4 \beta_2^3 (\beta_2 - 1)$, and it follows

$$\begin{aligned}
A^{(0)} &= -2s Q_A Q_{A'} Q_B Q_{B'} g^4 \frac{1}{(2\pi)^8} \int d\alpha_1 \int \beta_2 \int d^2\mathbf{k} \int d^2\mathbf{l}_1 \int d^2\mathbf{l}_2 \\
&\times N_c^2 \delta^{a_1 a_2} \delta^{a_1 a_2} \text{Tr}(T^A T^{A'}) \text{Tr}(T^B T^{B'}) \frac{1}{\mathbf{k}^2} \frac{1}{(\mathbf{k} - \mathbf{q})^2} \\
&\times \frac{(2\alpha_1)^2 (1 - \alpha_1)(1 - \beta_2)}{\alpha_1 \beta_2} \\
&\times \frac{(2\alpha_1 - 1)^{\frac{1}{2}} (2\alpha_1 - 1)^{\frac{1}{2}}}{((1 - \alpha_1)s\alpha_1\gamma_A - \mathbf{l}_1^2)((1 - \alpha_1)s\alpha_1\gamma_A - \alpha_1\mathbf{l}_1^2 - s\alpha_1\beta_q(1 - \alpha_1) - (1 - \alpha_1)(\mathbf{l}_1 - \mathbf{q})^2)} \\
&\times \frac{\beta_2^3 (\beta_2 - 1)}{((1 - \beta_2)s\beta_2\gamma_B - \mathbf{l}_2^2)((1 - \beta_2)s\beta_2\gamma_B - \beta_2\mathbf{l}_2^2 + s\beta_2\alpha_q(1 - \beta_2) - (1 - \beta_2)(\mathbf{l}_2 + \mathbf{q})^2)}. \tag{2.98}
\end{aligned}$$

With the relations $s\gamma_{A,B} = -Q_{A,B}^2$ and $s\gamma_{A',B'} = -Q_{A',B'}^2$, see Eq. (2.44), as well as with $\alpha_q = \frac{\mathbf{q}^2}{s} - \frac{Q_{B'}^2 - Q_B^2}{s}$ and $\beta_q = -\frac{\mathbf{q}^2}{s} + \frac{Q_{A'}^2 - Q_A^2}{s}$, see Eq. (2.46), we get

$$\begin{aligned}
A^{(0)} &= 8 s Q_A Q_{A'} Q_B Q_{B'} g^4 N_c^2 \delta^{a_1 a_2} \delta^{a_1 a_2} \text{Tr}(T^A T^{A'}) \text{Tr}(T^B T^{B'}) \\
&\times \frac{1}{(2\pi)^8} \int d\alpha_1 \int d\beta_2 \int d^2 \mathbf{k} \int d^2 \mathbf{l}_1 \int d^2 \mathbf{l}_2 \alpha_1 \beta_2^2 (\alpha_1 - 1/2)^2 (1 - \beta_2)^2 (1 - \alpha_1) \\
&\times \frac{1}{\mathbf{k}^2} \frac{1}{(\mathbf{k} - \mathbf{q})^2} \\
&\times \frac{1}{(\mathbf{l}_1^2 + \alpha_1(1 - \alpha_1)Q_A^2)((\mathbf{l}_1 - (1 - \alpha_1)\mathbf{q})^2 + \alpha_1(1 - \alpha_1)Q_{A'}^2)} \\
&\times \frac{1}{(\mathbf{l}_2^2 + \beta_2(1 - \beta_2)Q_B^2)((\mathbf{l}_2 + (1 - \beta_2)\mathbf{q})^2 + \beta_2(1 - \beta_2)Q_{B'}^2)}. \tag{2.99}
\end{aligned}$$

The traces over the $SU(4)_R$ generators is given in Eqs. (2.86) and (2.87). We use $\alpha_s = \frac{g^2}{4\pi}$ and introduce the scalar symmetry factor 1/2:

$$\begin{aligned}
A^{(0)} &= 8 s \alpha_s^2 Q_A Q_{A'} Q_B Q_{B'} N_c^2 \delta^{a_1 a_2} \delta^{a_1 a_2} \\
&\times \int d\alpha_1 \int d\beta_2 \int \frac{d^2 \mathbf{k}}{(2\pi)^2} \int \frac{d^2 \mathbf{l}_1}{(2\pi)^2} \int \frac{d^2 \mathbf{l}_2}{(2\pi)^2} \alpha_1 \beta_2^2 (\alpha_1 - 1/2)^2 (1 - \beta_2)^2 (1 - \alpha_1) \\
&\times \frac{1}{\mathbf{k}^2} \frac{1}{(\mathbf{k} - \mathbf{q})^2} \\
&\times \frac{1}{(\mathbf{l}_1^2 + \alpha_1(1 - \alpha_1)Q_A^2)((\mathbf{l}_1 - (1 - \alpha_1)\mathbf{q})^2 + \alpha_1(1 - \alpha_1)Q_{A'}^2)} \\
&\times \frac{1}{(\mathbf{l}_2^2 + \beta_2(1 - \beta_2)Q_B^2)((\mathbf{l}_2 + (1 - \beta_2)\mathbf{q})^2 + \beta_2(1 - \beta_2)Q_{B'}^2)}. \tag{2.100}
\end{aligned}$$

Eq. (2.100) is the result for the whole amplitude $A^{(0)}$. The impact factors can be read off easily with the help of Eq. (2.81). The scalar impact factor \mathbb{D}_{S1}^{LL} for diagram S1 is

$$\begin{aligned}
\mathbb{D}_{S1}^{LL} &= 2 Q_A Q_{A'} \alpha_s N_c \delta^{a_1 a_2} \int_0^1 d\alpha_1 \int \frac{d^2 \mathbf{l}_1}{(2\pi)^2} \alpha_1 (\alpha_1 - 1/2)^2 (1 - \alpha_1) \\
&\times \frac{1}{(\mathbf{l}_1^2 + \alpha_1(1 - \alpha_1)Q_A^2)((\mathbf{l}_1 - (1 - \alpha_1)\mathbf{q})^2 + \alpha_1(1 - \alpha_1)Q_{A'}^2)}, \tag{2.101}
\end{aligned}$$

the fermion impact factor \mathbb{D}_{F1}^{LL} for diagram F1 is

$$\begin{aligned}
\mathbb{D}_{F1}^{LL} &= 2 Q_B Q_{B'} \alpha_s N_c \delta^{a_1 a_2} \int_0^1 d\beta_2 \int \frac{d^2 \mathbf{l}_2}{(2\pi)^2} \beta_2^2 (1 - \beta_2)^2 \\
&\times \frac{1}{(\mathbf{l}_2^2 + \beta_2(1 - \beta_2)Q_B^2)((\mathbf{l}_2 + (1 - \beta_2)\mathbf{q})^2 + \beta_2(1 - \beta_2)Q_{B'}^2)}. \tag{2.102}
\end{aligned}$$

We have considered a scalar impact factor in the upper part of the diagram in Fig. 2.3 and a fermion impact factor in the lower part. To get an impact factor, which can be

inserted in the upper part of the diagram, from the one computed in the lower part of the diagram, we perform the following substitutions in (2.102),

$$\begin{aligned} \mathbf{l}_2 &\rightarrow \mathbf{l}_1, & \mathbf{k} &\rightarrow -\mathbf{k}, & \mathbf{q} &\rightarrow -\mathbf{q}, \\ \beta_2 &\rightarrow \alpha_1, & Q_{B,B'} &\rightarrow Q_{A,A'} \end{aligned} \quad (2.103)$$

and vice versa. The upper impact factor for F1 is

$$\begin{aligned} \mathbb{D}_{F1}^{LL} &= 2Q_A Q_{A'} \alpha_s N_c \delta^{a_1 a_2} \int_0^1 d\alpha_1 \int \frac{d^2 \mathbf{l}_1}{(2\pi)^2} \alpha_1^2 (1 - \alpha_1)^2 \\ &\times \frac{1}{(\mathbf{l}_1^2 + \alpha_1(1 - \alpha_1)Q_A^2)((\mathbf{l}_1 - (1 - \alpha_1)\mathbf{q})^2 + \alpha_1(1 - \alpha_1)Q_{A'}^2)}. \end{aligned} \quad (2.104)$$

From now on, we only examine impact factors from an upper loop. For convenience we change the notation to

$$\mathbf{l}_1 = \mathbf{l} \quad \text{and} \quad \alpha_1 = \alpha. \quad (2.105)$$

The impact factors for diagrams S2-S4 and F2-F4 in Figs. 2.5 and 2.4 are computed in a similar way as S1 and F1. The coupling of the gluons to the loop is the only difference. The loop momenta are changed, but the computation itself stays the same. We give the results for the impact factors here. We define

$$\begin{aligned} \mathbf{N}_1 &= \mathbf{l}, & \mathbf{N}_2 &= \mathbf{l} - \mathbf{k}, \\ \mathbf{N}'_1 &= \mathbf{l} - (1 - \alpha)\mathbf{q}, & \mathbf{N}'_2 &= \mathbf{l} - \mathbf{k} + \alpha\mathbf{q}, \\ D_1 &= \mathbf{N}_1^2 + \alpha(1 - \alpha)Q_A^2, & D_2 &= \mathbf{N}_2^2 + \alpha(1 - \alpha)Q_A^2, \\ D'_1 &= \mathbf{N}'_1{}^2 + \alpha(1 - \alpha)Q_{A'}^2, & D'_2 &= \mathbf{N}'_2{}^2 + \alpha(1 - \alpha)Q_{A'}^2. \end{aligned} \quad (2.106)$$

With these definitions the fermion and scalar impact factors $\phi_i^{\lambda\lambda'}$ in Eq. (2.83), shown in Fig. 2.4 and Fig. 2.5 respectively, are

$$\begin{aligned} \phi_{F1}^{LL} &= 2Q_A Q_{A'} \frac{\alpha^2(1 - \alpha)^2}{D_1 D'_1}, & \phi_{S1}^{LL} &= 2Q_A Q_{A'} \frac{\alpha(1 - \alpha)(1/2 - \alpha)^2}{D_1 D'_1}, \\ \phi_{F2}^{LL} &= -2Q_A Q_{A'} \frac{\alpha^2(1 - \alpha)^2}{D_1 D'_2}, & \phi_{S2}^{LL} &= -2Q_A Q_{A'} \frac{\alpha(1 - \alpha)(1/2 - \alpha)^2}{D_1 D'_2}, \\ \phi_{F3}^{LL} &= -2Q_A Q_{A'} \frac{\alpha^2(1 - \alpha)^2}{D_2 D'_1}, & \phi_{S3}^{LL} &= -2Q_A Q_{A'} \frac{\alpha(1 - \alpha)(1/2 - \alpha)^2}{D_2 D'_1}, \\ \phi_{F4}^{LL} &= 2Q_A Q_{A'} \frac{\alpha^2(1 - \alpha)^2}{D_2 D'_2}, & \phi_{S4}^{LL} &= 2Q_A Q_{A'} \frac{\alpha(1 - \alpha)(1/2 - \alpha)^2}{D_2 D'_2}. \end{aligned} \quad (2.107) \quad (2.108)$$

Eqs. (2.107) and (2.108) represent the impact factors with longitudinal polarization vectors of the R -currents. Now, we use transverse polarization vectors (2.59)-(2.61) for the incoming and outgoing R -currents. The resulting impact factors are

$$\begin{aligned}
\phi_{F1}^{hh'} &= \frac{1}{2D_1 D_1'} \left[(1 - hi\alpha) \boldsymbol{\epsilon}^{(h)} \cdot \boldsymbol{\epsilon}^{(h')*} \mathbf{N}_1 \cdot \mathbf{N}_1' \right. \\
&\quad + \left(-4\alpha(1 - \alpha) + i(h - h')(1 - \alpha) \right) \boldsymbol{\epsilon}^{(h)} \cdot \mathbf{N}_1 \mathbf{N}_1' \cdot \boldsymbol{\epsilon}^{(h')*} \\
&\quad \left. - (1 - hi\alpha) \left(\boldsymbol{\epsilon}^{(h)} \cdot \mathbf{l} (1 - \alpha) \mathbf{q} \cdot \boldsymbol{\epsilon}^{(h')*} - \boldsymbol{\epsilon}^{(h)} \cdot (1 - \alpha) \mathbf{q} \mathbf{l} \cdot \boldsymbol{\epsilon}^{(h')*} \right) \right], \\
\phi_{F2}^{hh'} &= -\frac{1}{2D_1 D_2'} \left[\boldsymbol{\epsilon}^{(h)} \cdot \boldsymbol{\epsilon}^{(h')*} \mathbf{N}_1 \cdot \mathbf{N}_2' \right. \\
&\quad + \left(-4\alpha(1 - \alpha) + i(h - h')(1 - 2\alpha) \right) \boldsymbol{\epsilon}^{(h)} \cdot \mathbf{N}_1 \mathbf{N}_2' \cdot \boldsymbol{\epsilon}^{(h')*} \\
&\quad \left. - \boldsymbol{\epsilon}^{(h)} \cdot \mathbf{l} (\mathbf{k} - \alpha \mathbf{q}) \cdot \boldsymbol{\epsilon}^{(h')*} + \boldsymbol{\epsilon}^{(h)} \cdot (\mathbf{k} - \alpha \mathbf{q}) \mathbf{l} \cdot \boldsymbol{\epsilon}^{(h')*} \right], \\
\phi_{F3}^{hh'} &= -\frac{1}{2D_2 D_1'} \left[\boldsymbol{\epsilon}^{(h)} \cdot \boldsymbol{\epsilon}^{(h')*} \mathbf{N}_2 \cdot \mathbf{N}_1' \right. \\
&\quad + \left(-4\alpha(1 - \alpha) + i(h - h')(1 - 2\alpha) \right) \boldsymbol{\epsilon}^{(h)} \cdot \mathbf{N}_2 \mathbf{N}_1' \cdot \boldsymbol{\epsilon}^{(h')*} \\
&\quad \left. + \boldsymbol{\epsilon}^{(h)} \cdot (\mathbf{l} - \mathbf{k}) (\mathbf{k} - (1 - \alpha) \mathbf{q}) \cdot \boldsymbol{\epsilon}^{(h')*} - \boldsymbol{\epsilon}^{(h)} \cdot (\mathbf{k} - (1 - \alpha) \mathbf{q}) (\mathbf{l} - \mathbf{k}) \cdot \boldsymbol{\epsilon}^{(h')*} \right], \\
\phi_{F4}^{hh'} &= \frac{1}{2D_2 D_2'} \left[(1 + hi(1 - \alpha)) \boldsymbol{\epsilon}^{(h)} \cdot \boldsymbol{\epsilon}^{(h')*} \mathbf{N}_2 \cdot \mathbf{N}_2' \right. \\
&\quad + \left(-4\alpha(1 - \alpha) - i(h - h')\alpha \right) \boldsymbol{\epsilon}^{(h)} \cdot \mathbf{N}_2 \mathbf{N}_2' \cdot \boldsymbol{\epsilon}^{(h')*} \\
&\quad \left. + (1 + hi(1 - \alpha)) \left(\boldsymbol{\epsilon}^{(h)} \cdot (\mathbf{l} - \mathbf{k}) \alpha \mathbf{q} \cdot \boldsymbol{\epsilon}^{(h')*} - \boldsymbol{\epsilon}^{(h)} \cdot \alpha \mathbf{q} (\mathbf{l} - \mathbf{k}) \cdot \boldsymbol{\epsilon}^{(h')*} \right) \right], \tag{2.109}
\end{aligned}$$

$$\begin{aligned}
\phi_{S1}^{hh'} &= 2 \frac{\alpha(1 - \alpha)}{D_1 D_1'} \boldsymbol{\epsilon}^{(h)} \cdot \mathbf{N}_1 \mathbf{N}_1' \cdot \boldsymbol{\epsilon}^{(h')*}, \\
\phi_{S2}^{hh'} &= -2 \frac{\alpha(1 - \alpha)}{D_1 D_2'} \boldsymbol{\epsilon}^{(h)} \cdot \mathbf{N}_1 \mathbf{N}_2' \cdot \boldsymbol{\epsilon}^{(h')*}, \\
\phi_{S3}^{hh'} &= -2 \frac{\alpha(1 - \alpha)}{D_2 D_1'} \boldsymbol{\epsilon}^{(h)} \cdot \mathbf{N}_2 \mathbf{N}_1' \cdot \boldsymbol{\epsilon}^{(h')*}, \\
\phi_{S4}^{hh'} &= 2 \frac{\alpha(1 - \alpha)}{D_2 D_2'} \boldsymbol{\epsilon}^{(h)} \cdot \mathbf{N}_2 \mathbf{N}_2' \cdot \boldsymbol{\epsilon}^{(h')*}. \tag{2.110}
\end{aligned}$$

A closer look at the impact factors $\phi_F^{hh'}$ identifies some cancellations. The last two terms of each $\phi_F^{hh'}$ cancel each other due to the angular integration in the transverse momentum \mathbf{l} , see Eq. (2.83). If we combine the two denominators, introducing a Feynman parameter and perform a shift in the \mathbf{l} integration in the integrand of (2.83), the shift cancels in the numerator and the remaining terms in the numerator depend upon the angle only through the $\cos \theta$ in the scalar product of the polarization vectors. Therefore, the result of the θ integration vanishes.

The terms proportional to h and h' also cancel because $N_2 \rightarrow -N_1$ and $N'_2 \rightarrow -N'_1$ after a change of variables, $\mathbf{l} \rightarrow -\mathbf{l} + \mathbf{k}$ and $\alpha \rightarrow 1 - \alpha$. The cancellation takes place between $\phi_{F1}^{hh'}$ and $\phi_{F4}^{hh'}$ as well as between $\phi_{F2}^{hh'}$ and $\phi_{F3}^{hh'}$.

After considering purely transverse or longitudinal polarization for all R -currents, we now choose different polarizations for incoming and outgoing R -currents. The impact factors ϕ^{Lh} for incoming longitudinally and outgoing transversely polarized R -currents are

$$\begin{aligned}
\phi_{F1}^{Lh} &= Q_A \frac{\alpha(1-\alpha)(1-2\alpha-hi)}{D_1 D'_1} \mathbf{N}'_1 \cdot \boldsymbol{\epsilon}^{(h)*}, \\
\phi_{F2}^{Lh} &= -Q_A \frac{\alpha(1-\alpha)(1-2\alpha-hi)}{D_1 D'_2} \mathbf{N}'_2 \cdot \boldsymbol{\epsilon}^{(h)*}, \\
\phi_{F3}^{Lh} &= -Q_A \frac{\alpha(1-\alpha)(1-2\alpha-hi)}{D_2 D'_1} \mathbf{N}'_1 \cdot \boldsymbol{\epsilon}^{(h)*}, \\
\phi_{F4}^{Lh} &= Q_A \frac{\alpha(1-\alpha)(1-2\alpha-hi)}{D_2 D'_2} \mathbf{N}'_2 \cdot \boldsymbol{\epsilon}^{(h)*}, \tag{2.111}
\end{aligned}$$

$$\begin{aligned}
\phi_{S1}^{Lh} &= -Q_A \frac{\alpha(1-\alpha)(1-2\alpha)}{D_1 D'_1} \mathbf{N}'_1 \cdot \boldsymbol{\epsilon}^{(h)*}, \\
\phi_{S2}^{Lh} &= Q_A \frac{\alpha(1-\alpha)(1-2\alpha)}{D_1 D'_2} \mathbf{N}'_2 \cdot \boldsymbol{\epsilon}^{(h)*}, \\
\phi_{S3}^{Lh} &= Q_A \frac{\alpha(1-\alpha)(1-2\alpha)}{D_2 D'_1} \mathbf{N}'_1 \cdot \boldsymbol{\epsilon}^{(h)*}, \\
\phi_{S4}^{Lh} &= -Q_A \frac{\alpha(1-\alpha)(1-2\alpha)}{D_2 D'_2} \mathbf{N}'_2 \cdot \boldsymbol{\epsilon}^{(h)*}. \tag{2.112}
\end{aligned}$$

For transverse-longitudinal polarization we get

$$\begin{aligned}
\phi_{F1}^{hL} &= Q_{A'} \frac{\alpha(1-\alpha)(1-2\alpha-hi)}{D_1 D'_1} \boldsymbol{\epsilon}^{(h)} \cdot \mathbf{N}_1, \\
\phi_{F2}^{hL} &= -Q_{A'} \frac{\alpha(1-\alpha)(1-2\alpha-hi)}{D_1 D'_2} \boldsymbol{\epsilon}^{(h)} \cdot \mathbf{N}_1, \\
\phi_{F3}^{hL} &= -Q_{A'} \frac{\alpha(1-\alpha)(1-2\alpha-hi)}{D_2 D'_1} \boldsymbol{\epsilon}^{(h)} \cdot \mathbf{N}_2, \\
\phi_{F4}^{hL} &= Q_{A'} \frac{\alpha(1-\alpha)(1-2\alpha-hi)}{D_2 D'_2} \boldsymbol{\epsilon}^{(h)} \cdot \mathbf{N}_2, \tag{2.113}
\end{aligned}$$

$$\begin{aligned}
\phi_{S1}^{hL} &= -Q_{A'} \frac{\alpha(1-\alpha)(1-2\alpha)}{D_1 D'_1} \boldsymbol{\epsilon}^{(h)} \cdot \mathbf{N}_1, \\
\phi_{S2}^{hL} &= Q_{A'} \frac{\alpha(1-\alpha)(1-2\alpha)}{D_1 D'_2} \boldsymbol{\epsilon}^{(h)} \cdot \mathbf{N}_1,
\end{aligned}$$

$$\begin{aligned}
\phi_{S3}^{hL} &= Q_{A'} \frac{\alpha(1-\alpha)(1-2\alpha)}{D_2 D_1'} \boldsymbol{\epsilon}^{(h)} \cdot \mathbf{N}_2, \\
\phi_{S4}^{hL} &= -Q_{A'} \frac{\alpha(1-\alpha)(1-2\alpha)}{D_2 D_2'} \boldsymbol{\epsilon}^{(h)} \cdot \mathbf{N}_2.
\end{aligned} \tag{2.114}$$

The terms proportional to the helicity h again cancel between ϕ_{F1} and ϕ_{F4} as well as between ϕ_{F2} and ϕ_{F3} after a change of variables, $\mathbf{l} \rightarrow -\mathbf{l} + \mathbf{k}$ and $\alpha \rightarrow 1 - \alpha$.

2.5.2 Full Impact Factors

Summarizing the results we have the full impact factors $\mathbb{D}^{\lambda\lambda'aa'}$ given by the sum of all scalar and all fermion impact factors. The final result for longitudinal-longitudinal polarization is

$$\mathbb{D}^{LLaa'} = \delta^{aa'} \frac{N_c \alpha_s}{2} Q_A Q_{A'} \int_0^1 d\alpha \int \frac{d^2\mathbf{l}}{(2\pi)^2} \alpha(1-\alpha) \left(\frac{1}{D_1} - \frac{1}{D_2} \right) \left(\frac{1}{D_1'} - \frac{1}{D_2'} \right). \tag{2.115}$$

A simplification occurs in the sum of fermion and scalar impact factors with transverse-transverse helicity. The terms from the scalar sector cancel exactly with the pieces from the fermion sector, which have remained after the simplification described after Eq. (2.110). Finally, only one term proportional to $\boldsymbol{\epsilon}^{(h)} \cdot \boldsymbol{\epsilon}^{(h')*} = \delta^{hh'}$ is left for each diagram, and the result is

$$\mathbb{D}^{hh'aa'} = \delta^{aa'} \delta^{hh'} \frac{N_c \alpha_s}{2} Q_A Q_{A'} \int_0^1 d\alpha \int \frac{d^2\mathbf{l}}{(2\pi)^2} \left(\frac{N_1}{D_1} - \frac{N_2}{D_2} \right) \left(\frac{N_1'}{D_1'} - \frac{N_2'}{D_2'} \right). \tag{2.116}$$

In the case of different polarizations for incoming and outgoing R -currents, the fermionic pieces, that have remained after simplification, cancel completely with the corresponding scalar impact factors,

$$\mathbb{D}^{Lh'aa'} = 0. \tag{2.117}$$

These results highlight a striking difference compared with the QCD results [47]. In QCD, helicity conservation only holds in the forward case, $t = 0$. In $\mathcal{N} = 4$ SYM, all off-diagonal terms in the polarization indices vanish for arbitrary $t = -\mathbf{q}^2$ due to the cancellation between the scalar and the fermionic part. Helicity conservation is a consequence of the supersymmetry of the theory.

3 The Six Point Function in $\mathcal{N} = 4$ SYM

In the last chapter, we have computed the four point function of R -currents in $\mathcal{N} = 4$ SYM in the Regge limit. The next step is to investigate the elastic scattering of more than two R -currents. Higher order correlation functions provide first unitarity corrections to the BFKL Pomeron. Unitarity corrections are believed to restore unitarity, which is violated at high energies by the BFKL Pomeron, see section 1.2.1. Accordingly, we analyze the six point function of R -currents in this chapter.

As we have seen, the four point function of R -currents in $\mathcal{N} = 4$ SYM in the Regge limit is dominated by the BFKL Pomeron. The supersymmetry only affects the impact factors in the amplitude, the reggeization of the amplitude stays the same. In a six point correlation function, the effect of the supersymmetry is expected to be more distinct since the structure of the diagrams is more complex, for example the BKP equations and the triple Pomeron vertex are included.

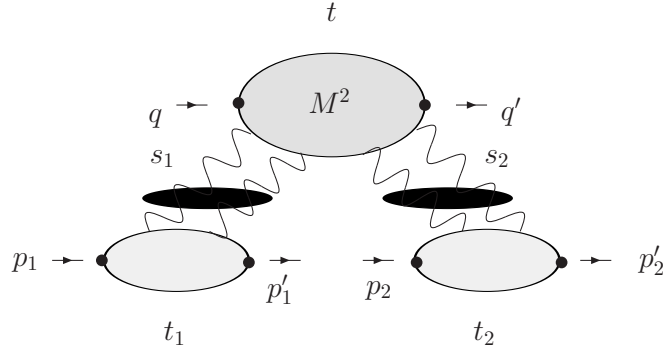
In the following, we study the six point function of R -currents in $\mathcal{N} = 4$ SYM in the triple Regge limit in the LLA. First, we [42] perform the computations for arbitrary N_c . In the last part of this chapter, we take the large N_c -limit of the six point function, see our publication in Ref. [43]. In the large N_c -limit, the strong coupling regime of $\mathcal{N} = 4$ SYM is related to the weakly coupled type IIB string theory via the AdS/CFT-correspondence. We will make use of this fact in the following chapters.

3.1 Setup of the Computation

In analogy to the four point function in Eq. (2.39) we define the six point amplitude of R -currents in $\mathcal{N} = 4$ SYM in momentum space as

$$\begin{aligned}
 & i(2\pi)^4 \delta(p_A + p_B + p_C - p_{A'} - p_{B'} - p_{C'}) A_R(s, t, \dots)^{\mu_A \mu_B \mu_C \mu_{A'} \mu_{B'} \mu_{C'}} \\
 = & \int \prod_i d^4 x_i e^{-ip_A \cdot x_A - ip_B \cdot x_B - ip_C \cdot x_C - ip_{A'} \cdot x_{A'} - ip_{B'} \cdot x_{B'} - ip_{C'} \cdot x_{C'}} \\
 & \times \langle J_R^{A\mu_A}(x_A) J_R^{B\mu_B}(x_B) J_R^{C\mu_C}(x_C) J_R^{A'\mu_{A'}}(x_{A'}) J_R^{B'\mu_{B'}}(x_{B'}) J_R^{C'\mu_{C'}}(x_{C'}) \rangle. \quad (3.1)
 \end{aligned}$$

The correlator is the analog of a six point function of virtual photons in QCD, see section 1.2.1. We are interested in the high energy limit of the six point amplitude (3.1). Its kinematics are shown in Fig. 3.1. The amplitude depends on three energy variables, $s_1 = (q + p_1)^2$, $s_2 = (q' + p_2')^2$, and $M^2 = (q + p_1 - p_1')^2$ and on the momentum

Figure 3.1: Kinematics of a six point amplitude of R -currents

transfer variables $t = (q - q')$, $t_1 = (p_1 - p'_1)^2$, and $t_2 = (p_2 - p'_2)^2$. Hence, the triple Regge limit is given by

$$s_1, s_2 \gg M^2 \gg t, t_1, t_2. \quad (3.2)$$

The total energy of the scattering process is $S = (q + p_1 + p_2)^2$.

We again use a Sudakov decomposition of the momenta and choose the lightlike reference vectors q' and p . Internal momenta are then written as

$$k = \alpha q' + \beta p + k_\perp \quad \text{with} \quad k_\perp^2 = -\mathbf{k}^2, \quad (3.3)$$

and it is

$$\begin{aligned} s &= 2p \cdot q, \quad S = 4p \cdot q = 2s, \\ q &= q' - xp \quad \text{with} \quad x = 2p \cdot q / Q^2, \quad \text{and} \quad M^2 = x_P s \quad \text{with} \quad x_P \ll 1. \end{aligned} \quad (3.4)$$

Furthermore, we choose two incoming momenta two be equal,

$$p_1 = p_2 = p. \quad (3.5)$$

In deep inelastic scattering on two weakly bound nucleons in QCD, the momenta belong to the two incoming nucleons. The outgoing momenta are

$$p'_1 = p(1 - x_P) + p_{1\perp} \quad \text{and} \quad p'_2 = p(1 + x_P) + p_{2\perp}, \quad (3.6)$$

that is the outgoing R -currents are allowed to have small losses of longitudinal and transverse momenta. In the triple Regge limit, Eq. (3.2), a multi-particle amplitude has an analytic expression [50],

$$\begin{aligned} T_{3 \rightarrow 3}(s_1, s_2, M^2; t_1, t_2, t) &= \frac{s_1 s_2}{M^2} \int \frac{d\omega_1 d\omega_2 d\omega}{(2\pi i)^3} s_1^{\omega_1} s_2^{\omega_2} (M^2)^{\omega - \omega_1 \omega_2} \xi(\omega_1) \xi(\omega_2) \\ &\times \xi(\omega, \omega_1, \omega_2) \cdot F(\omega, \omega_1, \omega_2; t, t_1, t_2) + \dots \end{aligned} \quad (3.7)$$

The partial wave $F(\omega, \omega_1, \omega_2; t, t_1, t_2)$ is related via a triple Mellin transform to the amplitude $T_{3 \rightarrow 3}$. The variables ω , ω_1 , and ω_2 are connected to the angular momenta

j , j_1 and j_2 by $\omega = j - 1$, $\omega_1 = j_1 - 1$, and $\omega_2 = j_2 - 1$. The dots represent three further terms that appear in the triple Regge limit. Since they do not contribute to the M^2 -discontinuity, we are interested in in the following computations, we do not show them here. The signature factors are given by

$$\xi(\omega) = -\pi \frac{e^{-i\pi\omega} - 1}{\sin(\pi\omega)} \quad \text{and} \quad \xi(\omega, \omega_1, \omega_2) = -\pi \frac{e^{-i\pi(\omega - \omega_1 - \omega_2)} - 1}{\sin(\pi(\omega - \omega_1 - \omega_2))}. \quad (3.8)$$

To compute the amplitude $T_{3 \rightarrow 3}$ in the high energy limit, we take the triple energy discontinuity in s_1 , s_2 , and M^2 . That is the reason why we are only interested in terms with a M^2 -discontinuity in the analytic expression (3.7). The triple energy discontinuity reads

$$\begin{aligned} & \text{disc}_{s_1} \text{disc}_{s_2} \text{disc}_{M^2} T_{3 \rightarrow 3} \\ &= \pi^3 \frac{s_1 s_2}{M^2} \int \frac{d\omega_1 d\omega_2 d\omega}{(2\pi i)^3} s_1^{\omega_1} s_2^{\omega_2} (M^2)^{\omega - \omega_1 - \omega_2} \cdot F(\omega, \omega_1, \omega_2; t_1, t_2, t). \end{aligned} \quad (3.9)$$

In Fig. 3.2, two examples of a six point function are shown. The dashed lines illustrate the discontinuities in s_1 , M^2 , and s^2 . These diagrams represent the LLA for the six point amplitude in the triple Regge limit. That means, for each gluon we have a large logarithm of an energy variable.

The general structure of the six point amplitude diagrams is the following: There are three different t -channel states: t , t_1 , and t_2 , each with its own angular momentum j , j_1 , and j_2 . In order to have, in the LLA, color singlet t -channel states, which couple to one R -current at the top and to two R -currents at the bottom of the diagram, the diagrams must contain four t -channel gluons at the lower end and two, three, or four t -channel gluons at the upper end. Wavy t -channel lines in the diagrams symbolize reggeized gluons. Interactions between different t -channel gluons are described by kernels. The impact factors describe the coupling of the t -channel gluons to the incoming and outgoing R -currents. An important part of each diagram is the lowest interaction between the gluons, the so called branching vertex, below which the upper t -channel breaks up into the channels t_1 and t_2 . Above the branching vertex the gluons evolve according to the BKP equation, below the branching vertex the gluons interact only pairwise according to the BFKL equation and form two disconnected BFKL Pomerons.

3.2 Impact Factors

The impact factors consist, as in the case of a four point function in $\mathcal{N} = 4$ SYM, of fermions and scalars in the adjoint representation of the gauge group, and the complete impact factors are given by the sum over all possible ways in which the gluons can couple to the fermions and scalars. We present results for fermion and scalar impact factors with three and four gluons. These impact factors and the two gluon impact factors, which have already been given in section 2.5.2, appear in the

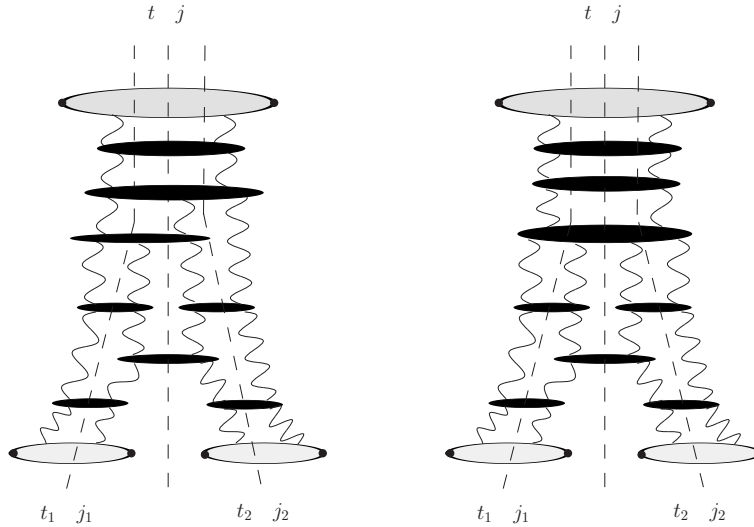


Figure 3.2: Some contributions to the triple energy discontinuity of the six point function of R -currents in the LLA

six point function diagrams. The impact factors with Weyl fermions for $\mathcal{N} = 4$ SYM can be related to the impact factors in QCD with Dirac fermions. The scalar impact factors have no counterpart in QCD and are completely new results [42].

3.2.1 Fermion Impact Factors

In this section, we explain the relation between fermion impact factors in $\mathcal{N} = 4$ SYM and QCD. We start with the simplest example: the two gluon impact factors. In $\mathcal{N} = 4$ SYM, the Weyl fermions are in the adjoint representation of the gauge group. Instead of N_c fundamental fermions in QCD we now have $N_c^2 - 1$ adjoint fermions, that is the color trace $\text{Tr}(t^a t^b) = \delta^{ab}/2$ is replaced by $\text{Tr}(T^a T^b) = N_c \delta^{ab}$ with $(T^a)_{bc} = -if_{abc}$, see section 2.2.1. Moreover, we identify the left- and righthanded parts of a massless Dirac fermion with a Weyl fermion in the standard way. Thus, the impact factor with a massless Dirac fermion is twice the impact factor with a Weyl fermion. Next, we consider the $U(1)$ charges e_F of the global $SU(4)_R$ symmetry, which are the analogs of the electric charges e_q . We get a factor, see also Eq. (2.86),

$$R_F = \frac{\sum e_F^2}{\sum e_q^2} = \frac{\text{Tr}(T^A T^A)}{\sum e_q^2} = \frac{1}{2 \sum e_q^2}. \quad (3.10)$$

For scalars the factor R_S resulting from the trace over $SU(4)_R$ generators is, Eq. (2.87),

$$R_S = \text{Tr}(T^A T^A) = 1. \quad (3.11)$$

We need this relation in the next section. Altogether, we have a relative factor F between two gluon impact factors with Weyl and Dirac fermions, which is

$$F = 2N_c R \quad \text{with} \quad R = \frac{1}{2} R_F. \quad (3.12)$$

Next we consider three gluon impact factors. In QCD, it is known, that the three gluon impact factors can be decomposed in terms of the two gluon impact factor [16, 17]:

$$D_{F,(3;0)}^{a_1 a_2 a_3}(\mathbf{k}_1, \mathbf{k}_2, \mathbf{k}_3) = \frac{1}{2} g f_{a_1 a_2 a_3} [D_{F,(2;0)}(12, 3) - D_{F,(2;0)}(13, 2) + D_{F,(2;0)}(1, 23)]. \quad (3.13)$$

We have introduced the notation $D_{F,(3;0)}^{a_1 a_2 a_3}(\mathbf{k}_1, \mathbf{k}_2, \mathbf{k}_3)$ for a three gluon impact factor in QCD. The arguments k_i are the momenta of the gluons and a_i their color labels. Furthermore, we have used the following shorthand notation for the two gluon impact factor,

$$D_{(2;0)}(12, 3) = D_{(2;0)}(\mathbf{k}_1 + \mathbf{k}_2, \mathbf{k}_3), \quad (3.14)$$

and similar expressions for the other two gluon impact factors in Eq. (3.13). With Eq. (3.13) and the factor F in Eq. (3.12), the relation of a fermion impact factor with three gluons in $\mathcal{N} = 4$ SYM to a three gluon impact factor in QCD is given by

$$\begin{aligned} \mathbb{D}_{F,(3;0)}^{a_1 a_2 a_3}(\mathbf{k}_1, \mathbf{k}_2, \mathbf{k}_3) &= 2N_c R D_{F,(3;0)}^{a_1 a_2 a_3}(\mathbf{k}_1, \mathbf{k}_2, \mathbf{k}_3) \\ &= \frac{1}{2} g f_{a_1 a_2 a_3} [\mathbb{D}_{F,(2;0)}(12, 3) - \mathbb{D}_{F,(2;0)}(13, 2) + \mathbb{D}_{F,(2;0)}(1, 23)]. \end{aligned} \quad (3.15)$$

The symbol $\mathbb{D}_{(i;0)}$ denotes impact factors in $\mathcal{N} = 4$ SYM as before in section 2.5. We have introduced the index $(i; 0)$ to distinguish the impact factors from the gluon amplitudes \mathbb{D}_i in section 3.3 later. We observe the reggeization of the gluons in the impact factor: In any two gluon impact factor in Eq. (3.15), two gluons combine and act as a single gluon. This is the same reggeization as known from QCD [17, 18].

For impact factors with four gluons the situation is more complicated because the color structure of the diagrams is different. We have for a pair of diagrams [42]

$$\text{Tr}(T^a T^b T^c T^d) + \text{Tr}(T^d T^c T^b T^a) = 2N_c d^{abcd} + \delta_{ab} \delta_{cd} + \delta_{ac} \delta_{bd} + \delta_{ad} \delta_{bc} \quad (3.16)$$

with

$$d^{abcd} = \text{Tr}(T^a T^b T^c T^d) + \text{Tr}(T^d T^c T^b T^a). \quad (3.17)$$

The relation of the impact factor $\mathbb{D}_{F,(4;0)}^{a_1 a_2 a_3 a_4}(\mathbf{k}_1, \mathbf{k}_2, \mathbf{k}_3, \mathbf{k}_4)$ to the QCD one is

$$\begin{aligned} \mathbb{D}_{F,(4;0)}^{a_1 a_2 a_3 a_4}(\mathbf{k}_1, \mathbf{k}_2, \mathbf{k}_3, \mathbf{k}_4) \\ = 2N_c R D_{(4;0)}^{a_1 a_2 a_3 a_4}(\mathbf{k}_1, \mathbf{k}_2, \mathbf{k}_3, \mathbf{k}_4) + \mathbb{D}_{F,(4;0)\text{Dir}}^{a_1 a_2 a_3 a_4}(\mathbf{k}_1, \mathbf{k}_2, \mathbf{k}_3, \mathbf{k}_4). \end{aligned} \quad (3.18)$$

The additional piece $\mathbb{D}_{F,(4;0)\text{Dir}}^{a_1 a_2 a_3 a_4}$ is a consequence of the delta tensors in Eq. (3.16) and cannot be related to QCD impact factors. The meaning of the subscript Dir will become clear in the next sections. The impact factor $\mathbb{D}_{F,(4;0)}^{a_1 a_2 a_3 a_4}$ expressed in terms of the two gluon impact factors in $\mathcal{N} = \text{SYM}$ is

$$\begin{aligned} \mathbb{D}_{F,(4;0)}^{a_1 a_2 a_3 a_4}(\mathbf{k}_1, \mathbf{k}_2, \mathbf{k}_3, \mathbf{k}_4) \\ = -g^2 d^{a_1 a_2 a_3 a_4} [\mathbb{D}_{F,(2;0)}(123, 4) + \mathbb{D}_{F,(2;0)}(1, 234) - \mathbb{D}_{F,(2;0)}(14, 23)] \\ - g^2 d^{a_1 a_2 a_3 a_4} [\mathbb{D}_{F,(2;0)}(134, 2) + \mathbb{D}_{F,(2;0)}(124, 3) - \mathbb{D}_{F,(2;0)}(12, 34) - \mathbb{D}_{F,(2;0)}(13, 24)] \\ + \mathbb{D}_{F,(4;0)\text{Dir}}^{a_1 a_2 a_3 a_4}(\mathbf{k}_1, \mathbf{k}_2, \mathbf{k}_3, \mathbf{k}_4). \end{aligned} \quad (3.19)$$

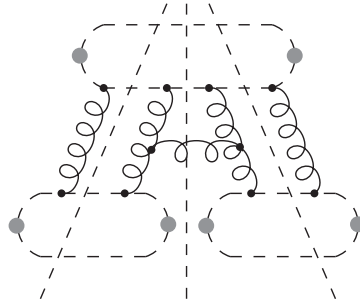
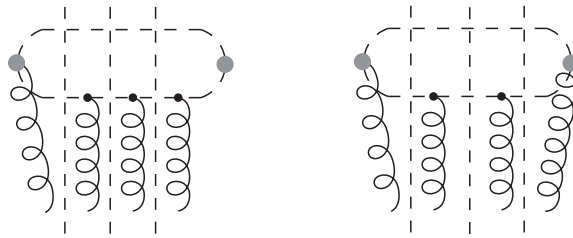


Figure 3.3: A scalar six point function

Figure 3.4: Two of the additional scalar diagrams in which gluons couple directly to an R -current

Furthermore, the additional part expressed in terms of the two gluon impact factor reads

$$\begin{aligned}
& \mathbb{D}_{F,(4;0)\text{Dir}}^{a_1 a_2 a_3 a_4}(\mathbf{k}_1, \mathbf{k}_2, \mathbf{k}_3, \mathbf{k}_4) \\
&= -g^2 \frac{1}{2N_c} (\delta_{a_1 a_2} \delta_{a_3 a_4} + \delta_{a_1 a_3} \delta_{a_2 a_4} + \delta_{a_1 a_4} \delta_{a_2 a_3}) \\
&\quad \times [\mathbb{D}_{F,(2;0)}(123, 4) + \mathbb{D}_{F,(2;0)}(124, 3) + \mathbb{D}_{F,(2;0)}(134, 2) + \mathbb{D}_{F,(2;0)}(1, 234) \\
&\quad - \mathbb{D}_{F,(2;0)}(12, 34) - \mathbb{D}_{F,(2;0)}(13, 24) - \mathbb{D}_{F,(2;0)}(14, 23)]. \tag{3.20}
\end{aligned}$$

Due to the symmetry of $\mathbb{D}_{F,(2;0)}$, the additional term is completely symmetric in its color and momentum arguments.

3.2.2 Scalar Impact Factors

We now come to the scalar impact factors. One scalar six point function is pictured in Fig. 3.3. We show that it is possible to relate the three and four gluon scalar impact factors $\mathbb{D}_{S,(3;0)}$ and $\mathbb{D}_{S,(4;0)}$ to the two gluon scalar impact factor $\mathbb{D}_{S,(2;0)}$ in the same way as for fermions.

We first consider the so-called additional diagrams, see Fig. 3.4. They are analogs of the diagrams S5-S9 in Fig. 2.5 for the two gluon impact factor. Fortunately, the additional diagrams are suppressed due to the same reason as in the case of two t -channel gluons. Every contraction of the gluon polarization tensor, Eq. (2.88), with the polarization vector of the R -current provides one power of s less than the leading

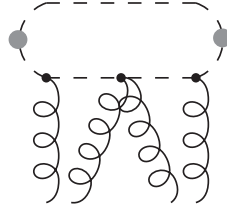


Figure 3.5: A scalar diagram, which does not contribute to the discontinuity

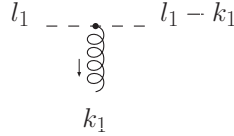


Figure 3.6: A scalar-gluon vertex

diagrams. Therefore, only diagrams with gluons coupled directly to the scalar lines contribute at high energies to the scalar impact factor.

Furthermore, diagrams as in Fig. 3.5 do not contribute to the discontinuity, which we are considering.

Because of the suppression of the additional diagrams, the scalar impact factors with more than two gluons can be expressed in terms of the two gluon impact factor $\mathbb{D}_{S,(2;0)}$. The reduction mechanism is similar to the one with fermion loops. We explain the mechanism in the following.

A scalar-gluon vertex, Fig. 3.6, contracted with the leading longitudinal part $(2p_\mu q'_\nu)/s$ of the gluon propagator, Eq.(2.88), is proportional to $s\alpha$. α is the Sudakov component of the scalar loop momentum l_1 . Let us now consider two adjacent gluons, which couple to the scalar loop. Each scalar-gluon vertex is contracted with the longitudinal momentum p from the polarization tensor of the t -channel gluons. Furthermore, the scalar propagator between the two vertices is on-shell because we are taking the discontinuity, resulting in a delta function. We obtain

$$\begin{array}{c}
 l_1 \text{ --- } \times \text{ --- } l_1 - k_1 - k_2 \\
 \begin{array}{c} \circ \\ \circ \\ \circ \end{array} \quad \begin{array}{c} \circ \\ \circ \\ \circ \end{array} \\
 \downarrow \quad \downarrow \\
 k_1 \quad k_2
 \end{array}
 \sim 2\pi i \delta((l - k_1)^2) (2l_1 - k_1) \cdot p (l - k_1 + l - k_1 - k_2) \cdot p. \quad (3.21)$$

Making use of the Sudakov decomposition, we find

$$\begin{aligned}
 & \delta((l - k_1)^2) (2l_1 - k_1) \cdot p (l - k_1 + l - k_1 - k_2) \cdot p \\
 & \sim s\alpha \delta((\beta - \beta_{k_1}) - (\mathbf{1} - \mathbf{k}_1)^2 / (s\alpha)) \sim
 \end{aligned}
 \begin{array}{c}
 l_1 \text{ --- } \text{ --- } l_1 - k_1 - k_2 \\
 \begin{array}{c} \circ \\ \circ \\ \circ \end{array} \\
 \swarrow \quad \searrow \\
 k_1 \quad k_2
 \end{array}, \quad (3.22)$$

which is the same as the one gluon-scalar vertex, but with the transverse gluon momentum given by the sum of both t -channel gluons. This means we observe reggeization of the gluons in the scalar part of the impact factors as well.

The scalar impact factors come in pairs. There are two diagrams each with the same momentum structure but the color trace in different order. The relative sign between these diagrams is $(-1)^n$; n is the number of gluons. Altogether, the decomposition of the three and four gluon impact factors into a sum of two gluon impact factors $\mathbb{D}_{S,(2;0)}$ works the same as for fermion impact factors. The results are

$$\mathbb{D}_{S,(3;0)}^{a_1 a_2 a_3}(\mathbf{k}_1, \mathbf{k}_2, \mathbf{k}_3) = \frac{1}{2} g f_{a_1 a_2 a_3} [\mathbb{D}_{S,(2;0)}(12, 3) - \mathbb{D}_{S,(2;0)}(13, 2) + \mathbb{D}_{S,(2;0)}(1, 23)] \quad (3.23)$$

and

$$\begin{aligned} & \mathbb{D}_{S,(4;0)}^{a_1 a_2 a_3 a_4}(\mathbf{k}_1, \mathbf{k}_2, \mathbf{k}_3, \mathbf{k}_4) \\ &= -g^2 d^{a_1 a_2 a_3 a_4} [\mathbb{D}_{S,(2;0)}(123, 4) + \mathbb{D}_{S,(2;0)}(1, 234) - \mathbb{D}_{S,(2;0)}(14, 23)] \\ & \quad -g^2 d^{a_1 a_2 a_3 a_4} [\mathbb{D}_{S,(2;0)}(134, 2) + \mathbb{D}_{S,(2;0)}(124, 2) - \mathbb{D}_{S,(2;0)}(12, 34) - \mathbb{D}_{S,(2;0)}(13, 24)] \\ & \quad + \mathbb{D}_{S,(4;0)\text{Dir}}^{a_1 a_2 a_3 a_4}(\mathbf{k}_1, \mathbf{k}_2, \mathbf{k}_3, \mathbf{k}_4) \end{aligned} \quad (3.24)$$

with $\mathbb{D}_{S,(2;0)\text{Dir}}^{a_1 a_2 a_3 a_4}(\mathbf{k}_1, \mathbf{k}_2, \mathbf{k}_3, \mathbf{k}_4)$ given by Eq. (3.20) with F replaced by S .

Since both the scalar and fermion impact factors show reggeization, the full impact factors $\mathbb{D}_{(3;0)}$ and $\mathbb{D}_{(4;0)}$ are given by the sum of fermion and scalar impact factors:

$$\begin{aligned} \mathbb{D}_{(3;0)} &= \mathbb{D}_{F,(3;0)} + \mathbb{D}_{S,(3;0)}, \\ \mathbb{D}_{(4;0)} &= \mathbb{D}_{F,(4;0)} + \mathbb{D}_{S,(4;0)} \end{aligned} \quad (3.25)$$

with arbitrary polarization of the R -currents.

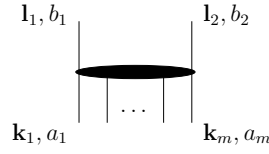
3.3 The Six Point Amplitude

After computation of the impact factors, we now study the six point amplitude. The amplitude is related to the partial wave $F(\omega, \omega_1, \omega_2; t, t_1, t_2)$, Eq. (3.7). The partial wave is obtained as the convolution of n -gluon amplitudes \mathbb{D}_n [42]:

$$\begin{aligned} F(\omega_1, \omega_2, \omega; t_1, t_2, t) &= 4 \mathbb{D}_2^{a_1 a_2}(\omega_1) \otimes_{12} \mathbb{D}_2^{a_3 a_4}(\omega_2) \otimes_{34} \\ & \left[\bar{\mathbb{D}}_{(4;0)}^{a_1 a_2 a_3 a_4}(\omega) + K_{2 \rightarrow 4}^{\{b\} \rightarrow \{a\}} \otimes \mathbb{D}_2^{b_1 b_2}(\omega) + \sum K_{2 \rightarrow 3}^{\{b\} \rightarrow \{a\}} \otimes \mathbb{D}_3^{b_1 b_2 b_3}(\omega) \right. \\ & \quad \left. + \sum' K_{2 \rightarrow 2}^{\{b\} \rightarrow \{a\}} \otimes \mathbb{D}_4^{b_1 b_2 b_3 b_4}(\omega) \right]. \end{aligned} \quad (3.26)$$

The relevant n -gluon amplitudes \mathbb{D}_n are obtained from the scattering amplitude applying suitable discontinuities. We refer to Ref. [17].

The amplitudes $\mathbb{D}_2(\omega_1)$ and $\mathbb{D}_2(\omega_2)$ combine the two lower impact factors $\mathbb{D}_{(2;0)}$ with their adjacent BFKL Green's functions and describe the evolution of two reggeized gluons below the branching vertex, respectively. To recapitulate, the branching vertex is the lowest interacting between the gluons after which the amplitude breaks up into two separate t -channels. The symbol \otimes_{12} (\otimes_{34}) denotes the convolution of the gluon

Figure 3.7: A diagrammatic representation of a $2 \rightarrow m$ kernel

amplitude $\mathbb{D}_2(\omega_1)$ ($\mathbb{D}_2(\omega_2)$) with the t -channel gluons 1 and 2 (3 and 4) and is defined as

$$\otimes_{12} = \int \frac{d^2 \mathbf{k}_1}{(2\pi)^3 \mathbf{k}_1 \mathbf{k}_2}. \quad (3.27)$$

\mathbf{k}_1 and \mathbf{k}_2 are the transverse gluon momenta.

The transitions between the gluons above the branching vertex are described by the kernels $K_{2 \rightarrow 4}^{\{b\} \rightarrow \{a\}}$, $K_{2 \rightarrow 3}^{\{b\} \rightarrow \{a\}}$, and $K_{2 \rightarrow 2}^{\{b\} \rightarrow \{a\}}$ [52], which act on the amplitudes $\mathbb{D}_2^{b_1 b_2}$, $\mathbb{D}_3^{b_1 b_2 b_3}$, and $\mathbb{D}_4^{b_1 b_2 b_3 b_4}$, respectively. The convolution symbol is defined as:

$$\otimes = \int \frac{d^2 \mathbf{l}_1}{(2\pi)^3 \mathbf{l}_1 \mathbf{l}_2}. \quad (3.28)$$

The kernels denote the interaction of two gluons resulting in m gluons while the other gluons of the amplitude keep their momenta and colors, see Fig. 3.7. The sums of the kernels extend over all possible interactions of the gluons under the condition that the gluons do not cross each other. The branching vertex itself is one of the $2 \rightarrow 4$, $2 \rightarrow 3$, or $2 \rightarrow 2$ kernels. One characteristic concerns the sum over $2 \rightarrow 2$ transitions. The branching vertex can be an interaction inside the gluon pairs (23), (13), (24), or (14), but not inside (12) or (34). The prime on the sum indicates that the interactions inside the gluon pairs (12) and (34) are not included.

$\bar{\mathbb{D}}_{(4;0)}$ is the unintegrated four gluon impact factor and describes the direct coupling of $\mathbb{D}_2(\omega_1)$ and $\mathbb{D}_2(\omega_2)$ to the upper impact factor. As long as we have one or more s -channel gluons that contribute to the M^2 -discontinuity, in addition to the particles in the loop, the invariant mass of the particles in the loop is integrated over. The integration is included in the usual impact factor $\mathbb{D}_{(4;0)}$. Without such s -channel gluons the mass of the particles in the loop coincides with the diffractive mass M , which is a fixed external parameter. Then the coupling of the four gluons to the loop is given by the triple discontinuity of the loop without integration over the diffractive mass and defines an unintegrated four gluon impact factor $\bar{\mathbb{D}}_{(4;0)}(\mathbf{k}_1, \mathbf{k}_2, \mathbf{k}_3, \mathbf{k}_4; M^2)$.

Following Refs. [15, 16, 17, 42], the partial wave can be decomposed into three parts:

$$F = F^{(R)} + F^{(I)} + F^{(\text{Dir})}. \quad (3.29)$$

The reggeizing part $F^{(R)}$ and the irreducible part $F^{(I)}$ with $\bar{\lambda} = \lambda/2$ are given by

$$F^{(R)}(\omega_1, \omega_2, \omega; t_1, t_2, t) = 4 \mathbb{D}_2^{a_1 a_2}(\omega_1) \otimes_{12} \mathbb{D}_2^{a_3 a_4}(\omega_2) \otimes_{34} \left[\bar{\mathbb{D}}_{(4;0)}^{a_1 a_2 a_3 a_4}(\omega) + (\omega - \omega_1 - \omega_2) \frac{\bar{\lambda}}{N_c} V_R \otimes \mathbb{D}_2^{a_1 a_2 a_3 a_4}(\omega) \right] \quad (3.30)$$

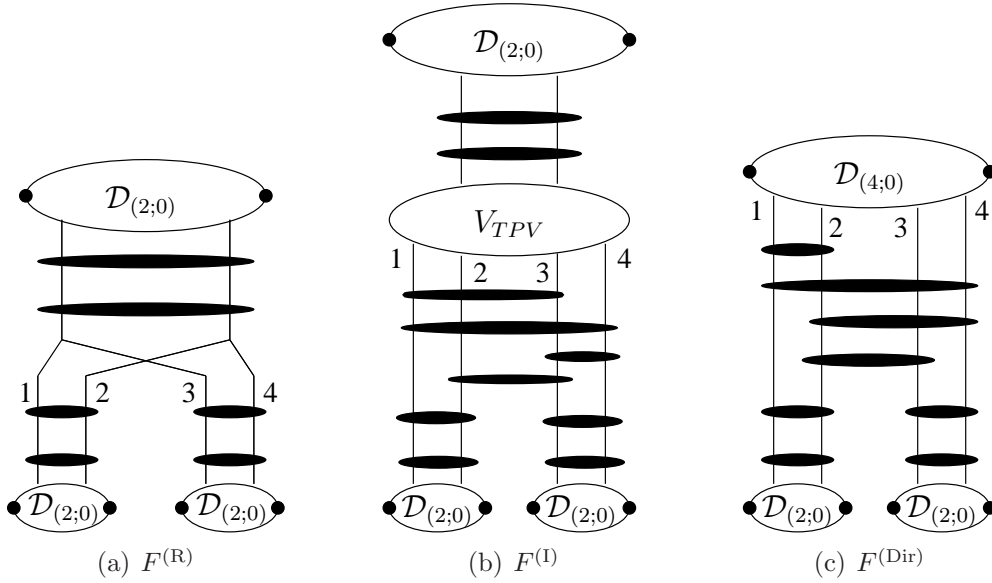


Figure 3.8: The three different parts of the six point partial wave $F(\omega, \omega_1, \omega_2)$ for arbitrary N_c

and

$$\begin{aligned}
 F^{(I)}(\omega_1, \omega_2, \omega; t_1, t_2, t) &= 4 \mathbb{D}_2^{a_1 a_2}(\omega_1) \otimes_{12} \mathbb{D}_2^{a_3 a_4}(\omega_2) \otimes_{34} \\
 &\quad \left[V_{TPV} \otimes \mathbb{D}_2^{a_1 a_2 a_3 a_4}(\omega) + \sum' K_{2 \rightarrow 2}^{\{b\} \rightarrow \{a\}} \otimes \mathbb{D}_4^{b_1 b_2 b_3 b_4}(\omega) \right].
 \end{aligned}
 \tag{3.31}$$

$F^{(R)}$ and $F^{(I)}$ have a similar structure, they are shown in Figs. 3.8(a) and 3.8(b). They contain the amplitudes $\mathbb{D}_2(\omega_1)$, $\mathbb{D}_2(\omega_2)$, and $\mathbb{D}_2(\omega)$, which combine the impact factors appearing at three different ends of the diagram, their connected BFKL Green's functions, and a triple vertex in the center. The explicit form of the vertices can be found in Ref. [52].

The term $F^{(R)}$ is a direct consequence of the reggeization of the gauge bosons, it is a superposition of two gluon amplitudes \mathbb{D}_2 . The gluons couple to the upper impact factor, interact according to the BFKL equation and then undergo a transition to four gluons via the triple vertex V_R . After the triple vertex the gluons 1 and 2 as well as the gluons 3 and 4 only interact pairwise according to the BFKL equation, that is we have two noninteracting BFKL Pomerons. In the special case in which we do not have s-channel gluons contributing to the M^2 -discontinuity, the direct coupling of the two Pomerons to the upper R -currents is given by the unintegrated impact factor $\mathbb{D}_{(4;0)}^{a_1 a_2 a_3 a_4}(\omega)$.

In the second term, $F^{(I)}$, two gluons again couple to the upper impact factor and interact according to the BFKL equation. Then the triple Pomeron vertex V_{TPV} transforms the two gluons to four, and they interact pairwise according to the BKP equations. The two disconnected Pomerons appear after the branching vertex. $F^{(R)}$

and $F^{(I)}$ are well known from QCD [17].

The last piece in Eq. (3.29), $F^{(\text{Dir})}$, pictured in Fig. 3.8(c), provides a new structure in $\mathcal{N} = 4$ SYM. It reads

$$F^{(\text{Dir})}(\omega, \omega_1, \omega_2; t_1, t_2, t) = 4 \mathbb{D}_2^{a_1 a_2}(\omega_1) \otimes_{12} \mathbb{D}_2^{a_3 a_4}(\omega_2) \otimes_{34} \left[\bar{\mathbb{D}}_{(4;0)}^{a_1 a_2 a_3 a_4}(\omega) + \sum' K_{2 \rightarrow 2}^{\{b\} \rightarrow \{a\}} \otimes \mathbb{D}_4^{b_1 b_2 b_3 b_4}(\omega) \right]. \quad (3.32)$$

Here, the four gluon BKP state couples directly to the upper impact factor. The partial wave $F^{(\text{Dir})}$ contains no triple vertex. After the branching vertex we once again obtain the two noninteracting Pomerons. The partial wave $F^{(\text{Dir})}$ also includes the unintegrated impact factor $\bar{\mathbb{D}}_{(4;0)}^{a_1 a_2 a_3 a_4}(\omega)$.

Now we compute the unintegrated impact factor $\bar{\mathbb{D}}_{(4;0)}^{a_1 a_2 a_3 a_4}$. To separate the color factor from the unintegrated impact factor, we introduce the notation

$$\bar{\mathbb{D}}_{(4;0)}^{a_1 a_2 a_3 a_4} = [2N_c d^{a_1 a_2 a_3 a_4} + \delta_{a_1 a_2} \delta_{a_3 a_4} + \delta_{a_1 a_3} \delta_{a_2 a_4} + \delta_{a_1 a_4} \delta_{a_2 a_3}] [\bar{\mathbb{D}}_{S,(4,0)} + \bar{\mathbb{D}}_{F,(4,0)}]. \quad (3.33)$$

$\bar{\mathbb{D}}_{S,(4,0)}$ and $\bar{\mathbb{D}}_{F,(4,0)}$ symbolize the scalar and fermion unintegrated impact factors, respectively. The structure of the unintegrated four gluon impact factor in QCD for the forward case $t = t_1 = t_2 = 0$ has been given in [17]. We evaluate the unintegrated impact factor in the forward case in $\mathcal{N} = 4$ SYM. There are 16 diagrams with a fermion and a scalar impact factor, respectively. To compute them explicitly, we take the discontinuity in s_1 , s_2 , and M^2 , but do not integrate over M . The results for Weyl fermions with $\mathbf{k}_1 = -\mathbf{k}_2 = \mathbf{k}$ and $\mathbf{k}_3 = -\mathbf{k}_4 = \mathbf{k}'$ are:

$$\begin{aligned} \bar{\mathbb{D}}_{F,(4,0)}^{hh'}(\mathbf{k}, -\mathbf{k}, \mathbf{k}', -\mathbf{k}'; M^2) &= \frac{R_F}{2} g^4 \frac{1}{(2\pi)^3} \int_0^1 d\alpha \int d^2 \mathbf{l} \alpha(\alpha-1) \delta(\alpha(1-\alpha)M^2 - \mathbf{l}^2) \\ &\times \left[-(2\alpha-1)^2 \boldsymbol{\epsilon}^{(h)} \cdot \left(\frac{\mathbf{l}+\mathbf{k}}{D(\mathbf{l}+\mathbf{k})} + \frac{\mathbf{l}-\mathbf{k}}{D(\mathbf{l}-\mathbf{k})} - 2 \frac{\mathbf{l}}{D(\mathbf{l})} \right) \right. \\ &\quad \times \left. \left(\frac{\mathbf{l}+\mathbf{k}'}{D(\mathbf{l}+\mathbf{k}')} + \frac{\mathbf{l}-\mathbf{k}'}{D(\mathbf{l}-\mathbf{k}')} - 2 \frac{\mathbf{l}}{D(\mathbf{l})} \right) \cdot \boldsymbol{\epsilon}^{(h')} \right. \\ &\quad + \boldsymbol{\epsilon}^{(h')} \cdot \left(\frac{\mathbf{l}+\mathbf{k}}{D(\mathbf{l}+\mathbf{k})} + \frac{\mathbf{l}-\mathbf{k}}{D(\mathbf{l}-\mathbf{k})} - 2 \frac{\mathbf{l}}{D(\mathbf{l})} \right) \left(\frac{\mathbf{l}+\mathbf{k}'}{D(\mathbf{l}+\mathbf{k}')} + \frac{\mathbf{l}-\mathbf{k}'}{D(\mathbf{l}-\mathbf{k}')} - 2 \frac{\mathbf{l}}{D(\mathbf{l})} \right) \cdot \boldsymbol{\epsilon}^{(h)} \\ &\quad \left. - \boldsymbol{\epsilon}^{(h)} \cdot \boldsymbol{\epsilon}^{(h')} \left(\frac{\mathbf{l}+\mathbf{k}}{D(\mathbf{l}+\mathbf{k})} + \frac{\mathbf{l}-\mathbf{k}}{D(\mathbf{l}-\mathbf{k})} - 2 \frac{\mathbf{l}}{D(\mathbf{l})} \right) \cdot \left(\frac{\mathbf{l}+\mathbf{k}'}{D(\mathbf{l}+\mathbf{k}')} + \frac{\mathbf{l}-\mathbf{k}'}{D(\mathbf{l}-\mathbf{k}')} - 2 \frac{\mathbf{l}}{D(\mathbf{l})} \right) \right]. \quad (3.34) \end{aligned}$$

We have contracted the impact factor with transversely polarized R -currents, given in Eqs. (2.59)-(2.61). The unintegrated impact factor for longitudinal polarization of

the R -currents, Eqs. (2.57) and (2.58), is

$$\begin{aligned} & \bar{\mathbb{D}}_{F,(4,0)}^{LL}(\mathbf{k}, -\mathbf{k}, \mathbf{k}', -\mathbf{k}'; M^2) \\ &= -4 \frac{R_F}{2} g^4 Q^2 \frac{1}{(2\pi)^3} \int_0^1 d\alpha \int d^2\mathbf{l} \alpha^3 (\alpha - 1)^3 \delta(\alpha(1 - \alpha)M^2 - \mathbf{l}^2) \\ & \quad \times \left(\frac{1}{D(\mathbf{l} + \mathbf{k})} + \frac{1}{D(\mathbf{l} - \mathbf{k})} - \frac{2}{D(\mathbf{l})} \right) \cdot \left(\frac{1}{D(\mathbf{l} + \mathbf{k}')} + \frac{1}{D(\mathbf{l} - \mathbf{k}')} - \frac{2}{D(\mathbf{l})} \right). \end{aligned} \quad (3.35)$$

The factor R_F and a factor 1/2 for Weyl fermions, see section 3.2, are included, but the color factor is not because we have written the color factor separately in Eq. (3.33). The denominators are given by

$$D(\mathbf{k}) = \alpha(\alpha - 1)Q^2 + \mathbf{k}^2. \quad (3.36)$$

Similarly, the scalar contributions to the unintegrated four gluon impact factors are

$$\begin{aligned} & \bar{\mathbb{D}}_{S,(4,0)}^{hh'}(\mathbf{k}, -\mathbf{k}, \mathbf{k}', -\mathbf{k}'; M^2) \\ &= g^4 \frac{1}{(2\pi)^3} \int_0^1 d\alpha \int d^2\mathbf{l} \alpha^2 (\alpha - 1)^2 \delta(\alpha(1 - \alpha)M^2 - \mathbf{l}^2) \\ & \quad \times \epsilon^{(h)} \cdot \left(\frac{\mathbf{l} + \mathbf{k}}{D(\mathbf{l} + \mathbf{k})} + \frac{\mathbf{l} - \mathbf{k}}{D(\mathbf{l} - \mathbf{k})} - 2 \frac{\mathbf{l}}{D(\mathbf{l})} \right) \left(\frac{\mathbf{l} + \mathbf{k}'}{D(\mathbf{l} + \mathbf{k}')} + \frac{\mathbf{l} - \mathbf{k}'}{D(\mathbf{l} - \mathbf{k}')} - 2 \frac{\mathbf{l}}{D(\mathbf{l})} \right) \cdot \epsilon^{(h')} \end{aligned} \quad (3.37)$$

and

$$\begin{aligned} & \bar{\mathbb{D}}_{S,(4,0)}^{LL}(\mathbf{k}, -\mathbf{k}, \mathbf{k}', -\mathbf{k}'; M^2) \\ &= g^4 Q^2 \frac{1}{(2\pi)^3} \int_0^1 d\alpha \int d^2\mathbf{l} (\alpha - 1/2)^2 \alpha^2 (\alpha - 1)^2 \delta(\alpha(1 - \alpha)M^2 - \mathbf{l}^2) \\ & \quad \times \left(\frac{1}{D(\mathbf{l} + \mathbf{k})} + \frac{1}{D(\mathbf{l} - \mathbf{k})} - \frac{2}{D(\mathbf{l})} \right) \left(\frac{1}{D(\mathbf{l} + \mathbf{k}')} + \frac{1}{D(\mathbf{l} - \mathbf{k}')} - \frac{2}{D(\mathbf{l})} \right). \end{aligned} \quad (3.38)$$

After integration over the angles of the momenta \mathbf{l} , \mathbf{k} , and \mathbf{k}' , it is possible to combine the fermion and scalar loops. The results are

$$\bar{\mathbb{D}}_{(4,0)}^{hh'}(\mathbf{k}, -\mathbf{k}, \mathbf{k}', -\mathbf{k}'; M^2) = \frac{g^4}{32} \delta^{hh'} \frac{1}{M^2} \int_0^1 d\alpha I_v(\mathbf{k}^2, \alpha, M^2) I_v(\mathbf{k}'^2, \alpha, M^2) \quad (3.39)$$

and

$$\bar{\mathbb{D}}_{(4,0)}^{LL}(\mathbf{k}, -\mathbf{k}, \mathbf{k}', -\mathbf{k}'; M^2) = \frac{g^4}{32} Q^2 \int_0^1 d\alpha \alpha^2 (1 - \alpha)^2 I_s(\mathbf{k}^2, \alpha, M^2) I_s(\mathbf{k}'^2, \alpha, M^2). \quad (3.40)$$

Here, we have defined:

$$\begin{aligned} \frac{1}{\mathbb{I}^2} I_v(\mathbf{k}^2, \alpha, M^2) &= \int_0^{2\pi} \frac{d\varphi}{2\pi} \left(\frac{1+\mathbf{k}}{D(1+\mathbf{k})} + \frac{1-\mathbf{k}}{D(1-\mathbf{k})} - 2\frac{1}{D(\mathbb{I})} \right) \\ &= \frac{1}{\mathbb{I}^2} \left(\frac{Q^2 - M^2}{Q^2 + M^2} - \frac{\mathbf{k}^2 + \alpha(1-\alpha)(Q^2 - M^2)}{\sqrt{(\mathbf{k}^2 + \alpha(1-\alpha)(Q^2 - M^2))^2 + 4\alpha^2(1-\alpha)^2 M^2 Q^2}} \right) \end{aligned} \quad (3.41)$$

and

$$\begin{aligned} I_s(\mathbf{k}^2, \alpha, M^2) &= \int_0^{2\pi} \frac{d\varphi}{2\pi} \left(\frac{1}{D(1+\mathbf{k})} + \frac{1}{D(1-\mathbf{k})} - \frac{2}{D(\mathbb{I})} \right) \\ &= 2 \left(\frac{1}{\sqrt{(\mathbf{k}^2 + \alpha(1-\alpha)(Q^2 - M^2))^2 + 4\alpha^2(1-\alpha)^2 M^2 Q^2}} - \frac{1}{\alpha(1-\alpha)(Q^2 + M^2)} \right), \end{aligned} \quad (3.42)$$

where φ denotes the angle of the vector \mathbf{k} , and we have used the delta functions to set $\mathbb{I}^2 = \alpha(1-\alpha)M^2$.

3.4 The Large N_c -Limit in a Topological Approach

The computation of the six point correlator in the last sections has been for arbitrary N_c . Now, we take the large N_c -limit, $N_c \rightarrow \infty$, since the AdS/CFT-correspondence relates the strong coupling regime of $\mathcal{N} = 4$ SYM in the large N_c -limit to supergravity in an AdS_5 background. Additionally, the large N_c -limit provides a different view on the color structure of diagrams in the high energy limit. In the so-called topological approach, the color structure can be projected onto surfaces, for example onto planes, spheres, or pairs-of-pants.

First, we recall the large N_c -limit of QCD with fermions in the fundamental representation [51]. The Fierz identity

$$(t^a)_j^i (t^a)_l^k = \delta_l^i \delta_j^k - \frac{1}{N_c} \delta_j^i \delta_l^k, \quad (3.43)$$

where $(t^a)_j^i$ denote the $SU(N_c)$ generators in the fundamental representation (with the normalization $\text{Tr}(t^a t^b) = \delta^{ab}$), and the identity

$$f^{abc} = \frac{1}{i\sqrt{2}} [\text{Tr}(t^a t^b t^c) - \text{Tr}(t^c t^b t^a)] \quad (3.44)$$

give rise to color diagrams with the following elements:

(i) for each quark in the fundamental representation a single line with an arrow indicating the flow from the upper to the lower index

$$\delta_j^i = i \longrightarrow j; \quad (3.45)$$

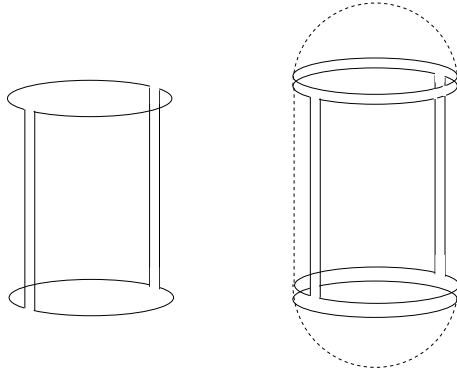


Figure 3.9: Cylinder topology for the $2 \rightarrow 2$ scattering in QCD (left) and the topology of a stretched sphere in $\mathcal{N} = 4$ SYM (right)

(ii) for each inner gluon a double line

$$\delta_l^i \delta_j^k = \begin{array}{c} \xrightarrow{i} \xrightarrow{l} \\ \xleftarrow{j} \xleftarrow{k} \end{array}; \quad (3.46)$$

(iii) for each triple gluon vertex

$$f^{abc} = \frac{1}{i\sqrt{2}} [\text{Tr}(t^a t^b t^c) - \text{Tr}(t^c t^b t^a)]. \quad (3.47)$$

As a result, each QCD diagram turns into a network of double and single lines. The resulting diagrams only represent the color factors. The momentum part has to be written separately. A usual Feynman diagram illustrates both the color factors and the momentum part.

The double line diagrams can be drawn on a two-dimensional surface with Euler number $\chi = 2 - 2h - b$, where h is the number of handles of the surface and b the number of boundaries or holes. A closed color loop always delivers a factor N_c , and a closed quark loop, compared to a corresponding gluon loop, is $1/N_c$ suppressed and leads to a boundary. For an arbitrary vacuum graph T one arrives at the following expansion in N_c

$$T = \sum_{h,b}^{\infty} N_c^{2-2h-b} T_{h,b}(\lambda), \quad (3.48)$$

where the 't Hooft-coupling λ is held fixed while N_c is taken to infinity. In this expansion, the leading diagrams are those, which have the topology of a sphere with zero handles and zero boundaries, $h = b = 0$. With quarks included the leading diagrams are those, which fit on a plane, that is $h = 0$, $b = 1$. Diagrams with two boundaries and zero handles, $b = 2$ and $h = 0$, can be drawn on the surface of a cylinder: the color diagram of the BFKL Pomeron in QCD lies on the surface of a cylinder, Fig. 3.9 left. Diagrams with three boundaries and zero handles, $b = 3$ and $h = 0$, fit on the surface of a pair-of-pants, see Fig. 3.10. One example for a diagram with such a color structure is the triple Pomeron vertex in QCD [52].

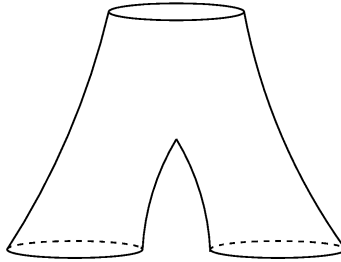
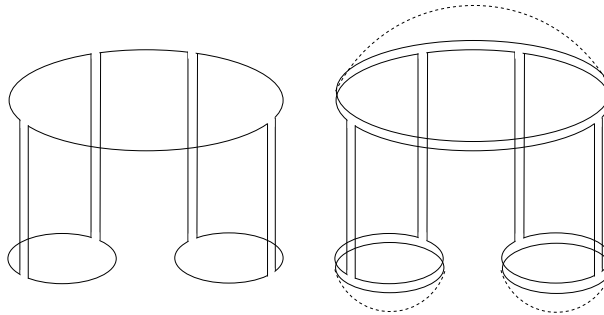


Figure 3.10: Pair-of-pants topology

Figure 3.11: Pair-of-pants topology for the $3 \rightarrow 3$ amplitude in QCD (left) and the deformed pair-of-pants topology in $\mathcal{N} = 4$ SYM (right)

In $\mathcal{N} = 4$ SYM, fermions and scalars belong to the adjoint representation of the gauge group, and in the topological description, they are represented by double lines as the gauge bosons. Then, fermions no longer define boundaries, and the color diagrams receive some changes. As a simple example, in QCD the BFKL Pomeron fits onto a cylinder with two boundaries defined by the closed quark loops, Fig. 3.9 left. In $\mathcal{N} = 4$ SYM, the top and the bottom loop obtain double lines and turn into caps, and the cylinder turns into a stretched sphere with zero handles and zero boundaries as shown in Fig. 3.9 right. The same happens for six point functions. The color diagrams for a six point function with fundamental fermions in QCD, Fig. 3.11 left, fit on a pair-of-pants [52]. In $\mathcal{N} = 4$ SYM with fermions and scalars in the adjoint representation, the loops of the impact factors turn into double lines, and the boundaries of the pair-of-pants are replaced by caps, Fig. 3.11 right.

If we are interested in a six point correlator of R -currents in $\mathcal{N} = 4$ SYM in the topological approach, we have to sum diagrams which lie on this surface. It turns out that there are three different classes of color diagrams, two already present in QCD and one new class. The separation into three classes of diagrams offers a better understanding of the structure of six point amplitudes already presented in the last section. The three classes of color diagrams are related to the three partial waves in Eq. (3.29). The different building blocks in the partial waves, the triple vertex V_R and the triple Pomeron vertex V_{TPV} as well as the additional partial wave $F^{(\text{Dir})}$ appear due to the different classes of color graphs.

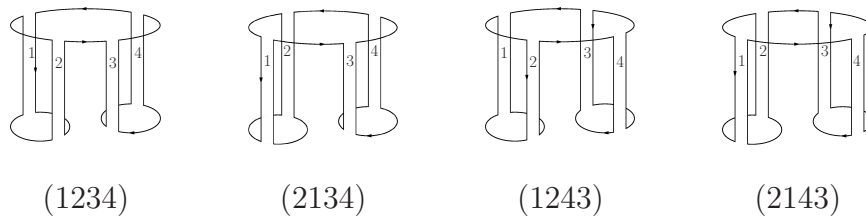


Figure 3.12: The four different orderings of color factors in the six point function in lowest order QCD

3.4.1 Diagrams on a Deformed Pair-of-Pants

We discuss the diagrams of a six point correlator of R -currents, which fit on a deformed pair-of-pants, shown in Fig. 3.11 right.

To start with a simple example, we first consider the cylinder topology. When we replace at the top of the cylinder the fermion in the fundamental representation in QCD, Fig. 3.9 left, by an adjoint fermion, we simply draw above the already existing color line of the fermion an additional closed color loop, which generates an additional factor N_c . The double line notation now also includes scalar loops. The two t -channel gluons are attached to the same color line of the closed loop, either to the lower line or to the upper one as shown in Fig. 3.9 right. Diagrams where the two t -channel lines are attached to different lines lose a factor N_c and are suppressed. A result of this simple observation is, the contribution of the adjoint fermions to the impact factors is proportional to N_c times that of a fundamental one. The different results for the traces of generators reflect this observation. In the fundamental representation, we have $\text{Tr}(t^a t^b) = \delta_{ab}$ whereas in the adjoint representation we have $\text{Tr}(T^a T^b) = N_c \delta_{ab}$. Note that our normalization of the fundamental generators deviates by a factor two from the standard normalization $\text{Tr}(\tau^a \tau^b) = \delta^{ab}/2$ in section 3.2.1.

Let us now turn to the six point function. In lowest order QCD, the four t -channel gluons couple to the upper loop in all possible ways, altogether there are 16 different diagrams. A closer look shows that we have inside the 16 diagrams four different orderings of color matrices. For the lowest order diagrams in the nonsupersymmetric QCD case, the four different structures are illustrated in Fig. 3.12. Switching to $\mathcal{N} = 4$ SYM, we simply perform for each of the three impact factors the substitution we have just described for the BFKL cylinder, and we obtain an additional factor N_c^3 . Whereas in QCD the analogous lowest order graphs fit on the surface of a pair-of-pants in Fig. 3.10, the diagrams now have the shape of a deformed sphere as once again shown in Fig. 3.13(a). Here both gluon cylinders are coupled to the same line of the upper loop.

A closer inspection shows another possible configuration in addition to Fig. 3.13(a): without losing a factor N_c , we can attach one of the cylinders to the outer loop, the other one to the inner loop, Fig. 3.13(b). This additional piece in the four gluon impact factor has no counterpart in QCD with fermions in the fundamental representation. It has first been found in [42]. An alternative way of drawing this graph is shown in

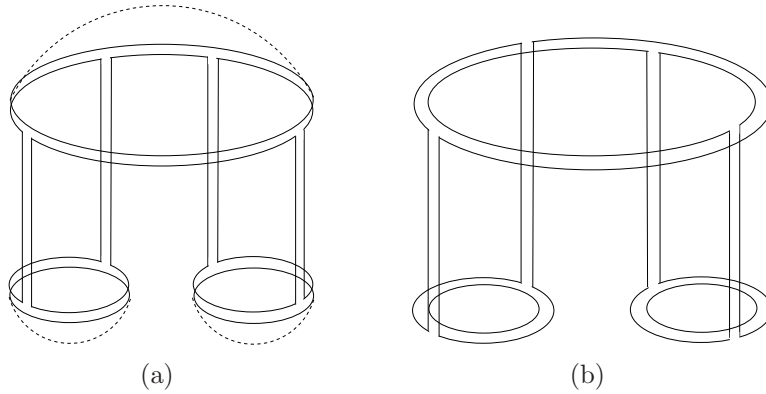


Figure 3.13: Pair-of-pants topology for the $3 \rightarrow 3$ amplitude in $\mathcal{N} = 4$ SYM: (a) a color configuration already present in QCD, and (b) a new one, which only exists for adjoint particles

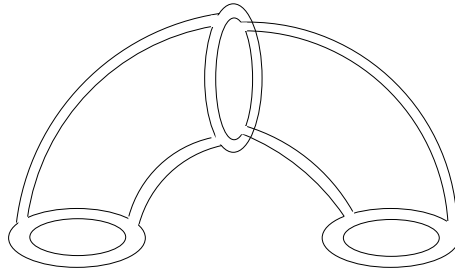


Figure 3.14: An alternative way of drawing Fig. 3.13(b)

Fig. 3.14.

Moving on to next-to-leading order (NLO) in the t'Hooft coupling λ , starting with one-loop corrections, we first note that for the diagram in Fig. 3.13(b), we can only insert $2 \rightarrow 2$ transitions inside the two cylinders: an example is shown in Fig. 3.15. In particular, any rung connecting the two cylinders loses a power of N_c . As a result, corrections to the diagram in Fig. 3.13(b) simply lead to two BFKL Pomeron coupled to the four gluon impact factor. This class of diagrams will be named direct: the two BFKL Pomerons couple directly to the impact factor. As discussed in Ref. [52], on the cylinder, each gluon rung comes in two different ways, one in front of the cylinder, the other one on the backside. This observation also applies to our $\mathcal{N} = 4$ SYM case.

Looking at the other diagram in Fig. 3.13, which is already present in nonsupersymmetric QCD, insertion of one more rung opens two distinct classes of graphs. Examples for these two classes are given in Fig. 3.16. It is suggestive to name them planar and nonplanar, respectively. By definition, planar graphs have the property by contracting closed color loops, they can be reduced to the $\mathcal{N} = 4$ SYM version of the graphs in Fig. 3.12. Beginning with the graph shown in Fig. 3.16 right, this is not possible for the nonplanar ones.

Altogether, we have to distinguish, starting at NLO, three different types of dia-

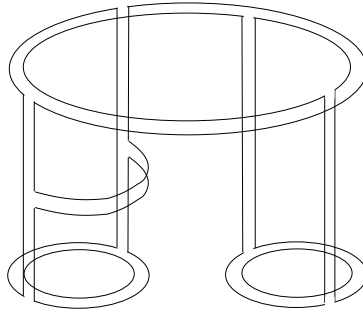


Figure 3.15: Example of a NLO diagram to Fig. 3.13(b)

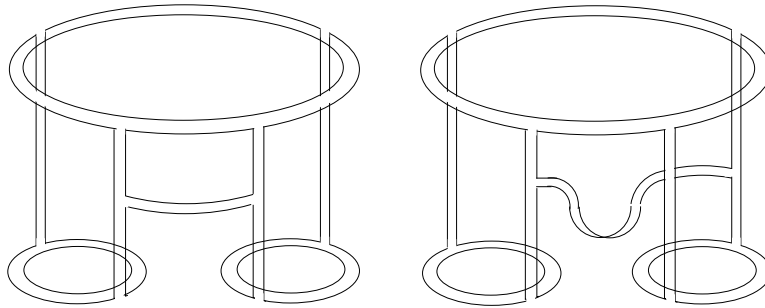


Figure 3.16: Two classes of diagrams: planar graphs (left) and nonplanar graphs (right)

grams: the direct, the planar, and the nonplanar diagrams. In the first case, the direct diagrams, the lowest interaction between the two cylinders, which defines the value of the diffractive mass M , is the upper impact factor itself. The four gluons couple directly to the upper loop via the impact factor $\bar{\mathbb{D}}_{(4,0)}$ without interaction between the two disconnected BFKL Pomerons.

The second type of diagrams are planar diagrams. At the upper loop, they start with two, three, or four gluons. These gluons undergo transitions by $2 \rightarrow 2$, $2 \rightarrow 3$, or $2 \rightarrow 4$ kernels. One of these transitions is the branching vertex, below which we always have four gluons. But any two gluons interact only pairwise after the branching vertex. They form once again the two noninteracting Pomerons.

Nonplanar diagrams are the last possibility. At the upper loop they can also start with two, three, or four gluons, and the structure above the branching vertex is the same as for planar diagrams. But the branching vertex itself now provides a nonplanar structure. Below this nonplanar vertex the known disconnected BFKL cylinders appear.

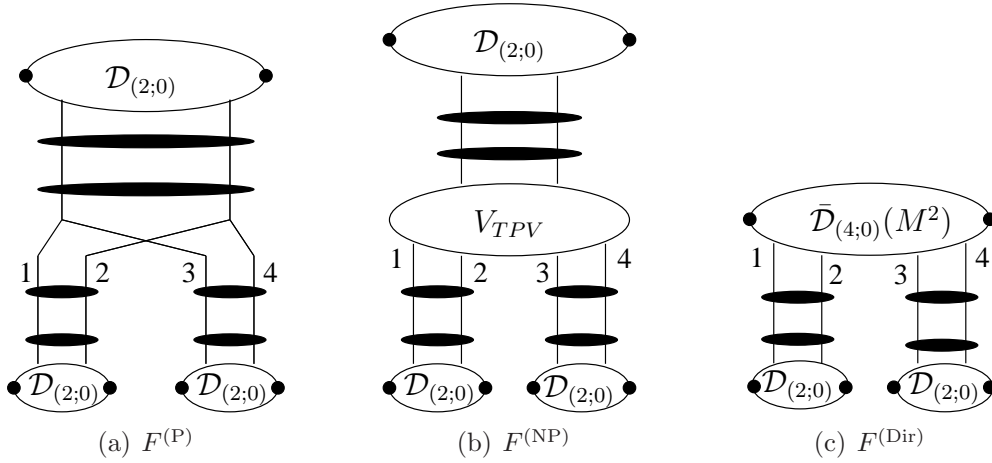


Figure 3.17: The three different parts of the six point partial wave $F(\omega, \omega_1, \omega_2)$ in the large N_c -limit

3.4.2 Analytic Expressions

We turn to the analytic expressions for the amplitude in the large N_c -limit. As in section 3.3, we split the partial wave F into three parts,

$$F = F^{(P)} + F^{(NP)} + F^{(\text{Dir})} \quad (3.49)$$

that are called planar, nonplanar, and direct. They are displayed in Fig. 3.17. We show that these three parts are related to the partial waves introduced in Eq. (3.29).

For the first two terms we can use the analytic representation in Eq. (3.7), and the explicit expressions are

$$F^{(P)}(\omega, \omega_1, \omega_2) = 4 \mathbb{D}_2^{(12)}(\omega_1) \otimes_{12} \mathbb{D}_2^{(34)}(\omega_2) \otimes_{34} \left[\bar{\mathbb{D}}_{(4;0)}(\omega) + (\omega - \omega_1 - \omega_2) \frac{\bar{\lambda}}{N_c} V_R \otimes \mathbb{D}_2(\omega) \right] \quad (3.50)$$

and

$$F^{(NP)}(\omega, \omega_1, \omega_2) = 4 \mathbb{D}_2^{(12)}(\omega_1) \otimes_{12} \mathbb{D}_2^{(34)}(\omega_2) \otimes_{34} \frac{\bar{\lambda}^2}{N_c} V_{\text{TPV}} \otimes \mathbb{D}_2(\omega). \quad (3.51)$$

The partial waves $F^{(P)}$ and $F^{(NP)}$ in the large N_c -limit have a similar structure as $F^{(R)}$ and $F^{(I)}$, Eqs. (3.30) and (3.31), for arbitrary N_c : The amplitudes $\mathbb{D}_2^{(12)}(\omega_1)$, $\mathbb{D}_2^{(34)}(\omega_2)$, $\mathbb{D}_2(\omega)$ appear at the three different ends of the diagram, and each partial wave has a triple vertex in the center. But there is one important difference in the large N_c -limit: The BKP states are suppressed. That is, the transition kernel $K_{2 \rightarrow 2}^{\{b\} \rightarrow \{a\}}$ in Eq. (3.31) has disappeared in $F^{(NP)}$. As a consequence the gluons below the triple vertex, that is the branching vertex, interact only pairwise according to the BFKL equation. In order to study BKP states in the large N_c -limit, correlations functions

with more than six R -currents have to be considered in which the BKP states are not suppressed.

The color graphs provide a new view on the two triple vertices. $F^{(P)}$ results from the planar diagrams, an example is shown in Fig. 3.16 left. The vertex is a consequence of the reggeization of the gauge bosons, and therefore the same vertex as in Eq. (3.30). The vertex in $F^{(NP)}$ is a result of the nonplanar structure of the color diagrams, one sample diagram is depicted in Fig. 3.16 right, and coincides with the triple Pomeron vertex in Eq. (3.31).

Finally, there is the partial wave $F^{(\text{Dir})}$ in Eq. (3.49). Here we have to use a different analytic expression for the amplitude $T_{3 \rightarrow 3}^{(\text{Dir})}$ as before,

$$T_{3 \rightarrow 3}^{(\text{Dir})}(s_1, s_2, M^2; t_1, t_2, t) = s_1 s_2 \int \frac{d\omega_1 d\omega_2}{(2\pi i)^2} s_1^{\omega_1} s_2^{\omega_2} (M^2)^{-\omega_1 \omega_2} \xi(\omega_1) \xi(\omega_2) \times F^{(\text{Dir})}(M^2, \omega_1, \omega_2; t, t_1, t_2). \quad (3.52)$$

The partial wave is given by

$$F^{(\text{Dir})}(M^2, \omega_1, \omega_2) = 4 \mathbb{D}_2^{(12)}(\omega_1) \otimes_{12} \mathbb{D}_2^{(34)}(\omega_2) \otimes_{34} \bar{\mathbb{D}}_{(4;0)}(M^2). \quad (3.53)$$

The BKP states, which appear for arbitrary N_c , Eq. (3.32), are again suppressed. As a consequence we have two disconnected BFKL Pomerons that couple directly to the upper impact factor. The coupling is described by the unintegrated impact factor $\bar{\mathbb{D}}_{(4;0)}(M^2)$, whose explicit expressions can be found in Eqs. (3.39) and (3.40). The partial wave $F^{(\text{Dir})}$ is subleading for large M^2 compared with the partial waves $F^{(P)}$ and $F^{(NP)}$. It contributes in the region of low mass M^2 .

In this chapter, we have investigated the scattering of six R -currents in the triple Regge limit. One main result is the new direct coupling of the exchanged gluons to the R -currents due to fermions and scalars, which are in the adjoint representation of the gauge group in $\mathcal{N} = 4$ SYM. Furthermore, we have written the scalar impact factors as a superposition of two gluon scalar impact factors. The triple vertices in $\mathcal{N} = 4$ SYM, V_R and the triple Pomeron vertex V_{TPV} , are the same as in QCD. They are independent of the coupling to the external R -currents, mediated by the impact factors, and not influenced by the supersymmetry. Altogether, the Regge factorization in the six point function of R -currents becomes apparent.

4 The Four Point Function in Supergravity

In the last two chapters, we have dealt with correlation functions of R -currents in $\mathcal{N} = 4$ SYM in the Regge limit at weak coupling. Now we like to address the strong coupling limit of R -current correlators in the Regge limit. We take advantage of the AdS/CFT-correspondence, which relates the strong coupling regime of $\mathcal{N} = 4$ SYM to a weakly coupled type IIB string theory on an AdS_5 background as explained in section 1.1. We perform our computations for large t'Hooft coupling λ in the large N_c -limit. With these limits, the full type IIB string theory reduces to classical supergravity.

The computations in the last two chapters in $\mathcal{N} = 4$ SYM have been realized for small t'Hooft coupling λ , that is at weak coupling. The supergravity computations are now performed for large t'Hooft coupling. Thus, the results of the respective computations are valid for different regimes of the coupling strength.

4.1 Setup of the Computation

We are interested in evaluating the four point amplitude of R -currents in momentum space defined in Eq. (2.39). However, we change the notation because the computation in supergravity takes place in five-dimensional Anti-de Sitter space. From now on, Greek indices label the $(d + 1)$ -dimensional space and run from 0 to 4. Latin indices refer to the four-dimensional Euclidean boundary of AdS_5 . With these changes we define the Euclidean amplitude in momentum space, $A(\vec{p}_i)$, as

$$i(2\pi)^4 \delta\left(\sum_i \vec{p}_i\right) A(\vec{p}_i)^{j_1 j_2 j_3 j_4} = \int \prod_{i=1}^4 d^4 x_i e^{-i\vec{p}_i \cdot \vec{x}_i} \langle J_R^{j_1}(\vec{x}_1) J_R^{j_2}(\vec{x}_2) J_R^{j_3}(\vec{x}_3) J_R^{j_4}(\vec{x}_4) \rangle. \quad (4.1)$$

\vec{x}_i and \vec{p}_i are four-dimensional Euclidean vectors, and the j_i label the spacial directions with $j_i = 1, \dots, 4$. We choose all momenta $\vec{p}_1, \dots, \vec{p}_4$ incoming. Again, we contract the amplitude with polarization vectors,

$$\mathcal{A}(|\vec{p}_i|; s, t)^{\lambda_1 \lambda_2 \lambda_3 \lambda_4} = \sum_{\lambda_i} \epsilon^{j_1(\lambda_1)}(\vec{p}_1) \epsilon^{j_2(\lambda_2)}(\vec{p}_2) \epsilon^{j_3(\lambda_3)}(\vec{p}_3)^* \epsilon^{j_4(\lambda_4)}(\vec{p}_4)^* A(\vec{p}_i)^{j_1 j_2 j_3 j_4}. \quad (4.2)$$

$\lambda_i = L, h$ denote the different polarizations, longitudinal or transverse. The resulting scattering amplitude \mathcal{A} depends on s, t , and the virtualities $Q_i^2 = |\vec{p}_i|^2$ of the incoming and outgoing R -currents.

Now, we fix some conventions about the five-dimensional Anti-de Sitter space AdS_5 . The Euclidean continuation of the five-dimensional Anti-de Sitter space is

$$ds^2 = \frac{1}{z_0^2}(dz_0^2 + d\vec{x}^2) \quad (4.3)$$

with $z_0 > 0$ and $\vec{x} = (x_1, \dots, x_4)$. Here we set the radius R to unity. The metric $g_{\mu\nu}$ is given by

$$g_{\mu\nu} = \frac{1}{z_0^2}\delta_{\mu\nu}. \quad (4.4)$$

In Euclidean notation, the energies s and t are

$$s = -(\vec{p}_1 + \vec{p}_2)^2 \quad \text{and} \quad -t = (\vec{p}_1 + \vec{p}_3)^2. \quad (4.5)$$

In order to take the Regge limit,

$$s \gg -t, Q_i^2, \quad (4.6)$$

we have to go to Minkowski space via Wick rotation.

The AdS/CFT-correspondence comes with a precise prescription, Eq. (1.9), how to compute correlation functions on both sides of the duality. For the computation on the supergravity side we need, see Eqs. (1.7) and (1.8), the classical supergravity action. It reads

$$S_{\text{sugra}} = \frac{1}{2\kappa^2} \int d^{d+1}z \sqrt{g}(-\mathcal{R} + \Lambda) + S_m. \quad (4.7)$$

\mathcal{R} is the scalar curvature. The covariant matter action S_m [40, 53, 54] is given by

$$S_m = \frac{1}{2\kappa^2} \int d^{d+1}z \sqrt{g} \left[\frac{1}{4}F_{\mu\nu}F^{\mu\nu} + \frac{ik}{24\sqrt{g}}\epsilon_{\mu\nu\rho\sigma\lambda}F_{\mu\nu}F_{\rho\sigma}A_\lambda - A_\mu J^\mu + \dots \right]. \quad (4.8)$$

We have the gravitational coupling κ with $2\kappa^2 = 15\pi^2 R^3/N_c^2$, and the coefficient k is an integer. $F_{\mu\nu}$ is the field strength of the gauge field A_μ . The dots denote higher order terms of A_μ . To lower indices, we use the five-dimensional metric in Eq. (4.4).

A_μ is a field in the bulk of supergravity; it lives in the five-dimensional Anti-de Sitter space. On the four-dimensional boundary at $z_0 = 0$ it has the value A_0 . According to the prescription in section 1.1.3, a supergravity field in the bulk with a certain boundary value is a source for an operator of the gauge theory, which lives on the four-dimensional boundary of AdS_5 . Here, the gauge field A_μ is a source for the R -current operator $J_R^{ji}(\vec{x}_i)$. The correlation function of n R -currents is then given by

$$\langle J_R(\vec{x}_1), \dots, J_R(\vec{x}_n) \rangle = \frac{\delta^n}{\delta A_0(\vec{x}_1) \dots \delta A_0(\vec{x}_n)} Z[A_0]_{\text{sugra}}|_{A_0=0}. \quad (4.9)$$

Using this relation in the actual computation, leads to a set of rules analog to Feynman rules and to a special class of Feynman diagrams, the so-called Witten diagrams [34]. An example is shown in Fig. 4.1, it is a three point function of R -currents. The

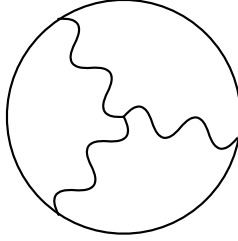


Figure 4.1: An example of a Witten diagram: a three point function with bulk-to-boundary gauge boson propagators

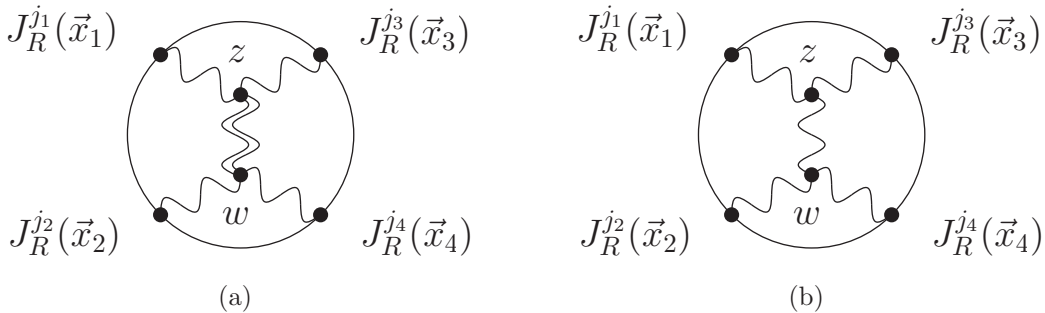


Figure 4.2: The graviton (a) and gauge boson (b) exchange Witten diagrams

R -currents are inserted at the boundary of AdS_5 , which is illustrated by a circle. Interactions take place in the interior. Wavy lines are gauge boson propagators, the ones shown here are bulk-to-boundary propagators connected by a vertex in the bulk. A second type of propagators are bulk-to-bulk-propagators, which connect two points in the interior of AdS_5 .

In our case, which is the four point function of R -currents in the classical supergravity limit, we have to consider Witten diagrams with a gauge boson exchange and with a graviton exchange in the bulk, respectively, see Fig. 4.2. The double wavy line symbolizes a graviton. In addition to the t -channel exchange diagrams, we also have to regard the exchange of the particles in the s - and u -channel. We expect the t -channel graviton exchange diagram to dominate with respect to the t -channel gauge boson exchange diagram. The exchanged particle with the highest spin provides the leading contribution to the amplitude. This is analog to the computation in $\mathcal{N} = 4$ SYM at weak coupling: The two gluon exchange diagrams, gluons are the particles with highest spin in $\mathcal{N} = 4$ SYM, dominate compared to the one-loop diagrams, in which fermion and scalars are exchanged in the t -channel.

The two Witten diagrams in Fig. 4.2 consist of three building blocks: the bulk-to-boundary propagator of the gauge boson, the bulk-to-bulk propagator of the gauge boson, and the bulk-to-bulk graviton propagator. The propagators are connected by vertices at the points z and w inside the bulk. In the following sections, we present explicit expressions for the propagators. Since we are interested in the Regge limit,

which is defined in momentum space, Eq. (4.6), we Fourier transform all propagators to momentum space.

4.1.1 Bulk-to-Bulk Propagator of the Gauge Boson

We start with the Fourier transformation of the bulk-to-bulk propagator of the gauge boson. In coordinate space it reads [55, 56]

$$G_{\mu\nu'}(z, w) = -(\partial_\mu \partial_{\nu'} u) F(u) + \partial_\mu \partial_{\nu'} S(u) \quad (4.10)$$

with the so-called chordal distance

$$u = \frac{(z - w)^2}{2z_0 w_0} \quad (4.11)$$

and the flat Euclidean distance $(z - w)^2 = \delta_{\mu\nu}(z - w)_\mu(z - w)_\nu$. ∂_μ is a derivative with respect to z_μ and $\partial_{\nu'}$ a derivative with respect to $w_{\nu'}$. $F(u)$ describes the propagation of the physical components of A_μ , it is the massive scalar propagator with $m^2 = -(d-1)$:

$$F(u) = C[u(2+u)]^{-(d-1)/2} \quad \text{with} \quad C = \frac{\Gamma(\frac{d-1}{2})}{(4\pi)^{(d+1)/2}}. \quad (4.12)$$

The function $S(u)$ is a gauge dependent function. In Refs. [55, 56], it has been explained that $S(u)$ can be discarded. We do not need its form in our further computations. The derivatives of the chordal distance u in Eq. (4.10) are given by

$$\partial_\mu \partial_{\nu'} u = -\frac{1}{z_0 w_0} \left(\delta_{\mu\nu'} + \frac{1}{w_0} (z - w)_\mu \delta_{\nu'0} + \frac{1}{z_0} (w - z)_{\nu'} \delta_{\mu0} - u \delta_{\mu0} \delta_{\nu'0} \right). \quad (4.13)$$

Therefore, $G_{\mu\nu'}(z, w)$ consists of four parts:

$$G_{\mu\nu'}(z, w) = G_{\mu\nu'}^1(z, w) + G_{\mu\nu'}^2(z, w) + G_{\mu\nu'}^3(z, w) + G_{\mu\nu'}^4(z, w). \quad (4.14)$$

Before we compute the Fourier transformation of these four terms, we rewrite the scalar propagator $F(u)$. We insert the chordal variable u and get

$$\begin{aligned} F(u) &= C \left(\frac{(z - w)^2}{2z_0 w_0} \left(2 + \frac{(z - w)^2}{2z_0 w_0} \right) \right)^{-(d-1)/2} \\ &= C 2^{(d-1)/2} \left(\frac{(z_0^2 + w_0^2 - 2z_0 w_0 + (\vec{z} - \vec{w})^2) \left(2 + \frac{z_0^2 + w_0^2 - 2z_0 w_0 + (\vec{z} - \vec{w})^2}{2z_0 w_0} \right)}{z_0 w_0} \right)^{\frac{1-d}{2}} \\ &= C 2^{d-1} \left(\frac{(z_0^2 + w_0^2 - 2z_0 w_0 + (\vec{z} - \vec{w})^2) (z_0^2 + w_0^2 + 2z_0 w_0 + (\vec{z} - \vec{w})^2)}{z_0^2 w_0^2} \right)^{\frac{1-d}{2}} \end{aligned}$$

$$\begin{aligned}
&= C \left(\frac{1}{2z_0 w_0} \right)^{1-d} \frac{1}{((z-w)^2(z-w^*)^2)^{\frac{d-1}{2}}} \\
&= C \left(\frac{1}{2z_0 w_0} \right)^{1-d} \frac{1}{(z_0^2 + w_0^2 + (\vec{z} - \vec{w})^2)^{d-1}} \frac{1}{(1-Y^2)^{\frac{d-1}{2}}} \\
&\qquad\qquad\qquad \text{with } Y = \frac{2z_0 w_0}{z_0^2 + w_0^2 + (\vec{z} - \vec{w})^2}.
\end{aligned} \tag{4.15}$$

Writing $F(u)$ as an infinite sum, we have

$$\begin{aligned}
F(u) &= C \left(\frac{2z_0 w_0}{z_0^2 + w_0^2 + (\vec{z} - \vec{w})^2} \right)^{d-1} \sum_{k=0}^{\infty} \frac{\Gamma(k + \frac{d-1}{2})}{\Gamma(\frac{d-1}{2})k!} Y^{2k} \\
&= C \sum_{k=0}^{\infty} \frac{\Gamma(k + \frac{d-1}{2})}{\Gamma(\frac{d-1}{2})k!} \left(\frac{2z_0 w_0}{z_0^2 + w_0^2 + (\vec{z} - \vec{w})^2} \right)^{2k-1+d} \\
&= \frac{\Gamma(\frac{d-1}{2})}{(4\pi)^{(d+1)/2}} \xi^{d-1} \sum_{k=0}^{\infty} \frac{\Gamma(k + \frac{d-1}{2})}{\Gamma(\frac{d-1}{2})\Gamma(k+1)} \xi^{2k} \\
&\qquad\qquad\qquad \text{with } \xi = \frac{2w_0 z_0}{z_0^2 + w_0^2 + (\vec{z} - \vec{w})^2}.
\end{aligned} \tag{4.16}$$

We define the Fourier transform of the bulk-to-bulk propagator $G_{\mu\nu'}(z, w)$ in Eq. (4.10) as

$$G_{\mu\nu'}(z_0, w_0, \vec{q}) = \int d^4x e^{i\vec{q}\cdot\vec{x}} G_{\mu\nu'}(z_0, w_0, \vec{x}) \quad \text{with } \vec{x} = \vec{z} - \vec{w}. \tag{4.17}$$

Then the Fourier transform of the first term of $G_{\mu\nu'}(z, w)$ is

$$\begin{aligned}
&G_{\mu\nu'}^1(z_0, w_0, \vec{q}) \\
&= \frac{1}{z_0 w_0} \delta_{\mu\nu'} \int d^4x e^{i\vec{q}\cdot\vec{x}} F(u) \\
&= \frac{1}{z_0 w_0} \delta_{\mu\nu'} \frac{\Gamma(\frac{d-1}{2})}{(4\pi)^{(d+1)/2}} \int d^4x e^{i\vec{q}\cdot\vec{x}} \sum_{k=0}^{\infty} \frac{\Gamma(k + \frac{d-1}{2})}{\Gamma(\frac{d-1}{2})\Gamma(k+1)} \left(\frac{2w_0 z_0}{z_0^2 + w_0^2 + \vec{x}^2} \right)^{2k+d-1}.
\end{aligned} \tag{4.18}$$

In order to evaluate the integral in Eq. (4.18), we introduce the Schwinger representation [40]. It reads

$$\begin{aligned}
I_m(x_0, \vec{q}) &= \int d^d x e^{i\vec{q}\cdot\vec{x}} \frac{1}{(x_0^2 + \vec{x}^2)^{m+1}} \\
&= \int d^d x e^{i\vec{q}\cdot\vec{x}} \left(\frac{1}{\Gamma(m+1)} \int_0^\infty d\tau \tau^m e^{-\tau(x_0^2 + \vec{x}^2)} \right) \\
&= \frac{\pi^{d/2}}{\Gamma(m+1)} \int_0^\infty d\tau \tau^{m-d/2} e^{-\tau x_0^2} e^{-\frac{\vec{q}^2}{4\tau}}
\end{aligned}$$

$$= \frac{2\pi^{d/2}}{\Gamma(m+1)} \left(\frac{|\vec{q}|}{2x_0} \right)^{m+1-d/2} K_{m+1-d/2}(|\vec{q}|x_0). \quad (4.19)$$

$K_m(x)$ is the modified Bessel function. We switch to $d = 4$ dimensions since this is the case of interest for us and apply the Schwinger representation. The Fourier transform of the first part of the bulk-to-bulk propagator is given by

$$\begin{aligned} G_{\mu\nu'}^1(z_0, w_0, \vec{q}) &= \delta_{\mu\nu'} \frac{\Gamma(\frac{3}{2})}{(4\pi)^{5/2}} \sum_{k=0}^{\infty} \frac{\Gamma(k + \frac{3}{2})}{\Gamma(\frac{3}{2})\Gamma(k+1)\Gamma(2k+3)} (2z_0w_0)^{2k+2} \\ &\quad \times \int d\tau \tau^{2k+2} \int d^4x e^{i\vec{q}\cdot\vec{x} - \tau(z_0^2 + w_0^2 + \vec{x}^2)} \\ &= \delta_{\mu\nu'} \frac{\Gamma(\frac{3}{2})}{(4\pi)^{5/2}} \sum_{k=0}^{\infty} \frac{\Gamma(k + \frac{3}{2})}{\Gamma(\frac{3}{2})\Gamma(k+1)\Gamma(2k+3)} (2w_0z_0)^{2k+2} \\ &\quad \times \pi^2 \int d\tau \tau^{2k} e^{-\tau(z_0^2 + w_0^2) - \frac{\vec{q}^2}{4\tau}} \\ &= \delta_{\mu\nu'} \sum_{k=0}^{\infty} \frac{(z_0w_0)^{2k+2}}{8\Gamma(k+1)\Gamma(k+2)} \left(\frac{\vec{q}^2}{4\bar{w}_0^2} \right)^{k+\frac{1}{2}} K_{2k+1}(|\vec{q}|\bar{w}_0). \end{aligned} \quad (4.20)$$

Here we have introduced the notation $\bar{w}_0 = \sqrt{z_0^2 + w_0^2}$. Next we consider the last term of $G_{\mu\nu'}(z, w)$ in Eq. (4.14). Compared to $G_{\mu\nu'}^1(z_0, w_0, \vec{q})$ it contains an additional factor u and different Kronecker symbols. It is given by

$$\begin{aligned} G_{\mu\nu'}^4(z, w) &= -\frac{1}{z_0w_0} \delta_{\mu 0} \delta_{\nu' 0} u F(u) \\ &= -C \delta_{\mu 0} \delta_{\nu' 0} \frac{1}{(z_0w_0)^2} 2^{d-2} (z_0^2 + w_0^2 - 2z_0w_0 + (\vec{z} - \vec{w})^2) \\ &\quad \times \left(\frac{(z_0^2 + w_0^2 - 2z_0w_0 + (\vec{z} - \vec{w})^2)(z_0^2 + w_0^2 + 2z_0w_0 + (\vec{z} - \vec{w})^2)}{z_0^2 w_0^2} \right)^{\frac{1-d}{2}} \\ &= -C \delta_{\mu 0} \delta_{\nu' 0} (z_0w_0)^{d-3} 2^{d-2} (z_0^2 + w_0^2 - 2z_0w_0 + (\vec{z} - \vec{w})^2) \\ &\quad \times \frac{1}{((z-w)^2(z-w^*)^2)^{\frac{d-1}{2}}} \\ &= -C \delta_{\mu 0} \delta_{\nu' 0} (z_0w_0)^{d-3} 2^{d-2} (z_0^2 + w_0^2 - 2z_0w_0 + (\vec{z} - \vec{w})^2) \\ &\quad \times \frac{1}{(z_0^2 + w_0^2 + (\vec{z} - \vec{w})^2)^{d-1}} \sum_{k=0}^{\infty} \frac{\Gamma(k + \frac{d-1}{2})}{\Gamma(\frac{d-1}{2})k!} \left(\frac{2z_0w_0}{z_0^2 + w_0^2 + (\vec{z} - \vec{w})^2} \right)^{2k} \\ &= -C \delta_{\mu 0} \delta_{\nu' 0} (z_0w_0)^{d-3} 2^{d-2} \sum_{k=0}^{\infty} \frac{\Gamma(k + \frac{d-1}{2})}{\Gamma(\frac{d-1}{2})k!} \\ &\quad \times \left[\frac{1}{(z_0^2 + w_0^2 + (\vec{z} - \vec{w})^2)^{d-2}} \left(\frac{2z_0w_0}{z_0^2 + w_0^2 + (\vec{z} - \vec{w})^2} \right)^{2k} \right. \\ &\quad \left. - \frac{1}{(z_0^2 + w_0^2 + (\vec{z} - \vec{w})^2)^{d-1}} \frac{(2z_0w_0)^{2k+1}}{(z_0^2 + w_0^2 + (\vec{z} - \vec{w})^2)^{2k}} \right]. \end{aligned} \quad (4.21)$$

Finally, we get

$$\begin{aligned}
G_{\mu\nu'}^4(z, w) &= -\delta_{\mu 0}\delta_{\nu' 0} \frac{\Gamma(\frac{d-1}{2})}{(4\pi)^{(d+1)/2}} 2^{d-2} \sum_{k=0}^{\infty} \frac{\Gamma(k + \frac{d-1}{2})}{\Gamma(\frac{d-1}{2})\Gamma(k+1)} \\
&\times \left[2^{2k} \frac{(z_0 w_0)^{2k+d-3}}{(z_0^2 + w_0^2 + (\vec{z} - \vec{w})^2)^{2k+d-2}} - 2^{2k+1} \frac{(z_0 w_0)^{2k+d-2}}{(z_0^2 + w_0^2 + (\vec{z} - \vec{w})^2)^{2k+d-1}} \right]. \tag{4.22}
\end{aligned}$$

The Fourier transform of $G_{\mu\nu'}^4(z_0, w_0, \vec{x})$ with $\vec{x} = \vec{z} - \vec{w}$ is defined as

$$\begin{aligned}
G_{\mu\nu'}^4(z_0, w_0, \vec{q}) &= -\delta_{\mu 0}\delta_{\nu' 0} \frac{\Gamma(\frac{d-1}{2})}{(4\pi)^{(d+1)/2}} 2^{d-2} \sum_{k=0}^{\infty} \frac{\Gamma(k + \frac{d-1}{2})}{\Gamma(\frac{d-1}{2})\Gamma(k+1)} \int d^d x e^{i\vec{q}\cdot\vec{x}} \\
&\times \left[2^{2k} \frac{(z_0 w_0)^{2k+d-3}}{(z_0^2 + w_0^2 + \vec{x}^2)^{2k+d-2}} - 2^{2k+1} \frac{(z_0 w_0)^{2k+d-2}}{(z_0^2 + w_0^2 + \vec{x}^2)^{2k+d-1}} \right]. \tag{4.23}
\end{aligned}$$

To perform the integral in $d = 4$ dimensions, we use the Schwinger representation, Eq. (4.19), again and get

$$\begin{aligned}
G_{\mu\nu'}^4(z_0, w_0, \vec{q}) &= -\delta_{\mu 0}\delta_{\nu' 0} \frac{\Gamma(\frac{3}{2})}{(4\pi)^{5/2}} 4 \sum_{k=0}^{\infty} \frac{\Gamma(k + \frac{3}{2})}{\Gamma(\frac{3}{2})\Gamma(k+1)} \\
&\times \left[2^{2k} (z_0 w_0)^{2k+1} \frac{1}{\Gamma(2k+2)} \int d\tau \tau^{2k+1} \int dx e^{i\vec{q}\cdot\vec{x} - \tau(z_0^2 + w_0^2 + \vec{x}^2)} \right. \\
&\quad \left. - 2^{2k+1} (z_0 w_0)^{2k+2} \frac{1}{\Gamma(2k+3)} \int d\tau \tau^{2k+2} \int dx e^{i\vec{q}\cdot\vec{x} - \tau(z_0^2 + w_0^2 + \vec{x}^2)} \right] \\
&= -\delta_{\mu 0}\delta_{\nu' 0} \frac{\Gamma(\frac{3}{2})}{(4\pi)^{5/2}} 4 \sum_{k=0}^{\infty} \frac{\Gamma(k + \frac{3}{2})}{\Gamma(\frac{3}{2})\Gamma(k+1)} \\
&\times \left[\frac{2^{2k} (z_0 w_0)^{2k+1}}{\Gamma(2k+2)} \pi^2 \int d\tau \tau^{2k-1} e^{-\tau(w_0^2 + z_0^2) - \frac{\vec{q}^2}{4\tau}} \right. \\
&\quad \left. - \frac{2^{2k+1} (z_0 w_0)^{2k+2}}{\Gamma(2k+3)} \pi^2 \int d\tau \tau^{2k} e^{-\tau(w_0^2 + z_0^2) - \frac{\vec{q}^2}{4\tau}} \right] \\
&= -\delta_{\mu 0}\delta_{\nu' 0} \frac{\Gamma(\frac{3}{2})}{(4\pi)^{5/2}} 4 \sum_{k=0}^{\infty} \frac{\Gamma(k + \frac{3}{2})}{\Gamma(\frac{3}{2})\Gamma(k+1)} \\
&\times \left[\frac{2^3 \pi^2}{\Gamma(2k+2)} \left(\frac{\vec{q}^2}{\vec{\omega}_0^2} \right)^k (z_0 w_0)^{2k+1} K_{2k}(|\vec{q}|\vec{\omega}_0) \right. \\
&\quad \left. - \frac{2^3 \pi^2}{\Gamma(2k+3)} \left(\frac{\vec{q}^2}{\vec{\omega}_0^2} \right)^{k+\frac{1}{2}} (z_0 w_0)^{2k+2} K_{2k+1}(|\vec{q}|\vec{\omega}_0) \right]
\end{aligned}$$

$$\begin{aligned}
&= -\delta_{\mu 0}\delta_{\nu' 0} \left[\frac{2^{-2k-3}}{\Gamma(1+k)\Gamma(1+k)} (z_0 w_0)^{2k+1} \left(\frac{\vec{q}^2}{\vec{\omega}_0^2} \right)^k K_{2k}(|\vec{q}|\vec{\omega}_0) \right. \\
&\quad \left. - \frac{2^{-2k-4}}{\Gamma(1+k)\Gamma(2+k)} (z_0 w_0)^{2k+2} \left(\frac{\vec{q}^2}{\vec{\omega}_0^2} \right)^{k+\frac{1}{2}} K_{2k+1}(|\vec{q}|\vec{\omega}_0) \right]. \quad (4.24)
\end{aligned}$$

In order to obtain the Fourier transform of the full bulk-to-bulk propagator, we still have to transform the second and the third term of $G_{\mu\nu'}(z, w)$ in Eq. (4.14). The second term is

$$\begin{aligned}
G_{\mu\nu'}^2(z, w) &= \frac{1}{z_0 w_0^2} (z-w)_\mu \delta_{\nu' 0} F(u) \\
&= C \delta_{\nu' 0} \frac{1}{z_0 w_0^2} ((z_0 - w_0)\delta_{\mu 0} + (z-w)_j \delta_{\mu j}) \frac{(2z_0 w_0)^{d-1}}{((z-w)^2 (z-w^*)^2)^{\frac{d-1}{2}}} \\
&= C \delta_{\nu' 0} \frac{(2z_0 w_0)^{d-1}}{z_0 w_0^2} ((z_0 - w_0)\delta_{\mu 0} + (z-w)_j \delta_{\mu j}) \\
&\quad \times \frac{1}{(z_0^2 + w_0^2 + (\vec{z} - \vec{w})^2)^{d-1}} \sum_{k=0}^{\infty} \frac{\Gamma(k + \frac{d-1}{2})}{\Gamma(\frac{d-1}{2})k!} \left(\frac{2z_0 w_0}{z_0^2 + w_0^2 + (\vec{z} - \vec{w})^2} \right)^{2k} \\
&= \frac{\Gamma(\frac{d-1}{2})}{(4\pi)^{(d+1)/2}} \delta_{\nu' 0} \frac{(2z_0 w_0)^{d-1}}{z_0 w_0^2} \\
&\quad \times \left[\frac{(z_0 - w_0)\delta_{\mu 0}}{(z_0^2 + w_0^2 + (\vec{z} - \vec{w})^2)^{d-1}} \sum_{k=0}^{\infty} \frac{\Gamma(k + \frac{d-1}{2})}{\Gamma(\frac{d-1}{2})k!} \left(\frac{2z_0 w_0}{z_0^2 + w_0^2 + (\vec{z} - \vec{w})^2} \right)^{2k} \right. \\
&\quad \left. + \delta_{\mu j} \sum_{k=0}^{\infty} \frac{\Gamma(k + \frac{d-1}{2})}{\Gamma(\frac{d-1}{2})k!} \partial_{x_j} \frac{(2z_0 w_0)^{2k}}{(z_0^2 + w_0^2 + (\vec{z} - \vec{w})^2)^{2k+d-2}} \frac{1}{2(-2k-d+2)} \right]. \quad (4.25)
\end{aligned}$$

Its Fourier transform reads

$$\begin{aligned}
&G_{\mu\nu'}^2(z_0, w_0, \vec{q}) \\
&= \delta_{\nu' 0} \frac{\Gamma(\frac{d-1}{2})}{(4\pi)^{(d+1)/2}} \frac{(2z_0 w_0)^{d-1}}{z_0 w_0^2} \int d^4 x e^{i\vec{q}\cdot\vec{x}} \\
&\quad \times \left[\frac{(z_0 - w_0)\delta_{\mu 0}}{(z_0^2 + w_0^2 + \vec{x}^2)^{d-1}} \sum_{k=0}^{\infty} \frac{\Gamma(k + \frac{d-1}{2})}{\Gamma(\frac{d-1}{2})k!} \left(\frac{2z_0 w_0}{z_0^2 + w_0^2 + \vec{x}^2} \right)^{2k} \right. \\
&\quad \left. + \delta_{\mu j} \sum_{k=0}^{\infty} \frac{\Gamma(k + \frac{d-1}{2})}{\Gamma(\frac{d-1}{2})k!} \partial_{x_j} \frac{(2z_0 w_0)^{2k}}{(z_0^2 + w_0^2 + \vec{x}^2)^{2k+d-2}} \frac{1}{2(-2k-d+2)} \right]. \quad (4.26)
\end{aligned}$$

In $d = 4$ dimensions, we get

$$\begin{aligned}
G_{\mu\nu'}^2(z_0, w_0, \vec{q}) &= \delta_{\nu'0} \frac{\Gamma(\frac{3}{2})}{(4\pi)^{5/2}} \frac{(2z_0w_0)^3}{z_0w_0^2} \int d^4x e^{i\vec{q}\cdot\vec{x}} \\
&\times \left[(z_0 - w_0)\delta_{\mu 0} \sum_{k=0}^{\infty} \frac{\Gamma(k + \frac{3}{2})}{\Gamma(\frac{3}{2})\Gamma(k+1)} \frac{(2z_0w_0)^{2k}}{(z_0^2 + w_0^2 + \vec{x}^2)^{2k+3}} \right. \\
&\quad \left. + iq_j\delta_{\mu j} \sum_{k=0}^{\infty} \frac{\Gamma(k + \frac{3}{2})}{\Gamma(\frac{3}{2})\Gamma(k+1)} \frac{1}{2(2k+2)} \frac{(2z_0w_0)^{2k}}{(z_0^2 + w_0^2 + \vec{x}^2)^{2k+2}} \right].
\end{aligned} \tag{4.27}$$

We use the Schwinger representation in Eq. (4.19) once again and arrive at

$$\begin{aligned}
G_{\mu\nu'}^2(z_0, w_0, \vec{q}) &= \delta_{\nu'0} \frac{\Gamma(\frac{3}{2})}{(4\pi)^{5/2}} \frac{(2z_0w_0)^3}{z_0w_0^2} \sum_{k=0}^{\infty} \frac{\Gamma(k + \frac{3}{2})}{\Gamma(\frac{3}{2})\Gamma(k+1)} (2z_0w_0)^{2k} \\
&\times \left[(z_0 - w_0)\delta_{\mu 0} \frac{1}{\Gamma(2k+3)} \int d\tau \tau^{2k+2} \int dx e^{i\vec{q}\cdot\vec{x} - \tau(z_0^2 + w_0^2 + \vec{x}^2)} \right. \\
&\quad \left. + iq_j\delta_{\mu j} \frac{1}{2(2k+2)} \frac{1}{\Gamma(2k+2)} \int d\tau \tau^{2k+1} \int dx e^{i\vec{q}\cdot\vec{x} - \tau(z_0^2 + w_0^2 + \vec{x}^2)} \right] \\
&= \delta_{\nu'0} \frac{\Gamma(\frac{3}{2})}{(4\pi)^{5/2}} \frac{(2z_0w_0)^3}{z_0w_0^2} \sum_{k=0}^{\infty} \frac{\Gamma(k + \frac{3}{2})}{\Gamma(\frac{3}{2})\Gamma(k+1)} (2z_0w_0)^{2k} \\
&\times \left[(z_0 - w_0)\delta_{\mu 0} \frac{1}{\Gamma(2k+3)} \pi^2 \int d\tau \tau^{2k} e^{-\tau(z_0^2 + w_0^2) - \frac{\vec{q}^2}{4\tau}} \right. \\
&\quad \left. + iq_j\delta_{\mu j} \frac{1}{2(2k+2)} \frac{1}{\Gamma(2k+2)} \pi^2 \int d\tau \tau^{2k-1} e^{-\tau(z_0^2 + w_0^2) - \frac{\vec{q}^2}{4\tau}} \right] \\
&= \delta_{\nu'0} z_0^{2k+2} w_0^{2k+1} \frac{2^{-2k-4}}{\Gamma(1+k)\Gamma(2+k)} \\
&\times \left[(z_0 - w_0)\delta_{\mu 0} \left(\frac{\vec{q}^2}{\bar{\omega}_0^2}\right)^{k+\frac{1}{2}} K_{2k+1}(|\vec{q}|\bar{\omega}_0) + iq_j\delta_{\mu j} \left(\frac{\vec{q}^2}{\bar{\omega}_0^2}\right)^k K_{2k}(|\vec{q}|\bar{\omega}_0) \right].
\end{aligned} \tag{4.28}$$

Finally, we consider the third term in $G_{\mu\nu'}(z, w)$:

$$G_{\mu\nu'}^3(z, w) = \frac{1}{z_0^2 w_0} (z - w)_{\nu'} \delta_{\mu 0} F(u). \tag{4.29}$$

The Fourier transform of $G_{\mu\nu'}^3(z, w)$ can be deduced from $G_{\mu\nu'}^2(z_0, w_0, \vec{q})$ since

$$G_{\mu\nu'}^3(z, w) = -\frac{w_0}{z_0} G_{\nu'\mu}^2(z, w). \tag{4.30}$$

Thus, the Fourier transform is given by

$$\begin{aligned}
G_{\mu\nu'}^3(z_0, w_0, \vec{q}) &= -\delta_{\mu 0} z_0^{2k+1} w_0^{2k+2} \frac{2^{-2k-4}}{\Gamma(1+k)\Gamma(2+k)} \\
&\times \left[(z_0 - w_0) \delta_{\nu' 0} \left(\frac{\vec{q}^2}{\bar{\omega}_0^2} \right)^{k+\frac{1}{2}} K_{2k+1}(|\vec{q}|\bar{\omega}_0) + i q_j \delta_{\nu' j} \left(\frac{\vec{q}^2}{\bar{\omega}_0^2} \right)^k K_{2k}(|\vec{q}|\bar{\omega}_0) \right]. \tag{4.31}
\end{aligned}$$

Altogether, the bulk-to-bulk propagator of the gauge boson in momentum space reads

$$\begin{aligned}
G_{\mu\nu'}(z_0, w_0, \vec{q}) &= G_{\mu\nu'}^1 + G_{\mu\nu'}^2 + G_{\mu\nu'}^3 + G_{\mu\nu'}^4 \\
&= \delta_{\mu\nu'} \sum_{k=0}^{\infty} \frac{2^{-2k-4}}{\Gamma(1+k)\Gamma(2+k)} (w_0 z_0)^{2k+2} \left(\frac{\vec{q}^2}{\bar{\omega}_0^2} \right)^{k+\frac{1}{2}} K_{2k+1}(|\vec{q}|\bar{\omega}_0) \\
&\quad - \delta_{\mu 0} \delta_{\nu' 0} \left(\sum_{k=0}^{\infty} \frac{2^{-2k-3}}{\Gamma(1+k)\Gamma(1+k)} (w_0 z_0)^{2k+1} \left(\frac{\vec{q}^2}{\bar{\omega}_0^2} \right)^k K_{2k}(|\vec{q}|\bar{\omega}_0) \right. \\
&\quad \quad \left. - \sum_{k=0}^{\infty} \frac{2^{-2k-4}}{\Gamma(1+k)\Gamma(2+k)} (w_0 z_0)^{2k+2} \left(\frac{\vec{q}^2}{\bar{\omega}_0^2} \right)^{k+\frac{1}{2}} K_{2k+1}(|\vec{q}|\bar{\omega}_0) \right) \\
&\quad + \delta_{\mu 0} \delta_{\nu' 0} \sum_{k=0}^{\infty} \frac{2^{-2k-4}}{\Gamma(1+k)\Gamma(2+k)} (w_0 z_0)^{2k+1} \left(\frac{\vec{q}^2}{\bar{\omega}_0^2} \right)^{k+\frac{1}{2}} \\
&\quad \quad \quad \times (z_0 - w_0)^2 K_{2k+1}(|\vec{q}|\bar{\omega}_0) \\
&\quad + \delta_{\nu' 0} \delta_{\mu j} i q_j \sum_{k=0}^{\infty} \frac{2^{-2k-4}}{\Gamma(1+k)\Gamma(2+k)} z_0^{2k+2} w_0^{2k+1} \left(\frac{\vec{q}^2}{\bar{\omega}_0^2} \right)^k K_{2k}(|\vec{q}|\bar{\omega}_0) \\
&\quad - \delta_{\mu 0} \delta_{\nu' j} i q_j \sum_{k=0}^{\infty} \frac{2^{-2k-4}}{\Gamma(1+k)\Gamma(2+k)} z_0^{2k+1} w_0^{2k+2} \left(\frac{\vec{q}^2}{\bar{\omega}_0^2} \right)^k K_{2k}(|\vec{q}|\bar{\omega}_0). \tag{4.32}
\end{aligned}$$

Now we specify the propagator depending on whether the second index ν' is equal j or 0. First, we choose $\nu' = j$,

$$\begin{aligned}
G_{\mu j}(z_0, w_0, \vec{q}) &= \sum_{k=0}^{\infty} \frac{2^{-3} z_0 w_0}{\Gamma(1+k)\Gamma(2+k)} \\
&\times \left[\delta_{\mu j} \left(\frac{z_0^2 w_0^2 \vec{q}^2}{4\bar{\omega}_0^2} \right)^{k+\frac{1}{2}} K_{2k+1}(|\vec{q}|\bar{\omega}_0) - \delta_{\mu 0} \frac{i}{2} q_j w_0 \left(\frac{z_0^2 w_0^2 \vec{q}^2}{4\bar{\omega}_0^2} \right)^k K_{2k}(|\vec{q}|\bar{\omega}_0) \right]. \tag{4.33}
\end{aligned}$$

The second expression with $\nu' = 0$ is

$$\begin{aligned}
G_{\mu 0}(z_0, w_0, \vec{q}) &= \sum_{k=0}^{\infty} \frac{2^{-3} z_0 w_0}{\Gamma(1+k)\Gamma(2+k)} \\
&\times \left[\delta_{\mu 0} \frac{\bar{w}_0^2}{z_0 w_0} \left(\frac{z_0^2 w_0^2 \vec{q}^2}{4\bar{w}_0^2} \right)^{k+\frac{1}{2}} K_{2k+1}(|\vec{q}|\bar{w}_0) + \delta_{\mu j} \frac{i}{2} q_j z_0 \left(\frac{z_0^2 w_0^2 \vec{q}^2}{4\bar{w}_0^2} \right)^k K_{2k}(|\vec{q}|\bar{w}_0) \right. \\
&\left. - \delta_{\mu 0}(k+1) \left(\frac{z_0^2 w_0^2 \vec{q}^2}{4\bar{w}_0^2} \right)^k K_{2k}(|\vec{q}|\bar{w}_0) \right]. \tag{4.34}
\end{aligned}$$

4.1.2 Bulk-to-Boundary Propagator of the Gauge Boson

The bulk-to-boundary propagator of the gauge boson [34] is given by

$$G_{\mu j}(z, \vec{x}) = N_d \delta_{\mu j} \frac{z_0^{d-2}}{(z_0^2 + (\vec{z} - \vec{x})^2)^{d-1}} - N_d \delta_{\mu 0} \frac{z_0^{d-3} (z-x)_j}{(z_0^2 + (\vec{z} - \vec{x})^2)^{d-1}} \tag{4.35}$$

with the normalization

$$N_d = \frac{(d-2)\Gamma(d)}{2\pi^{d/2}(d-1)\Gamma(d/2)}. \tag{4.36}$$

Due to this normalization, the bulk-to-boundary propagator $G_{ij}(z, \vec{x})$ becomes $\delta_{ij}\delta^{(d)}(\vec{z} - \vec{x})$ in the limit $z_0 \rightarrow 0$. The expression (4.35) is valid for $d > 2$.

To obtain the propagator in momentum space, we Fourier transform the propagator in Eq. (4.35):

$$\begin{aligned}
G_{\mu j}(z_0, \vec{p}) &= \int d^4 x e^{i\vec{p}\cdot(\vec{z}-\vec{x})} G_{\mu j}(z, \vec{x}) \\
&= N_d \delta_{\mu j} \int d^4 x e^{i\vec{p}\cdot(\vec{z}-\vec{x})} \frac{z_0^{d-2}}{(z_0^2 + (\vec{z} - \vec{x})^2)^{d-1}} \\
&\quad - N_d \delta_{\mu 0} \int d^4 x e^{i\vec{p}\cdot(\vec{z}-\vec{x})} \frac{z_0^{d-3} (z-x)_j}{(z_0^2 + (\vec{z} - \vec{x})^2)^{d-1}}. \tag{4.37}
\end{aligned}$$

We substitute $\vec{x} \rightarrow -\vec{x}' + \vec{z}$ in the integrand and get

$$\begin{aligned}
G_{\mu j}(z_0, \vec{p}) &= N_d \delta_{\mu j} \int d^4 x e^{i\vec{p}\cdot\vec{x}'} \frac{z_0^{d-2}}{(z_0^2 + \vec{x}'^2)^{d-1}} \\
&\quad - \frac{N_d}{2(d-2)} \delta_{\mu 0} \int d^4 x e^{i\vec{p}\cdot\vec{x}'} \partial_{x_j} \frac{z_0^{d-3}}{(z_0^2 + \vec{x}'^2)^{d-2}} \\
&= N_d \delta_{\mu j} \int d^4 x e^{i\vec{p}\cdot\vec{x}'} \frac{z_0^{d-2}}{(z_0^2 + \vec{x}'^2)^{d-1}} \\
&\quad - \frac{N_d}{2(d-2)} \delta_{\mu 0} \int d^4 x e^{i\vec{p}\cdot\vec{x}'} i p_j \frac{z_0^{d-3}}{(z_0^2 + \vec{x}'^2)^{d-2}}. \tag{4.38}
\end{aligned}$$

The Schwinger representation, Eq. (4.19), in $d = 4$ dimensions is used to evaluate the integrals:

$$\begin{aligned}
G_{\mu j}(z_0, \vec{p}) &= \delta_{\mu j} \frac{N_4 z_0^2}{\Gamma(3)} \int d\tau \tau^2 \int d^4 x e^{i\vec{p}\cdot\vec{x}' - \tau(z_0^2 + \vec{x}'^2)} \\
&\quad + \frac{i N_4 z_0 p_j}{4\Gamma(2)} \delta_{\mu 0} \int d\tau \tau \int d^4 x e^{i\vec{p}\cdot\vec{x}' - \tau(z_0^2 + \vec{x}'^2)} \\
&= \delta_{\mu j} \frac{N_4 z_0^2 \pi^2}{2} \int d\tau e^{-\tau z_0^2 - \frac{p^2}{4\tau}} + i p_j \frac{N_4 z_0 \pi^2}{4} \delta_{\mu 0} \int d\tau \tau^{-1} e^{-\tau z_0^2 - \frac{p^2}{4\tau}} \\
&= \delta_{\mu j} \frac{N_4 \pi^2}{2} z_0 |\vec{p}| K_1(|\vec{p}| z_0) + \delta_{\mu 0} i p_j \frac{N_4 \pi^2}{2} z_0 K_0(|\vec{p}| z_0). \tag{4.39}
\end{aligned}$$

The normalization constant N_4 can be read off from Eq. (4.36). It is $N_4 = 2/\pi^2$. The bulk-to-boundary propagator of the gauge boson in momentum space finally reads

$$G_{\mu j}(z_0, \vec{p}) = z_0 [|\vec{p}| \delta_{\mu j} K_1(|\vec{p}| z_0) + i p_j \delta_{\mu 0} K_0(|\vec{p}| z_0)]. \tag{4.40}$$

4.1.3 Bulk-to-Bulk Propagator of the Graviton

We consider the bulk-to-bulk propagator of the graviton [56]:

$$G_{\mu\nu; \mu'\nu'} = (\partial_\mu \partial_{\mu'} u \partial_\nu \partial_{\nu'} u + \partial_\mu \partial_{\nu'} u \partial_\nu \partial_{\mu'} u) G(u) + g_{\mu\nu} g_{\mu'\nu'} H(u) + \dots \tag{4.41}$$

The dots symbolize terms of the form $\partial_\rho X$ with $\rho = \mu, \mu', \nu, \nu'$. The functions $G(u)$ and $H(u)$ are the physical terms of the propagator, see Ref. [56]. The derivatives of the chordal distance u in Eq. (4.41) have already been given in Eq. (4.13). $G(u)$ is the massless scalar propagator. It reads

$$G(u) = C_d 2^d u^{-d} {}_2F_1(d, (d+1)/2; d+1; -2u^{-1}) \quad \text{with} \quad C_d = \frac{\Gamma(\frac{d+1}{2})}{(4\pi)^{\frac{d+1}{2}} d}. \tag{4.42}$$

F denotes the hypergeometric function. An explicit expression for $H(u)$ can be found in Ref. [56]. In $d = 4$ dimensions, the massless scalar propagator can be written as

$$G(u) = -\frac{1}{8\pi^2} \left(\frac{(1+u)(2(1+u)^2 - 3)}{(u(2+u))^{\frac{3}{2}}} - 2 \right). \tag{4.43}$$

We insert the chordal distance, Eq. (4.11), and arrive at

$$\begin{aligned}
G(z, w) &= -\frac{1}{8\pi^2} \left(-2 + \frac{4(z_0^2 + w_0^2 + (\bar{z} - \bar{w})^2)(-3 + \frac{(z_0^2 + w_0^2 + (\bar{z} - \bar{w})^2)^2}{2z_0^2 w_0^2})z_0^2 w_0^2}{((z_0^2 + w_0^2 - 2z_0 w_0 + (\bar{z} - \bar{w})^2)(z_0^2 + w_0^2 + 2z_0 w_0 + (\bar{z} - \bar{w})^2))^{\frac{3}{2}}} \right) \\
&= -\frac{1}{4\pi^2} \left(-1 + \frac{2(z_0^2 + w_0^2 + (\bar{z} - \bar{w})^2)(-3z_0^2 w_0^2 + \frac{1}{2}(z_0^2 + w_0^2 + (\bar{z} - \bar{w})^2)^2)}{((\bar{w} - \bar{z})^2(\bar{w} - \bar{z}^*)^2)^{\frac{3}{2}}} \right) \\
&= -\frac{1}{4\pi^2} \left(-1 + \frac{2(-3z_0^2 w_0^2 + \frac{1}{2}(z_0^2 + w_0^2 + (\bar{z} - \bar{w})^2)^2)}{(z_0^2 + w_0^2 + (\bar{w} - \bar{z})^2)^2} \frac{1}{(1 - Y^2)^{\frac{3}{2}}} \right), \\
&\qquad\qquad\qquad \text{again with } Y = \frac{2z_0 w_0}{z_0^2 + w_0^2 + (\bar{z} - \bar{w})^2}.
\end{aligned} \tag{4.44}$$

We rewrite this as

$$\begin{aligned}
G(z, w) &= -\frac{1}{4\pi^2} \left(-1 + \frac{2(-3z_0^2 w_0^2 + \frac{1}{2}(z_0^2 + w_0^2 + (\bar{z} - \bar{w})^2)^2)}{(z_0^2 + w_0^2 + (\bar{z} - \bar{w})^2)^2} \sum_{k=0}^{\infty} \frac{\Gamma(k + \frac{3}{2})}{\Gamma(\frac{3}{2})k!} Y^{2k} \right) \\
&= -\frac{1}{4\pi^2} \left(-1 + \sum_{k=0}^{\infty} \frac{\Gamma(k + \frac{3}{2})}{\Gamma(\frac{3}{2})k!} \frac{(2z_0 w_0)^{2k} (-6z_0^2 w_0^2 + (z_0^2 + w_0^2 + (\bar{z} - \bar{w})^2)^2)}{(z_0^2 + w_0^2 + (\bar{z} - \bar{w})^2)^{2k+2}} \right) \\
&= -\frac{1}{4\pi^2} \left(-1 + \sum_{k=0}^{\infty} \frac{\Gamma(k + \frac{3}{2})}{\Gamma(\frac{3}{2})k!} (2z_0 w_0)^{2k} \frac{-6z_0^2 w_0^2}{(z_0^2 + w_0^2 + (\bar{z} - \bar{w})^2)^{2k+2}} \right. \\
&\quad \left. + \sum_{k=0}^{\infty} \frac{\Gamma(k + \frac{3}{2})}{\Gamma(\frac{3}{2})k!} (2z_0 w_0)^{2k} \frac{1}{(z_0^2 + w_0^2 + (\bar{z} - \bar{w})^2)^{2k}} \right) \\
&= -\frac{1}{4\pi^2} \left(-1 + \sum_{k=0}^{\infty} \frac{\Gamma(k + \frac{3}{2})}{\Gamma(\frac{3}{2})k!} (2w_0 z_0)^{2k} \frac{-6z_0^2 w_0^2}{(z_0^2 + w_0^2 + (\bar{z} - \bar{w})^2)^{2k+2}} \right. \\
&\quad \left. + 1 + \sum_{k=1}^{\infty} \frac{\Gamma(k + \frac{3}{2})}{\Gamma(\frac{3}{2})k!} (2z_0 w_0)^{2k} \frac{1}{(z_0^2 + w_0^2 + (\bar{z} - \bar{w})^2)^{2k}} \right). \tag{4.45}
\end{aligned}$$

The substitution $k \rightarrow k' = k + 1$ leads to

$$\begin{aligned}
G(z, w) &= -\frac{1}{4\pi^2} \sum_{k=0}^{\infty} \frac{\Gamma(k + \frac{3}{2})}{\Gamma(\frac{3}{2})k!} (2z_0 w_0)^{2k} \\
&\quad \times \left(\frac{-6z_0^2 w_0^2}{(z_0^2 + w_0^2 + (\bar{z} - \bar{w})^2)^{2k+2}} + \frac{k + \frac{3}{2}}{k + 1} \frac{(2z_0 w_0)^2}{(z_0^2 + w_0^2 + (\bar{z} - \bar{w})^2)^{2k}} \right) \\
&= \frac{1}{2\pi^2} \sum_{k=0}^{\infty} \frac{\Gamma(k + \frac{3}{2})k}{\Gamma(\frac{3}{2})(k + 1)!} \frac{2^{2k} (z_0 w_0)^{2k+2}}{(z_0^2 + w_0^2 + (\bar{z} - \bar{w})^2)^{2k+2}}. \tag{4.46}
\end{aligned}$$

We substitute $\vec{x} = \vec{z} - \vec{w}$, and the Fourier transform reads

$$\begin{aligned}
G(z_0, w_0, \vec{q}) &= \int d^4x e^{i\vec{q}\cdot\vec{x}} G(z_0, w_0, \vec{x}) \\
&= \frac{1}{2\pi^2} \int d^4x e^{i\vec{q}\cdot\vec{x}} \sum_{k=0}^{\infty} \frac{\Gamma(k + \frac{3}{2})k}{\Gamma(\frac{3}{2})(k+1)!} \frac{2^{2k}(z_0w_0)^{2k+2}}{(z_0^2 + w_0^2 + \vec{x}^2)^{2k+2}} \\
&= \frac{1}{2\pi^2} \sum_{k=0}^{\infty} \frac{\Gamma(k + \frac{3}{2})k}{\Gamma(\frac{3}{2})(k+1)!} \frac{2^{2k}(z_0w_0)^{2k+2}}{\Gamma(2k+2)} \int d\tau \tau^{2k+1} \int d^4x e^{i\vec{q}\cdot\vec{x} - \tau(z_0^2 + w_0^2 + \vec{x}^2)} \\
&= \frac{1}{2\pi^2} \sum_{k=0}^{\infty} \frac{\Gamma(k + \frac{3}{2})k}{\Gamma(\frac{3}{2})(k+1)!} \frac{2^{2k}(z_0w_0)^{2k+2}}{\Gamma(2k+2)} \pi^2 \int d\tau \tau^{2k-1} e^{-\tau(z_0^2 + w_0^2) - \frac{\vec{q}^2}{4\tau}} \\
&= \frac{1}{2} \sum_{k=0}^{\infty} \frac{\Gamma(k + \frac{3}{2})k}{\Gamma(\frac{3}{2})\Gamma(2k+2)(k+1)!} 2^{2k}(z_0w_0)^{2k+2} 2^{1-2k} \left(\frac{\vec{q}^2}{\bar{\omega}_0^2}\right)^k K_{2k}(|\vec{q}|\bar{\omega}_0).
\end{aligned} \tag{4.47}$$

The term with $k = 0$ does not contribute to the sum, we substitute $k \rightarrow k' = k + 1$ again and arrive at

$$\begin{aligned}
G(z_0, w_0, \vec{q}) &= \sum_{k=0}^{\infty} \frac{\Gamma(k + \frac{5}{2})(k+1)}{\Gamma(\frac{3}{2})\Gamma(2k+4)(k+2)!} (w_0z_0)^{2k+4} \left(\frac{\vec{q}^2}{\bar{\omega}_0^2}\right)^{k+1} K_{2k+2}(|\vec{q}|\bar{\omega}_0) \\
&= \sum_{k=0}^{\infty} \frac{1}{2^{2(1+k)}} \frac{1}{\Gamma(1+k)\Gamma(3+k)} (w_0z_0)^{2k+4} \left(\frac{\vec{q}^2}{\bar{\omega}_0^2}\right)^{k+1} K_{2k+2}(|\vec{q}|\bar{\omega}_0).
\end{aligned} \tag{4.48}$$

This is the Fourier transform of the massless scalar propagator $G(u)$. In the full bulk-to-bulk propagator, Eq. (4.41), $G(u)$ is multiplied with the derivatives of the chordal variable u , which are given in Eq. (4.13). In the following, it turns out that only the first term in Eq. (4.13), proportional to one Kronecker symbol, contributes in the Regge limit. The term proportional to $H(u)$ in the bulk-to-bulk propagator does not contribute in the Regge limit as well. Accordingly, we define the part of the bulk-to-bulk graviton propagator, which gives the leading contribution the Regge limit in momentum space as

$$\begin{aligned}
G_{\mu\nu;\mu'\nu'}^{(1)}(z_0, w_0, \vec{q}) \\
:= (\delta_{\mu\mu'}\delta_{\nu\nu'} + \delta_{\mu\nu'}\delta_{\nu\mu'}) \sum_{k=0}^{\infty} \frac{(z_0w_0)^{2k+2}}{\Gamma(1+k)\Gamma(3+k)} \left(\frac{\vec{q}^2}{4\bar{\omega}_0^2}\right)^{k+1} K_{2k+2}(|\vec{q}|\bar{\omega}_0).
\end{aligned} \tag{4.49}$$

4.2 Graviton Exchange

We compute the amplitude $\mathcal{A}(|\vec{p}_i|, s, t)$ of the graviton exchange diagram shown in Fig. 4.2(a) in the Regge limit, see Eq. (4.6). We switch to the Minkowski metric

$g = \text{diag}(+, -, -, -)$, but for simplicity we continue using the previous notation. That means the four vector \vec{p}_j now stands for $(p_{j;4}, p_{j;1}, p_{j;2}, p_{j;3})$ with $|\vec{p}_j|^2 = -p_{j;4}^2 + p_{j;1}^2 + p_{j;2}^2 + p_{j;3}^2 = -p_j^2$. Latin indices continue to run from 1 to 4, and Greek indices run from 0 to 4.

The contribution of one graviton exchange in the t -channel to the four point function of R -currents is

$$I^{\text{GR}} = \frac{1}{4} \int \frac{d^4 z dz_0}{z_0} \int \frac{d^4 w dw_0}{w_0} T_{(13)\mu\nu}(z) G_{\mu\nu;\mu'\nu'}(z, w) T_{(24)\mu'\nu'}(w). \quad (4.50)$$

Here we suppress some multiplicative constants, which can be restored from the action (4.8). The graviton exchange in the t -channel is described by the bulk-to-bulk propagator of the graviton $G_{\mu\nu;\mu'\nu'}(z, w)$. The coupling of the R -currents inserted at the boundary of AdS_5 to the exchanged graviton is given by the so-called stress-energy tensor $T_{(13)\mu\nu}(z)$. The index (13) denotes the stress-energy tensor for R -currents inserted at the points \vec{x}_1 and \vec{x}_3 at the boundary. A similar definition is valid for the stress-energy tensor $T_{(24)\mu'\nu'}(w)$. The explicit coupling between the R -currents and the graviton is mediated by the bulk-to-boundary propagator of the gauge boson, which is included in the stress-energy tensor. In the next paragraph, we compute the stress-energy tensor in momentum space.

4.2.1 Stress-Energy Tensor

The stress-energy tensor is defined as

$$T_{\mu\nu} = -\frac{2}{\sqrt{g}} \frac{\partial S_m}{\partial g^{\mu\nu}} = -2 \frac{\partial S_m}{\partial g^{\mu\nu}} + g^{\mu\nu} S_m \quad (4.51)$$

with the matter action S_m given in Eq. (4.8). The definition of the stress-energy tensor results in

$$\begin{aligned} T_{\mu\nu} &= F_{\mu\rho} F_{\nu}^{\rho} - \frac{1}{4} g_{\mu\nu} F_{\rho\sigma} F^{\rho\sigma} \\ &= \partial_{[\mu} A_{\rho]} \partial_{[\nu} A^{\rho]} - \frac{1}{4} g_{\mu\nu} \partial_{[\rho} A_{\sigma]} \partial^{[\rho} A^{\sigma]}. \end{aligned} \quad (4.52)$$

The square brackets denote antisymmetrization in the indices. The gauge boson field in the bulk $A_\mu(z)$ is connected with the boundary field $A_i(\vec{x})$ by the bulk-to-boundary propagator of the gauge boson:

$$A_\mu(z) = \int d^4 \vec{x} G_{\mu i}(z, \vec{x}) A_i(\vec{x}). \quad (4.53)$$

Relation (4.53) and variation of the stress-energy tensor with respect to the boundary field $A_i(\vec{x})$ leads to

$$\begin{aligned} T_{(13)\mu\nu} &= z_0^2 \partial_{[\mu} G_{\rho]k_3}(z, \vec{x}_3) \partial_{[\nu} G_{\rho]k_1}(z, \vec{x}_1) + z_0^2 \partial_{[\mu} G_{\rho]k_1}(z, \vec{x}_1) \partial_{[\nu} G_{\rho]k_3}(z, \vec{x}_3) \\ &\quad - \frac{1}{2} z_0^2 g_{\mu\nu} \partial_{[\rho} G_{\sigma]k_1}(z, \vec{x}_1) \partial_{[\rho} G_{\sigma]k_3}(z, \vec{x}_3). \end{aligned} \quad (4.54)$$

A similar expression exists for $T_{(24)\mu'\nu'}$. T satisfies the four-dimensional Ward identity by construction. We are interested in the stress-energy tensor in momentum space. In order to determine its expression, we define its Fourier transform as

$$T_{(13)\mu\nu}(z, \vec{x}_1, \vec{x}_3) = \frac{1}{(2\pi)^8} \int dp_1 dp_3 e^{i\vec{p}_1 \cdot \vec{x}_1 + i\vec{p}_3 \cdot \vec{x}_3} e^{-i(\vec{p}_1 + \vec{p}_3) \cdot \vec{z}} \tilde{T}_{\mu\nu}(z, \vec{p}_1, \vec{p}_3). \quad (4.55)$$

Our computations of the graviton exchange amplitude have shown that only the first two terms of $T_{(13)\mu\nu}$ in Eq. (4.54) contribute in the Regge limit. The reason will become clear in the next section. Thus for convenience, we only Fourier transform the first two terms of the stress-energy tensor here. To this end, we use the Fourier transformation of the bulk-to-boundary propagator of the gauge boson,

$$G_{\mu j}(z, \vec{x}) = \int \frac{d^4 p}{(2\pi)^4} e^{i\vec{p} \cdot (\vec{x} - \vec{z})} G_{\mu j}(z_0, \vec{p}) \quad (4.56)$$

We insert this expression into the first two terms of Eq. (4.54) and get

$$\begin{aligned} & T_{(13)\mu\nu}(z, \vec{x}_1, \vec{x}_3) \\ & \approx z_0^2 \partial_{[\mu} \left(\int \frac{d^4 p_1}{(2\pi)^4} e^{i\vec{p}_1 \cdot (\vec{x}_1 - \vec{z})} G_{\rho]k_1}(z_0, \vec{p}_1) \right) \partial_{\nu} \left(\int \frac{d^4 p_3}{(2\pi)^4} e^{i\vec{p}_3 \cdot (\vec{x}_3 - \vec{z})} G_{\rho]k_3}(z_0, \vec{p}_3) \right) \\ & \quad + \mu \leftrightarrow \nu. \end{aligned} \quad (4.57)$$

From now on, the symbol \approx denotes that we only consider terms contributing in the Regge limit. $\mu \leftrightarrow \nu$ symbolizes the exchange of indices and stands for the second term in Eq. (4.54). The derivatives in Eq. (4.57) are given by

$$\begin{aligned} & \partial_{[\mu} \left(e^{i\vec{p}_1 \cdot (\vec{x}_1 - \vec{z})} G_{\rho]k_1}(z_0, \vec{p}_1) \right) \\ & = \partial_{[\mu} \left(e^{i\vec{p}_1 \cdot (\vec{x}_1 - \vec{z})} \right) G_{\rho]k_1}(z_0, \vec{p}_1) + e^{i\vec{p}_1 \cdot (\vec{x}_1 - \vec{z})} \delta_{\mu 0} \partial_{[\mu} G_{\rho]k_1}(z_0, \vec{p}_1) \\ & = -ip_{1[\mu} e^{i\vec{p}_1 \cdot (\vec{x}_1 - \vec{z})} G_{\rho]k_1}(z_0, \vec{p}_1) + e^{i\vec{p}_1 \cdot (\vec{x}_1 - \vec{z})} \delta_{\mu 0} \partial_{[\mu} G_{\rho]k_1}(z_0, \vec{p}_1) \end{aligned} \quad (4.58)$$

and thus, the stress-energy tensor reads

$$\begin{aligned} & T_{(13)\mu\nu}(z, \vec{x}_1, \vec{x}_3) \\ & \approx \frac{1}{(2\pi)^8} \int dp_1 dp_3 e^{i\vec{p}_1 \cdot \vec{x}_1 + i\vec{p}_3 \cdot \vec{x}_3} e^{-i(\vec{p}_1 + \vec{p}_3) \cdot \vec{z}} z_0^2 \\ & \quad \times \left[-ip_{1[\mu} G_{\rho]k_1}(z_0, \vec{p}_1) + \partial_0 \delta_{[\mu 0} G_{\rho]k_1}(z_0, \vec{p}_1) \right] \\ & \quad \times \left[-ip_{3[\nu} G_{\rho]k_3}(z_0, \vec{p}_3) + \partial_0 \delta_{[\nu 0} G_{\rho]k_3}(z_0, \vec{p}_3) \right] \\ & \quad + \mu \leftrightarrow \nu \\ & = \frac{1}{(2\pi)^8} \int dp_1 dp_3 e^{i\vec{p}_1 \cdot \vec{x}_1 + i\vec{p}_3 \cdot \vec{x}_3} e^{-i(\vec{p}_1 + \vec{p}_3) \cdot \vec{z}} z_0^2 \\ & \quad \times \left[-p_{1[\mu} G_{\rho]k_1}(z_0, \vec{p}_1) p_{3[\nu} G_{\rho]k_3}(z_0, \vec{p}_3) + \partial_0 \delta_{[\mu 0} G_{\rho]k_1}(z_0, \vec{p}_1) \partial_0 \delta_{[\nu 0} G_{\rho]k_3}(z_0, \vec{p}_3) \right. \\ & \quad \left. - ip_{3\nu} G_{\rho k_3}(z_0, \vec{p}_3) \partial_0 \delta_{\mu 0} G_{\rho k_1}(z_0, \vec{p}_1) - ip_{1\mu} G_{\rho k_1}(z_0, \vec{p}_1) \partial_0 \delta_{\nu 0} G_{\rho k_3}(z_0, \vec{p}_3) \right] \\ & \quad + \mu \leftrightarrow \nu. \end{aligned} \quad (4.59)$$

Only the first term contributes in the Regge limit. We have

$$T_{(13)\mu\nu}(z, \vec{x}_1, \vec{x}_3) \approx -\frac{1}{(2\pi)^8} \int dp_1 dp_3 e^{i\vec{p}_1 \cdot \vec{x}_1 + i\vec{p}_3 \cdot \vec{x}_3} e^{-i(\vec{p}_1 + \vec{p}_3) \cdot \vec{z}} z_0^2 \times \left[p_{1[\mu} G_{\rho]k_1}(z_0, \vec{p}_1) p_{3[\nu} G_{\rho]k_3}(z_0, \vec{p}_3) + \mu \leftrightarrow \nu \right]. \quad (4.60)$$

The bulk-to-boundary propagator in momentum space is given in Eq. (4.40). We insert the explicit form of the propagator and get

$$\begin{aligned} T_{(13)\mu\nu}(z, \vec{x}_1, \vec{x}_3) &\approx -\frac{1}{(2\pi)^8} \int dp_1 dp_3 e^{i\vec{p}_1 \cdot \vec{x}_1 + i\vec{p}_3 \cdot \vec{x}_3} e^{-i(\vec{p}_1 + \vec{p}_3) \cdot \vec{z}} z_0^4 \\ &\times p_{1[\mu} (|\vec{p}_1| K_1(|\vec{p}_1|z_0) \delta_{\rho]k_1} + i p_{1k_1} K_0(|\vec{p}_1|z_0) \delta_{\rho]0}) \\ &\times p_{3[\nu} (|\vec{p}_3| K_1(|\vec{p}_3|z_0) \delta_{\rho]k_3} + i p_{3k_3} K_0(|\vec{p}_3|z_0) \delta_{\rho]0}) \\ &+ \mu \leftrightarrow \nu \\ &\approx -\frac{1}{(2\pi)^8} \int dp_1 dp_3 e^{i\vec{p}_1 \cdot \vec{x}_1 + i\vec{p}_3 \cdot \vec{x}_3} e^{-i(\vec{p}_1 + \vec{p}_3) \cdot \vec{z}} z_0^4 \\ &\times p_{1[\mu} p_{3[\nu} (|\vec{p}_1| |\vec{p}_3| K_1(|\vec{p}_1|z_0) K_1(|\vec{p}_3|z_0) \delta_{\rho]k_1} \delta_{\rho]k_3} \\ &- p_{1k_1} p_{3k_3} K_0(|\vec{p}_1|z_0) K_0(|\vec{p}_3|z_0) \delta_{\rho]0} \delta_{\rho]0}) \\ &+ \mu \leftrightarrow \nu \\ &\approx -\frac{1}{(2\pi)^8} \int dp_1 dp_3 e^{i\vec{p}_1 \cdot \vec{x}_1 + i\vec{p}_3 \cdot \vec{x}_3} e^{-i(\vec{p}_1 + \vec{p}_3) \cdot \vec{z}} z_0^4 (\delta_{\mu j_1} \delta_{\nu j_3} + \delta_{\nu j_1} \delta_{\mu j_3}) \\ &\times (|\vec{p}_1| |\vec{p}_3| K_1(|\vec{p}_1|z_0) K_1(|\vec{p}_3|z_0) (p_{1j_1} \delta_{\rho k_1} - p_{1\rho} \delta_{j_1 k_1}) (p_{3j_3} \delta_{\rho k_3} - p_{3\rho} \delta_{j_3 k_3}) \\ &- K_0(|\vec{p}_1|z_0) K_0(|\vec{p}_3|z_0) (p_{1j_1} p_{1k_1} \delta_{\rho 0} - p_{1\rho} p_{1k_1} \delta_{j_1 0}) (p_{3j_3} p_{3k_3} \delta_{\rho 0} - p_{3\rho} p_{3k_3} \delta_{j_3 0})). \end{aligned} \quad (4.61)$$

Once again, only two terms give the leading contribution in the Regge limit, see the next section for an explanation. They read

$$\begin{aligned} T_{(13)\mu\nu}(z, \vec{x}_1, \vec{x}_3) &\approx \frac{z_0^4}{(2\pi)^8} \int dp_1 dp_3 e^{i\vec{p}_1 \cdot \vec{x}_1 + i\vec{p}_3 \cdot \vec{x}_3} e^{-i(\vec{p}_1 + \vec{p}_3) \cdot \vec{z}} (\delta_{\mu j_1} \delta_{\nu j_3} + \delta_{\nu j_1} \delta_{\mu j_3}) \\ &\times (K_0(|\vec{p}_1|z_0) K_0(|\vec{p}_3|z_0) p_{1j_1} p_{3j_3} p_{1k_1} p_{3k_3} \\ &- |\vec{p}_1| |\vec{p}_3| K_1(|\vec{p}_1|z_0) K_1(|\vec{p}_3|z_0) p_{1j_1} p_{3j_3} \delta_{k_1 k_3}). \end{aligned} \quad (4.62)$$

We have computed the stress-energy tensor in coordinate space given by a Fourier transform in Eq. (4.55). For convenience, we write the expression here again:

$$T_{(13)\mu\nu}(z, \vec{x}_1, \vec{x}_3) = \frac{1}{(2\pi)^8} \int dp_1 dp_3 e^{i\vec{p}_1 \cdot \vec{x}_1 + i\vec{p}_3 \cdot \vec{x}_3} e^{-i(\vec{p}_1 + \vec{p}_3) \cdot \vec{z}} \tilde{T}_{\mu\nu}(z, \vec{p}_1, \vec{p}_3). \quad (4.63)$$

From Eqs. (4.62) and (4.63) we can read off the leading contribution of the stress-energy tensor in momentum space in the Regge limit. We get

$$\begin{aligned} \tilde{T}_{(13)\mu\nu}(z, \vec{p}_1, \vec{p}_3) &\approx z_0^4 (\delta_{\mu j_1} \delta_{\nu j_3} + \delta_{\nu j_1} \delta_{\mu j_3}) p_{1j_1} p_{3j_3} (K_0(|\vec{p}_1|z_0) K_0(|\vec{p}_3|z_0) p_{1k_1} p_{3k_3} \\ &- |\vec{p}_1| |\vec{p}_3| K_1(|\vec{p}_1|z_0) K_1(|\vec{p}_3|z_0) \delta_{k_1 k_3}). \end{aligned} \quad (4.64)$$

4.2.2 Graviton Exchange Amplitude

We define the Fourier transform of the graviton exchange contribution I^{GR} given in Eq. (4.50):

$$\begin{aligned}\tilde{I}^{\text{GR}}(\vec{p}_i) &= \int \prod_i d^4 x_i e^{-i \sum_j \vec{p}_j \cdot \vec{x}_j} I^{\text{GR}}(\vec{x}_i) \\ &= (2\pi)^4 \delta^{(4)}\left(\sum_i \vec{p}_i\right) \frac{1}{4} \int \frac{dz_0}{z_0} \int \frac{dw_0}{w_0} \tilde{T}_{(13)\mu\nu}(z_0, \vec{p}_1, \vec{p}_3) \\ &\quad \times G_{\mu\nu;\mu'\nu'}(z_0, w_0, \vec{p}_1 + \vec{p}_3) \tilde{T}_{(24)\mu'\nu'}(w_0, \vec{p}_2, \vec{p}_4)\end{aligned}\quad (4.65)$$

with the bulk-to-bulk propagator of the graviton $G_{\mu\nu;\mu'\nu'}(z_0, w_0, \vec{p}_1 + \vec{p}_3)$ given in Eq. (4.49) and the stress-energy tensor given in Eq. (4.64).

Let us now explain why only certain terms of the stress-energy tensor contribute to the leading behavior of the amplitude in the Regge limit. In coordinate space, each term of the stress-energy tensor in Eq. (4.54) has two derivatives, which are replaced by momenta after Fourier transformation. These momenta are combined with momenta from the second stress-energy tensor. We are interested in the highest power of the energy s in the amplitude. Contraction of the momenta \vec{p}_1 and \vec{p}_3 with the momenta \vec{p}_2 and \vec{p}_4 gives terms proportional to s . On the other hand, contractions of \vec{p}_1 with \vec{p}_3 or of \vec{p}_2 with \vec{p}_4 give subleading contributions. Any other contraction, for example with a zero-component of a momentum gives a subleading contribution as well.

The same arguments also apply for the bulk-to-bulk propagator $G_{\mu\nu;\mu'\nu'}^{(1)}$ introduced in Eq. (4.49). $G_{\mu\nu;\mu'\nu'}^{(1)}$ contains all terms of the propagator, which contribute to the highest power of s in the amplitude in the Regge limit.

The bulk-to-bulk propagator $G_{\mu\nu;\mu'\nu'}^{(1)}$ can be written in a different form:

$$\tilde{G}_{ij;i'j'}^{(1)}(z_0, w_0, \vec{q}) \approx \frac{4}{s^2(z_0 w_0)^2} (p_{2i} p_{1_i'} p_{2_j} p_{1_{j'}} + p_{2_i} p_{1_{j'}} p_{2_j} p_{1_i'}) \tilde{G} \quad (4.66)$$

using a Sudakov decomposition of the momenta with the lightlike vectors p_1 and p_2 . This is the expected form for a propagator of a spin two particle in the Regge limit. It is similar to a propagator of a spin one gauge boson in the Regge limit. The leading high energy behavior of a spin one gauge boson comes from a particular t -channel helicity state, which contributes through the tensor

$$\frac{2p_{2_j} p_{1_{j'}}}{s}, \quad (4.67)$$

see also Eq. (2.88) and below. Here j (j') denotes the upper (lower) Lorentz index of the t -channel exchange propagator, and the propagator is contracted with large momentum p_1 (p_2) at the upper (lower) vertex. Accordingly, the leading behavior of the graviton propagator in Eq. (4.66) can be interpreted as the symmetrized tensor product of two spin one gauge bosons.

We insert the explicit expressions of the graviton propagator (4.49) and of the stress-energy tensor (4.64) in the Regge limit into Eq. (4.65) and get

$$\begin{aligned}
\tilde{I}_{\text{Regge}}^{\text{GR}}(\vec{p}_i) &= (2\pi)^4 \delta^{(4)}\left(\sum_i \vec{p}_i\right) \frac{1}{4} \int \frac{dz_0}{z_0} \int \frac{dw_0}{w_0} \\
&\times z_0^4 (\delta_{\mu'j_1} \delta_{\nu'j_3} + \delta_{\nu'j_1} \delta_{\mu'j_3}) p_{1j_1} p_{3j_3} \left[|\vec{p}_1| |\vec{p}_3| K_1(|\vec{p}_1|z_0) K_1(|\vec{p}_3|z_0) \delta_{k_1 k_3} \right. \\
&\quad \left. - K_0(|\vec{p}_1|z_0) K_0(|\vec{p}_3|z_0) p_{1k_1} p_{3k_3} \right] \\
&\times w_0^4 (\delta_{\mu'j_2} \delta_{\nu'j_4} + \delta_{\nu'j_2} \delta_{\mu'j_4}) p_{2j_2} p_{4j_4} \left[|\vec{p}_2| |\vec{p}_4| K_1(|\vec{p}_2|w_0) K_1(|\vec{p}_4|w_0) \delta_{k_2 k_4} \right. \\
&\quad \left. - K_0(|\vec{p}_2|w_0) K_0(|\vec{p}_4|w_0) p_{2k_2} p_{4k_4} \right] \\
&\times (\delta_{\mu\mu'} \delta_{\nu\nu'} + \delta_{\mu\nu'} \delta_{\nu\mu'}) \sum_{k=0}^{\infty} \frac{(z_0 w_0)^{2k+2}}{\Gamma(1+k)\Gamma(3+k)} \left(\frac{|\vec{p}_1 + \vec{p}_3|^2}{4\bar{w}_0^2} \right)^{k+1} K_{2k+2}(|\vec{p}_1 + \vec{p}_3|\bar{w}_0).
\end{aligned} \tag{4.68}$$

$\tilde{I}_{\text{Regge}}^{\text{GR}}$ denotes the leading contribution of the graviton exchange in the Regge limit. After contraction of the momenta, the highest order contribution is given by

$$\begin{aligned}
\tilde{I}_{\text{Regge}}^{\text{GR}}(\vec{p}_i) &= (2\pi)^4 \delta^{(4)}\left(\sum_i \vec{p}_i\right) \int dz_0 \int dw_0 \left((\vec{p}_1 \cdot \vec{p}_3)(\vec{p}_3 \cdot \vec{p}_4) + (\vec{p}_1 \cdot \vec{p}_4)(\vec{p}_3 \cdot \vec{p}_3) \right) \\
&\times \left(|\vec{p}_1| |\vec{p}_3| K_1(|\vec{p}_1|z_0) K_1(|\vec{p}_3|z_0) \delta_{k_1 k_3} - K_0(|\vec{p}_1|z_0) K_0(|\vec{p}_3|z_0) p_{1k_1} p_{3k_3} \right) \\
&\times \left(|\vec{p}_2| |\vec{p}_4| K_1(|\vec{p}_2|w_0) K_1(|\vec{p}_4|w_0) \delta_{k_2 k_4} - K_0(|\vec{p}_2|w_0) K_0(|\vec{p}_4|w_0) p_{2k_2} p_{4k_4} \right) \\
&\times \sum_{k=0}^{\infty} \frac{(z_0 w_0)^{2k+5}}{\Gamma(1+k)\Gamma(3+k)} \left(\frac{|\vec{p}_1 + \vec{p}_3|^2}{4\bar{w}_0^2} \right)^{k+1} K_{2k+2}(|\vec{p}_1 + \vec{p}_3|\bar{w}_0) \\
&= (2\pi)^4 \delta^{(4)}\left(\sum_i \vec{p}_i\right) \frac{s^2}{2} \int dz_0 \int dw_0 \\
&\times \left(|\vec{p}_1| |\vec{p}_3| K_1(|\vec{p}_1|z_0) K_1(|\vec{p}_3|z_0) \delta_{k_1 k_3} - K_0(|\vec{p}_1|z_0) K_0(|\vec{p}_3|z_0) p_{1k_1} p_{3k_3} \right) \\
&\times \left(|\vec{p}_2| |\vec{p}_4| K_1(|\vec{p}_2|w_0) K_1(|\vec{p}_4|w_0) \delta_{k_2 k_4} - K_0(|\vec{p}_2|w_0) K_0(|\vec{p}_4|w_0) p_{2k_2} p_{4k_4} \right) \\
&\times \sum_{k=0}^{\infty} \frac{(z_0 w_0)^{2k+5}}{\Gamma(1+k)\Gamma(3+k)} \left(\frac{|\vec{p}_1 + \vec{p}_3|^2}{4\bar{w}_0^2} \right)^{k+1} K_{2k+2}(|\vec{p}_1 + \vec{p}_3|\bar{w}_0).
\end{aligned} \tag{4.69}$$

The highest contribution to the graviton exchange amplitude in the Regge limit is proportional to s^2 . This is the expected result for the exchange of a spin two boson in the t -channel.

The last step left is to contract $\tilde{I}_{\text{Regge}}^{\text{GR}}(\vec{p}_i)$ with appropriate polarization vectors of the R -currents:

$$\tilde{\mathcal{I}}_{\text{Regge}}^{\text{GR}\lambda_1\lambda_2\lambda_3\lambda_4} = \sum_{\lambda_i} \epsilon^{k_1(\lambda_1)}(\vec{p}_1) \epsilon^{k_2(\lambda_2)}(\vec{p}_2) \epsilon^{k_3(\lambda_3)}(\vec{p}_3)^* \epsilon^{k_4(\lambda_4)}(\vec{p}_4)^* \tilde{I}_{\text{Regge}}^{\text{GR}k_1k_2k_3k_4}. \tag{4.70}$$

We use the polarization vectors introduced during the computation in $\mathcal{N} = 4$ SYM in section 2.3. They are defined in Minkowski space. Since we have switched to

Minkowski space in the supergravity computation as well, as explained at the beginning of this section, we are allowed to use them. Here, all R -currents are incoming. We use the shifted polarization vectors because the amplitude satisfies the Ward identities. We contract with longitudinal, Eqs. (2.57) and (2.58), as well as with transverse polarization vectors, Eqs. (2.59)-(2.61). The contraction with these polarization vectors gives no additional power of s . First, we contract with longitudinal polarization vectors, that is we choose $\lambda_i = L$. We get

$$\begin{aligned} \tilde{\mathcal{I}}_{\text{Regge}}^{\text{GRLLLL}} &= (2\pi)^4 \delta^{(4)} \left(\sum_i \vec{p}_i \right) \frac{s^2}{2} \int dz_0 \int dw_0 |\vec{p}_1| |\vec{p}_2| |\vec{p}_3| |\vec{p}_4| \\ &\quad \times K_0(|\vec{p}_1|z_0) K_0(|\vec{p}_3|z_0) K_0(|\vec{p}_2|w_0) K_0(|\vec{p}_4|w_0) \\ &\quad \times \sum_{k=0}^{\infty} \frac{(z_0 w_0)^{2k+5}}{\Gamma(1+k)\Gamma(3+k)} \left(\frac{|\vec{p}_1 + \vec{p}_3|^2}{4\bar{w}_0^2} \right)^{k+1} K_{2k+2}(|\vec{p}_1 + \vec{p}_3|\bar{w}_0). \end{aligned} \quad (4.71)$$

Only two terms of the right-hand side of Eq. (4.69) contribute. Similarly, we contract with transverse polarization vectors with the helicity $h = \pm$:

$$\begin{aligned} \tilde{\mathcal{I}}_{\text{Regge}}^{\text{GR}h_1 h_2 h_3 h_4} &= (2\pi)^4 \delta^{(4)} \left(\sum_i \vec{p}_i \right) \frac{s^2}{2} \int dz_0 \int dw_0 |\vec{p}_1| |\vec{p}_2| |\vec{p}_3| |\vec{p}_4| \\ &\quad \times (\epsilon_{\perp}^{(h_1)} \cdot \epsilon_{\perp}^{(h_3)*}) (\epsilon_{\perp}^{(h_2)} \cdot \epsilon_{\perp}^{(h_4)*}) K_1(|\vec{p}_1|z_0) K_1(|\vec{p}_3|z_0) K_1(|\vec{p}_2|w_0) K_1(|\vec{p}_4|w_0) \\ &\quad \times \sum_{k=0}^{\infty} \frac{(z_0 w_0)^{2k+5}}{\Gamma(1+k)\Gamma(3+k)} \left(\frac{|\vec{p}_1 + \vec{p}_3|^2}{4\bar{w}_0^2} \right)^{k+1} K_{2k+2}(|\vec{p}_1 + \vec{p}_3|\bar{w}_0). \end{aligned} \quad (4.72)$$

Again, only two terms of the right-hand side of Eq. (4.69) contribute. Finally, we choose a different polarization for the upper two and the lower two R -currents. The result is

$$\begin{aligned} \tilde{\mathcal{I}}_{\text{Regge}}^{\text{GR}h_1 L h_3 L} &= (2\pi)^4 \delta^{(4)} \left(\sum_i \vec{p}_i \right) \frac{s^2}{2} \int dz_0 \int dw_0 |\vec{p}_1| |\vec{p}_2| |\vec{p}_3| |\vec{p}_4| \\ &\quad \times (\epsilon_{\perp}^{(h_1)} \cdot \epsilon_{\perp}^{(h_3)*}) K_1(|\vec{p}_1|z_0) K_1(|\vec{p}_3|z_0) K_0(|\vec{p}_2|w_0) K_0(|\vec{p}_4|w_0) \\ &\quad \times \sum_{k=0}^{\infty} \frac{(z_0 w_0)^{2k+5}}{\Gamma(1+k)\Gamma(3+k)} \left(\frac{|\vec{p}_1 + \vec{p}_3|^2}{4\bar{w}_0^2} \right)^{k+1} K_{2k+2}(|\vec{p}_1 + \vec{p}_3|\bar{w}_0) \end{aligned} \quad (4.73)$$

for transverse-longitudinal polarization. There is a similar result for the reversed case. Different polarizations within the two upper R -currents, for example $\lambda_1 = L$ and $\lambda_3 = h$ or within the two lower R -currents, for example $\lambda_2 = L$ and $\lambda_4 = h$, give subleading contributions in s .

Let us rewrite our result for the leading contribution of a four point function of

R -currents with single graviton exchange in the t -channel as

$$\begin{aligned} \tilde{I}_{\text{Regge}}^{\text{GR}}(\vec{p}_i) &= (2\pi)^4 \delta^{(4)}\left(\sum_i \vec{p}_i\right) \frac{s^2}{2} \int dz_0 \int dw_0 \\ &\quad \times \Phi_{k_1 k_3}(\vec{p}_1, \vec{p}_3, z_0) \Sigma(|\vec{p}_1 + \vec{p}_3|, z_0, w_0) \Phi_{k_2 k_4}(\vec{p}_2, \vec{p}_4, w_0) \end{aligned} \quad (4.74)$$

with the graviton exchange propagator

$$\Sigma(z_0, w_0, |\vec{p}_1 + \vec{p}_3|) = \sum_{k=0}^{\infty} \frac{(z_0 w_0)^{2k+5}}{\Gamma(1+k)\Gamma(3+k)} \left(\frac{|\vec{p}_1 + \vec{p}_3|^2}{4\bar{w}_0^2} \right)^{k+1} K_{2k+2}(|\vec{p}_1 + \vec{p}_3| \bar{w}_0) \quad (4.75)$$

and with the two functions $\Phi_{k_1 k_3}$ and $\Phi_{k_2 k_4}$. $\Phi_{k_1 k_3}$ is defined as

$$\Phi_{k_1 k_3}(z_0, p_1, p_3) = \sum_{m=0,1} \tilde{W}_{k_1 k_3 m}(\vec{p}_1, \vec{p}_3) K_m(|\vec{p}_1| z_0) K_m(|\vec{p}_3| z_0), \quad (4.76)$$

and we have a similar definition for $\Phi_{k_2 k_4}$. The functions Φ are evocative of the impact factors in Eq. (2.81) in the computations in $\mathcal{N} = 4$ SYM. The term $\tilde{W}_{k_1 k_3 m}$ is given by

$$\tilde{W}_{k_1 k_3 m} = \delta_{k_1 k_3} |\vec{p}_1| |\vec{p}_3| \delta_{m,1} - p_{1k_1} p_{3k_3} \delta_{m,0}. \quad (4.77)$$

After contraction with polarization vectors, $\tilde{W}_{k_1 k_3 m}$ reads

$$\begin{aligned} \tilde{\mathcal{W}}_{\lambda_1 \lambda_3 m} &= \sum_{\lambda_1, \lambda_3} \epsilon^{k_1(\lambda_1)}(\vec{p}_1) \epsilon^{k_3(\lambda_3)}(\vec{p}_3)^* \tilde{W}_{k_1 k_3 m}(\vec{p}_1, \vec{p}_3) \\ &\approx |\vec{p}_1| |\vec{p}_3| (\delta_{m,1} \delta_{\lambda_1, h} \delta_{\lambda_3, h} + \delta_{m,0} \delta_{\lambda_1, L} \delta_{\lambda_3, L}). \end{aligned} \quad (4.78)$$

The first term with $m = 1$ contributes to transverse and the second term with $m = 0$ to longitudinal polarization. Helicity changing terms are suppressed in the Regge limit. Consequently, the helicity of the R -currents is conserved. In $\mathcal{N} = 4$ SYM at weak coupling, the elastic scattering of two R -currents also provides helicity conservation of the R -currents as shown in Eq. (2.117).

$\tilde{\mathcal{W}}_{\lambda_1 \lambda_3}$ only depends on the virtualities of the R -currents. Hence, the impact factor in the helicity basis, given by

$$\Phi_{\lambda_1 \lambda_3}(z_0, |\vec{p}_1|, |\vec{p}_3|) = \sum_{m=0,1} \tilde{\mathcal{W}}_{\lambda_1 \lambda_3 m}(|\vec{p}_1|, |\vec{p}_3|) K_m(|\vec{p}_1| z_0) K_m(|\vec{p}_3| z_0), \quad (4.79)$$

only depends on the virtualities and not on the momenta of the R -currents as well. The same is true in $\mathcal{N} = 4$ SYM: the impact factors (2.115)-(2.116) at weak coupling do not depend on the momenta of the external R -currents. Furthermore, we see in Eq. (4.79) that the Bessel function K_0 corresponds to the longitudinal polarization L , and the Bessel function K_1 corresponds to the transverse polarization h of the R -currents.

Finally, the scattering amplitude reads

$$\begin{aligned} \mathcal{A}_{\text{Regge}}^{\text{GR}\lambda_1\lambda_2\lambda_3\lambda_4}(|\vec{p}_i|, s, t) \\ = \frac{s^2}{2} \int dz_0 \int dw_0 \Phi^{\lambda_1\lambda_3}(z_0, |\vec{p}_1|, |\vec{p}_3|) \Sigma(|\vec{p}_1 + \vec{p}_3|, z_0, w_0) \Phi^{\lambda_2\lambda_4}(w_0, |\vec{p}_2|, |\vec{p}_4|). \end{aligned} \quad (4.80)$$

In the Regge limit, the scattering amplitude with a graviton exchange in the t -channel is proportional to s^2 . We also have to consider the exchange of a graviton in the s - and u -channel. In these cases, the third term of the stress-energy tensor is important, and at first sight, one might expect additional contributions of order s^2 . Nevertheless, the s - and u -channel contributions are suppressed by an additional factor s^{-1} , which comes in through the graviton propagator.

The amplitude in Eq. (4.80) has a factorized form like the four point amplitude of R -currents computed in $\mathcal{N} = 4$ SYM at weak coupling, see Eq. (2.81). Again, the amplitude contains two impact factors Φ which depend on the virtualities of the external R -currents. The impact factors are connected by the exchange propagator Σ . On the gauge theory side, we have two gluon propagators. In both amplitudes, the impact factors are convoluted by a two-dimensional integration: over the transverse components of the loop momentum and over two variables in the fifth dimension, respectively. Finally, the power of s in the amplitudes reflects the spin of the exchanged particles.

On the gauge theory side, we have the exchange of two gluons in the leading diagrams, see section 2.5, and the amplitude is proportional to s . In higher order of the gauge coupling g_{YM}^2 , the two gluon exchange is replaced by the BFKL Green's function, and the power of s is modified from 1 to $1 + \omega_0$. ω_0 is the leading singularity in the ω -plane. On the string theory side, we expect a similar behavior. In higher order diagrams, due to the expected reggeization of the graviton, the power behavior of s may be modified to $s^{2-\Delta}$ with the correction $\Delta = \mathcal{O}(1/\sqrt{\lambda})$. In order to compute this correction, computations of loop diagrams on the string side are necessary, that means the computations have to be performed beyond the supergravity limit.

4.3 Gauge Boson Exchange

The second diagram for a four point function of R -currents in the supergravity limit has a gauge boson exchange in the bulk. The leading term in the energy s comes from a gauge boson exchange in the t -channel, see Fig. 4.2(b). Contributions from s - and u -channel exchanges are suppressed by at least one power of s . In this section, we verify that the gauge boson exchange is subleading compared to the graviton exchange. We restrict ourselves to the Abelian part of the $SU(4)_R$ group as we have done in the $\mathcal{N} = 4$ SYM part.

The gauge boson exchange in the t -channel is described by the bulk-to-bulk propagator $G_{\mu_5\nu_5}(z, w)$, and the coupling of the bulk-to-bulk propagator to the bulk-to-boundary gauge boson propagators is given by the Chern-Simons interaction term in

the action (4.8),

$$\int d^4z dz_0 \epsilon_{\mu\nu\rho\sigma\lambda} \partial_\mu A_\nu(z) \partial_\rho A_\sigma(z) A_\lambda(z). \quad (4.81)$$

The gauge boson field in the bulk $A_\mu(z)$ is connected with the boundary field $A_i(\vec{x})$ by the bulk-to-boundary propagator of the gauge boson:

$$A_\mu(z) = \int d^4\vec{x} G_{\mu i}(z, \vec{x}) A_i(\vec{x}). \quad (4.82)$$

We use the rules of the AdS/CFT-correspondence and obtain the contribution of one gauge boson exchange in the t -channel to the four point function of R -currents,

$$\begin{aligned} I^{\text{CS}}(\vec{x}_i) &= \int d^4z dz_0 \int d^4w dw_0 \epsilon_{\mu_1\mu_2\mu_3\mu_4\mu_5} \epsilon_{\nu_1\nu_2\nu_3\nu_4\nu_5} \partial_{[\mu_1} G_{\mu_2]k_1}(z, \vec{x}_1) \partial_{[\mu_3} G_{\mu_4]k_3}(z, \vec{x}_3) \\ &\quad \times G_{\mu_5\nu_5}(z, w) \partial_{[\nu_1} G_{\nu_2]k_2}(w, \vec{x}_2) \partial_{[\nu_3} G_{\nu_4]k_4}(w, \vec{x}_4). \end{aligned} \quad (4.83)$$

The partial derivatives act on z and w , respectively. There are similar contributions as (4.83) that include derivatives on the bulk-to-bulk propagator. But all these contributions turn out to be identical to the above term due to the Bianchi identity. We have to transform $I^{\text{CS}}(\vec{x}_i)$ to momentum space since we like to take the Regge limit. We define the Fourier transform as

$$I^{\text{CS}}(\vec{x}_i) = \frac{1}{(2\pi)^{16}} \int \prod_i d^4p_i e^{i\sum_j \vec{p}_j \cdot \vec{x}_j} \tilde{I}^{\text{CS}}(\vec{p}_i). \quad (4.84)$$

The Fourier transform of the bulk-to-boundary propagator is given in Eq. (4.56),

$$G_{\mu_2 k_1}(z, \vec{x}_1) = \int \frac{d^4p_1}{(2\pi)^4} e^{-i\vec{p}_1 \cdot (\vec{z} - \vec{x}_1)} G_{\mu_2 k_1}(z_0, \vec{p}_1), \quad (4.85)$$

and derivatives of the bulk-to-boundary propagator in momentum space have been computed in Eq. (4.58). Similar expressions hold for the other bulk-to-boundary propagators in Eq. (4.83). We substitute $\vec{x} = \vec{z} - \vec{w}$ and $I^{\text{CS}}(\vec{x}_i)$ reads

$$\begin{aligned} I^{\text{CS}}(\vec{x}_i) &= \frac{1}{(2\pi)^{16}} \int d^4z dz_0 \int d^4w dw_0 \epsilon_{\mu_1\mu_2\mu_3\mu_4\mu_5} \epsilon_{\nu_1\nu_2\nu_3\nu_4\nu_5} \int \frac{d^4p}{(2\pi)^4} e^{i\vec{x} \cdot \vec{p}} \\ &\quad \times \int d^4p_1 d^4p_2 d^4p_3 d^4p_4 e^{i\vec{p}_1 \cdot \vec{x}_1} e^{i\vec{p}_2 \cdot \vec{x}_2} e^{i\vec{p}_3 \cdot \vec{x}_3} e^{i\vec{p}_4 \cdot \vec{x}_4} e^{-i(\vec{p}_1 + \vec{p}_3) \cdot \vec{z}} e^{-i(\vec{p}_2 + \vec{p}_4) \cdot \vec{w}} \\ &\quad \times [ip_{1[\mu_1} G_{\mu_2]k_1}(z_0, \vec{p}_1) + \partial_0 \delta_{[\mu_1 0} G_{\mu_2]k_1}(z_0, \vec{p}_1)] \\ &\quad \times [ip_{3[\mu_3} G_{\mu_4]k_2}(z_0, \vec{p}_3) + \partial_0 \delta_{[\mu_3 0} G_{\mu_4]k_2}(z_0, \vec{p}_3)] \\ &\quad \times G_{\mu_5\nu_5}(z_0, w_0, \vec{p}) \\ &\quad \times [ip_{2[\nu_1} G_{\nu_2]k_3}(w_0, \vec{p}_2) + \partial_0 \delta_{[\nu_1 0} G_{\nu_2]k_3}(w_0, \vec{p}_2)] \\ &\quad \times [ip_{4[\nu_3} G_{\nu_4]k_4}(w_0, \vec{p}_4) + \partial_0 \delta_{[\nu_3 0} G_{\nu_4]k_4}(w_0, \vec{p}_4)] \\ &\quad + \left(\begin{array}{c} \vec{p}_1 \leftrightarrow \vec{p}_3 \\ k_1 \leftrightarrow k_3 \end{array} \right) + \left(\begin{array}{c} \vec{p}_2 \leftrightarrow \vec{p}_4 \\ k_2 \leftrightarrow k_4 \end{array} \right) + \left(\begin{array}{c} \vec{p}_1 \leftrightarrow \vec{p}_3; \vec{p}_2 \leftrightarrow \vec{p}_4 \\ k_1 \leftrightarrow k_3; k_2 \leftrightarrow k_4 \end{array} \right). \end{aligned} \quad (4.86)$$

The brackets in the last line symbolize the exchange of momenta and indices. We drop these terms in the next formulas and reintroduce them in the final result. We integrate over \vec{z} , \vec{w} , and \vec{p} and arrive at

$$\begin{aligned}
I^{\text{CS}}(\vec{x}_i) &= \frac{1}{(2\pi)^{20}} \int dz_0 \int dw_0 \epsilon_{\mu_1\mu_2\mu_3\mu_4\mu_5} \epsilon_{\nu_1\nu_2\nu_3\nu_4\nu_5} \\
&\times \int d^4p_1 d^4p_2 d^4p_3 d^4p_4 e^{i\vec{p}_1 \cdot \vec{x}_1} e^{i\vec{p}_2 \cdot \vec{x}_2} e^{i\vec{p}_3 \cdot \vec{x}_3} e^{i\vec{p}_4 \cdot \vec{x}_4} (2\pi)^4 \delta^{(4)}(\sum \vec{p}_i) \\
&\times [ip_{1[\mu_1} G_{\mu_2]k_1}(z_0, \vec{p}_1) + \partial_0 \delta_{[\mu_1 0} G_{\mu_2]k_1}(z_0, \vec{p}_1)] \\
&\times [ip_{3[\mu_3} G_{\mu_4]k_3}(z_0, \vec{p}_3) + \partial_0 \delta_{[\mu_3 0} G_{\mu_4]k_3}(z_0, \vec{p}_3)] \\
&\times G_{\mu_5\nu_5}(z_0, w_0, \vec{p}) \\
&\times [ip_{2[\nu_1} G_{\nu_2]k_2}(w_0, \vec{p}_2) + \partial_0 \delta_{[\nu_1 0} G_{\nu_2]k_2}(w_0, \vec{p}_2)] \\
&\times [ip_{4[\nu_3} G_{\nu_4]k_4}(w_0, \vec{p}_4) + \partial_0 \delta_{[\nu_3 0} G_{\nu_4]k_4}(w_0, \vec{p}_4)]. \tag{4.87}
\end{aligned}$$

From this expression together with Eq. (4.84) we can read off I^{CS} in momentum space. We get

$$\begin{aligned}
\tilde{I}^{\text{CS}}(\vec{p}_i) &= \int dz_0 \int dw_0 \epsilon_{\mu_1\mu_2\mu_3\mu_4\mu_5} \epsilon_{\nu_1\nu_2\nu_3\nu_4\nu_5} (2\pi)^4 \delta^{(4)}(\sum \vec{p}_i) \\
&\times [ip_{1[\mu_1} G_{\mu_2]k_1}(z_0, \vec{p}_1) + \partial_0 \delta_{[\mu_1 0} G_{\mu_2]k_1}(z_0, \vec{p}_1)] \\
&\times [ip_{3[\mu_3} G_{\mu_4]k_3}(z_0, \vec{p}_3) + \partial_0 \delta_{[\mu_3 0} G_{\mu_4]k_3}(z_0, \vec{p}_3)] \\
&\times G_{\mu_5\nu_5}(z_0, w_0, \vec{p}) \\
&\times [ip_{2[\nu_1} G_{\nu_2]k_2}(w_0, \vec{p}_2) + \partial_0 \delta_{[\nu_1 0} G_{\nu_2]k_2}(w_0, \vec{p}_2)] \\
&\times [ip_{4[\nu_3} G_{\nu_4]k_4}(w_0, \vec{p}_4) + \partial_0 \delta_{[\nu_3 0} G_{\nu_4]k_4}(w_0, \vec{p}_4)]. \tag{4.88}
\end{aligned}$$

A straightforward but lengthy computation shows: The leading contribution of $\tilde{I}^{\text{CS}}(\vec{p}_i)$ in the Regge limit is given by $\mu_5 = m \neq 0$ and $\nu_5 = n \neq 0$ in the bulk-to-bulk propagator. With these conditions we have

$$\begin{aligned}
\tilde{I}^{\text{CS}}(\vec{p}_i) &\approx \int dz_0 \int dw_0 \epsilon_{0\mu_2\mu_3\mu_4m} \epsilon_{0\nu_2\nu_3\nu_4n} (2\pi)^4 \delta^{(4)}(\sum \vec{p}_i) G_{mn}(z_0, w_0, \vec{p}) \\
&\times [ip_{1[0} G_{\mu_2]k_1}(z_0, \vec{p}_1) + \partial_0 G_{\mu_2]k_1}(z_0, \vec{p}_1)] [ip_{3[\mu_3} G_{\mu_4]k_3}(z_0, \vec{p}_3)] \\
&\times [ip_{2[0} G_{\nu_2]k_2}(w_0, \vec{p}_2) + \partial_0 G_{\nu_2]k_2}(w_0, \vec{p}_2)] [ip_{4[\nu_3} G_{\nu_4]k_4}(w_0, \vec{p}_4)]. \tag{4.89}
\end{aligned}$$

The symbol \approx again denotes the leading contribution in the Regge limit. The derivative of the bulk-to-boundary propagator with respect to z_0 is

$$\partial_0 G_{\mu_2 k_1}(z_0, p_1) = -p_1^2 z_0 K_0(|\vec{p}|z_0) \delta_{k_1 \mu_2} + ip_{1k_1} (K_0(|\vec{p}|z_0) - |\vec{p}_1|z_0 K_1(|\vec{p}|z_0)) \delta_{\mu_2 0}. \tag{4.90}$$

Furthermore, we use the bulk-to-boundary propagator given in Eq. (4.40) to write

$$\begin{aligned}
\tilde{I}^{\text{CS}}(\vec{p}_i) &\approx \int dz_0 \int dw_0 \epsilon_{0\mu_2\mu_3\mu_4m} \epsilon_{0\nu_2\nu_3\nu_4n} (2\pi)^4 \delta^{(4)}\left(\sum \vec{p}_i\right) G_{mn}(z_0, w_0, \vec{p}) \\
&\quad \times [-ip_{1\mu_2} iz_0 p_{k_1} K_0(|\vec{p}_1|z_0) - p_1^2 \delta_{[\mu_1 0} \delta_{k_1 \mu_2]} z_0 K_0(|\vec{p}_1|z_0)] \\
&\quad \times [ip_{3[\mu_3} z_0 |\vec{p}_3| K_1(|\vec{p}_3|z_0) \delta_{\mu_4]k_3}] [ip_{4[\nu_3} w_0 |\vec{p}_4| K_1(|\vec{p}_4|w_0) \delta_{\nu_4]k_4}] \\
&\quad \times [-ip_{2\nu_2} iw_0 p_{k_2} K_0(|\vec{p}_2|w_0) - p_2^2 \delta_{[\nu_1 0} \delta_{k_2 \nu_2]} w_0 K_0(|\vec{p}_2|w_0)] \\
&= \int dz_0 \int dw_0 \epsilon_{0\mu_2\mu_3\mu_4m} \epsilon_{0\nu_2\nu_3\nu_4n} (2\pi)^4 \delta^{(4)}\left(\sum \vec{p}_i\right) G_{mn}(z_0, w_0, \vec{p}) \\
&\quad \times (-p_1^2 \delta_{[\mu_1 0} \delta_{k_1 \mu_2]} + p_{1\mu_2} p_{1k_1}) z_0 K_0(|\vec{p}_1|z_0) \\
&\quad \times (-p_2^2 \delta_{[\nu_1 0} \delta_{k_2 \nu_2]} + p_{2\nu_2} p_{2k_2}) w_0 K_0(|\vec{p}_2|w_0) \\
&\quad \times [ip_{3[\mu_3} z_0 |\vec{p}_3| K_1(|\vec{p}_3|z_0) \delta_{\mu_4]k_3}] [ip_{4[\nu_3} w_0 |\vec{p}_4| K_1(|\vec{p}_4|w_0) \delta_{\nu_4]k_4}]. \quad (4.91)
\end{aligned}$$

Now we insert the explicit expression of the bulk-to-bulk gauge boson propagator shown in Eq. (4.33) and have

$$\begin{aligned}
\tilde{I}^{\text{CS}}(\vec{p}_i) &\approx - \int dz_0 z_0^2 \int dw_0 w_0^2 \epsilon_{0\mu_2\mu_3\mu_4m} \epsilon_{0\nu_2\nu_3\nu_4n} (2\pi)^4 \delta^{(4)}\left(\sum \vec{p}_i\right) \delta_{lm} |\vec{p}_3| |\vec{p}_4| \\
&\quad \times (p_1^2 \delta_{\mu_2 k_1} - p_{1\mu_2} p_{1k_1}) (p_2^2 \delta_{\nu_2 k_2} - p_{2\nu_2} p_{2k_2}) \\
&\quad \times (p_{3\mu_3} \delta_{\mu_4 k_3} - p_{3\mu_4} \delta_{\mu_3 k_3}) (p_{4\nu_3} \delta_{\nu_4 k_4} - p_{4\nu_4} \delta_{\nu_3 k_4}) \\
&\quad \times K_0(|\vec{p}_1|z_0) K_1(|\vec{p}_3|z_0) K_0(|\vec{p}_2|w_0) K_1(|\vec{p}_4|w_0) \\
&\quad \times \sum_{k=0}^{\infty} \frac{(z_0 w_0)^{2k+2}}{2\Gamma(1+k)\Gamma(2+k)} \left(\frac{|\vec{p}_1 + \vec{p}_3|^2}{4\bar{w}_0^2}\right)^{k+\frac{1}{2}} K_{2k+1}(|\vec{p}_1 + \vec{p}_3|\bar{w}_0). \quad (4.92)
\end{aligned}$$

Next we perform all possible contractions of the momenta with the epsilon tensors. The resulting leading contribution in the Regge limit is

$$\begin{aligned}
\tilde{I}_{\text{Regge}}^{\text{CS}}(\vec{p}_i) &= (2\pi)^4 \delta^{(4)}\left(\sum \vec{p}_i\right) \tilde{W}_{k_1 k_2 k_3 k_4}^{\text{CS}} \int dz_0 z_0^2 \int dw_0 w_0^2 |\vec{p}_3| K_1(|\vec{p}_3|z_0) K_0(|\vec{p}_1|z_0) \\
&\quad \times \sum_{k=0}^{\infty} \frac{(z_0 w_0)^{2k+2}}{\Gamma(1+k)\Gamma(2+k)} \left(\frac{|\vec{p}_1 + \vec{p}_3|^2}{4\bar{w}_0^2}\right)^{k+\frac{1}{2}} K_{2k+1}(|\vec{p}_1 + \vec{p}_3|\bar{w}_0) \\
&\quad \times |\vec{p}_4| K_1(|\vec{p}_4|w_0) K_0(|\vec{p}_2|w_0) \\
&\quad + \begin{pmatrix} \vec{p}_1 \leftrightarrow \vec{p}_3 \\ k_1 \leftrightarrow k_3 \end{pmatrix} + \begin{pmatrix} \vec{p}_2 \leftrightarrow \vec{p}_4 \\ k_2 \leftrightarrow k_4 \end{pmatrix} + \begin{pmatrix} \vec{p}_1 \leftrightarrow \vec{p}_3; \vec{p}_2 \leftrightarrow \vec{p}_4 \\ k_1 \leftrightarrow k_3; k_2 \leftrightarrow k_4 \end{pmatrix} \quad (4.93)
\end{aligned}$$

with the polarization tensor

$$\begin{aligned}
\tilde{W}_{k_1 k_2 k_3 k_4}^{\text{CS}} &\approx t s p_{1k_1} p_{2k_2} \delta_{k_3 k_4} - s |\vec{p}_1|^2 |\vec{p}_2|^2 (\delta_{k_2 k_3} \delta_{k_1 k_4} - \delta_{k_1 k_2} \delta_{k_3 k_4}) + s p_{1k_1} p_{2k_2} q_{k_3} q_{k_4} \\
&\quad - s |\vec{p}_1|^2 p_{2k_2} (\delta_{k_1 k_4} q_{k_3} - \delta_{k_3 k_4} q_{k_1}) - s |\vec{p}_2|^2 p_{1k_1} (\delta_{k_3 k_4} q_{k_2} - \delta_{k_2 k_3} q_{k_4}) \quad (4.94)
\end{aligned}$$

with $\vec{q} = \vec{p}_1 + \vec{p}_3$. The last step in our computation is to contract the polarization tensor $\tilde{W}^{\text{CS}}(\vec{p}_i)$ with the polarization vectors of the R -currents,

$$\tilde{\mathcal{W}}^{\text{CS}\lambda_1\lambda_2\lambda_3\lambda_4}(\vec{p}_i) = \sum_{\lambda_i} \epsilon^{k_1(\lambda_1)}(\vec{p}_1) \epsilon^{k_2(\lambda_2)}(\vec{p}_2) \epsilon^{k_3(\lambda_3)}(\vec{p}_3)^* \epsilon^{k_4(\lambda_4)}(\vec{p}_4)^* \tilde{W}_{k_1k_2k_3k_4}^{\text{CS}}(\vec{p}_i). \quad (4.95)$$

The contraction with longitudinal polarization vectors, Eqs. (2.57) and (2.58), gives

$$\tilde{\mathcal{W}}^{\text{CSLLLL}}(\vec{p}_i) = 2t|\vec{p}_1||\vec{p}_2||\vec{p}_3||\vec{p}_4| \quad (4.96)$$

whereas contraction with transverse polarization vectors, Eqs. (2.59)-(2.61), results in

$$\begin{aligned} & \tilde{\mathcal{W}}^{\text{CS}h_1h_2h_3h_4}(\vec{p}_i) \\ &= -s|\vec{p}_1|^2|\vec{p}_2|^2((\vec{\epsilon}_\perp^{(h_2)} \cdot \vec{\epsilon}_\perp^{(h_3)*})(\vec{\epsilon}_\perp^{(h_1)} \cdot \vec{\epsilon}_\perp^{(h_4)*}) - (\vec{\epsilon}_\perp^{(h_3)*} \cdot \vec{\epsilon}_\perp^{(h_4)*})(\vec{\epsilon}_\perp^{(h_1)} \cdot \vec{\epsilon}_\perp^{(h_2)*})). \end{aligned} \quad (4.97)$$

There are two possible transverse polarizations, $h_i = \pm$. Looking at different combinations of transverse polarizations, we rewrite the polarization tensor as

$$\tilde{\mathcal{W}}^{\text{CS}h_1h_2h_3h_4}(\vec{p}_i) = -s|\vec{p}_1|^2|\vec{p}_2|^2(2\delta^{h_1h_2} - 1)\delta^{h_1h_3}\delta^{h_2h_4}. \quad (4.98)$$

Different polarizations of the upper two and lower to R -currents lead to

$$\tilde{\mathcal{W}}^{\text{CS}Lh_2Lh_4}(\vec{p}_i) = -|\vec{p}_1||\vec{p}_3||\vec{p}_2|^2((\vec{\epsilon}_\perp^{(h_2)} \cdot \vec{q}_\perp)(\vec{\epsilon}_\perp^{(h_4)*} \cdot \vec{q}_\perp). \quad (4.99)$$

We get a similar result for the reverse case. We see that only transverse polarization vectors contribute to the leading high energy behavior in the Regge limit. Therefore, the helicity of the R -currents is conserved. Let us rewrite the leading contribution of the gauge boson exchange to the four point function of R -currents as

$$\begin{aligned} \tilde{\mathcal{I}}_{\text{Regge}}^{\text{CS}} &= -(2\pi)^4\delta^{(4)}(\sum \vec{p}_i)(2\delta^{h_1h_2} - 1)s \\ &\times \int dz_0dw_0\Phi^{\text{CS}h_1h_3}(p_1, p_3; z_0)\Sigma^{\text{CS}}(|\vec{p}_1 + \vec{p}_3|, z_0, w_0)\Phi^{\text{CS}h_2h_4}(p_2, p_4; w_0). \end{aligned} \quad (4.100)$$

The term $(2\delta^{h_1h_2} - 1)$ changes the sign of the result depending on whether the two left R -currents have equal or opposite helicity. The exchange propagator reads

$$\begin{aligned} & \Sigma^{\text{CS}}(z_0, w_0, |\vec{p}_1 + \vec{p}_3|) \\ &= \sum_{k=0}^{\infty} \frac{(z_0w_0)^{2k+2}}{\Gamma(1+k)\Gamma(2+k)} \left(\frac{|\vec{p}_1 + \vec{p}_3|^2}{4\bar{w}_0^2} \right)^{k+\frac{1}{2}} K_{2k+1}(|\vec{p}_1 + \vec{p}_3|\bar{w}_0), \end{aligned} \quad (4.101)$$

and the functions Φ^{CS} have the form

$$\Phi^{\text{CS}h_1h_3}(z_0, |\vec{p}_1|, |\vec{p}_3|) = z_0^2|\vec{p}_1|^2|\vec{p}_3|K_1(|\vec{p}_3|z_0)K_0(|\vec{p}_1|z_0)\delta^{h_1h_3}. \quad (4.102)$$

We get a similar expression for $\Phi^{\text{CS}h_2h_4}(w_0, |\vec{p}_2|, |\vec{p}_4|)$. The functions Φ are again reminiscent of impact factors in $\mathcal{N} = 4$ SYM. The amplitude for gauge boson exchange finally reads

$$\begin{aligned} \mathcal{A}_{\text{Regge}}^{\text{CS}h_1h_2h_3h_4} &= -s (2\delta^{h_1h_2} - 1) \\ &\times \int dz_0 dw_0 \Phi^{\text{CS}h_1h_3}(z_0, |\vec{p}_1|, |\vec{p}_3|) \Sigma^{\text{CS}}(|\vec{p}|, z_0, w_0) \Phi^{\text{CS}h_2h_4}(w_0, |\vec{p}_2|, |\vec{p}_4|). \end{aligned} \tag{4.103}$$

The amplitude is proportional to s . As expected, the gauge boson exchange amplitude is subleading compared to the graviton exchange amplitude, which is proportional to s^2 . The highest spin particle, the graviton, provides the leading contribution to the four point function of R -currents in the Regge limit in classical supergravity.

Similar to the four point amplitude in $\mathcal{N} = 4$ SYM, the gauge boson exchange amplitude consists of two impact factors and an exchange propagator, convoluted by a two-dimensional integration. However, the amplitude is not completely factorized into an upper and a lower part due to the term $2\delta^{h_1h_2} - 1$. Other subleading terms proportional to s from the exchange of the graviton or the gauge boson in the s - and u -channel, may cancel this term and preserve the factorization of the amplitude.

5 The Six Point Function in Supergravity

After computing the four point function of R -currents in supergravity, we now proceed with the six point function of R -currents. In chapter 3, we have investigated the six point correlator at weak coupling in $\mathcal{N} = 4$ SYM. Now we address the strong coupling limit in the corresponding weakly coupled supergravity theory using the AdS/CFT-correspondence.

5.1 Setup of the Computation

We define the Euclidean version of the six point amplitude of R -currents $A(\vec{p}_i)$ in momentum space as

$$\begin{aligned} & i(2\pi)^4 \delta\left(\sum_i \vec{p}_i\right) A(\vec{p}_i)^{j_1 j_2 j_3 j_4 j_5 j_6} \\ &= \int \prod_{i=1}^6 d^4 x_i e^{-i\vec{p}_i \cdot \vec{x}_i} \langle J_R^{j_1}(\vec{x}_1) J_R^{j_2}(\vec{x}_2) J_R^{j_3}(\vec{x}_3) J_R^{j_4}(\vec{x}_4) J_R^{j_5}(\vec{x}_5) J_R^{j_6}(\vec{x}_6) \rangle. \end{aligned} \quad (5.1)$$

\vec{x}_i and \vec{p}_i are four-dimensional Euclidean vectors, and the j_i label the spacial directions with $j_i = 1, \dots, 4$. We choose all momenta $\vec{p}_1, \dots, \vec{p}_6$ to be incoming. In Euclidean notation the amplitude depends on the energy variables $s_1 = -(\vec{p}_1 + \vec{p}_2)^2$, $s_2 = -(\vec{p}_4 + \vec{p}_6)^2$, and $M^2 = -(\vec{p}_1 + \vec{p}_2 + \vec{p}_5)^2$ and on the momentum transfer variables $-t = (\vec{p}_1 + \vec{p}_4)^2$, $-t_1 = (\vec{p}_2 + \vec{p}_5)^2$, and $-t_2 = (\vec{p}_3 + \vec{p}_6)^2$. In order to take the triple Regge limit, given by

$$s_1, s_2 \gg M^2 \gg -t, -t_1, -t_2, \quad (5.2)$$

we have to go to Minkowski space via Wick rotation. We contract the amplitude with polarization vectors again,

$$\begin{aligned} & \mathcal{A}(|\vec{p}_i|; s, t, M^2, \dots)^{\lambda_1 \lambda_2 \lambda_3 \lambda_4 \lambda_5 \lambda_6} \\ &= \sum_{\lambda_i} \epsilon^{j_1(\lambda_1)}(\vec{p}_1) \epsilon^{j_2(\lambda_2)}(\vec{p}_2) \epsilon^{j_3(\lambda_3)}(\vec{p}_3) \epsilon^{j_4(\lambda_4)}(\vec{p}_4)^* \epsilon^{j_5(\lambda_5)}(\vec{p}_5)^* \epsilon^{j_6(\lambda_6)}(\vec{p}_6)^* A(\vec{p}_i)^{j_1 j_2 j_3 j_4 j_5 j_6}. \end{aligned} \quad (5.3)$$

As before, $\lambda_i = L, h$ denote the different polarizations, longitudinal or transverse. The resulting scattering amplitude \mathcal{A} depends on the energy and momentum transfer variables and on the virtualities $Q_i^2 = |\vec{p}_i|^2$ of the R -currents.

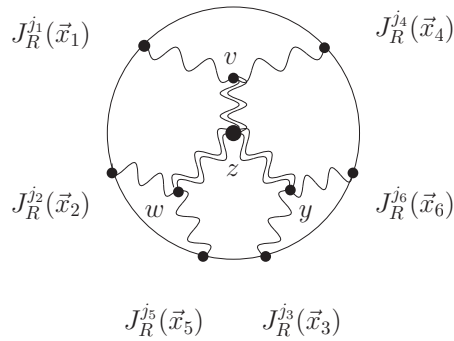


Figure 5.1: Witten diagram for the six point function of R -currents with a triple graviton vertex

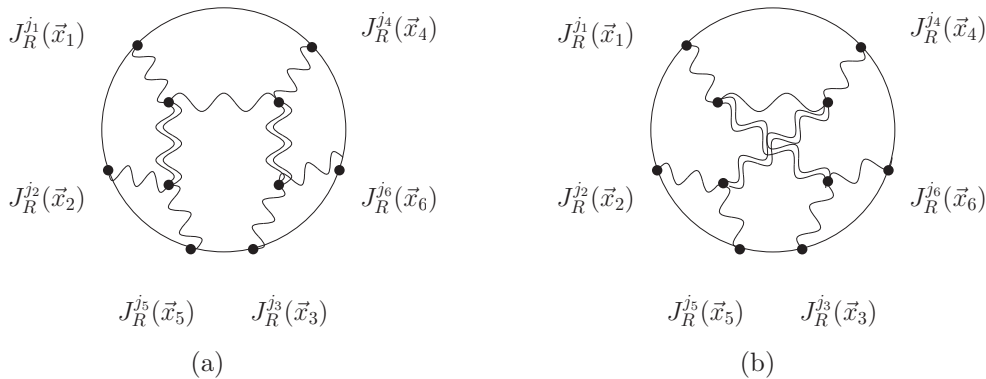


Figure 5.2: Witten diagrams for the six point function of R -currents with two graviton exchange

To compute the six point R -current amplitude (5.1) in classical supergravity, we again make use of Eq. (1.9), that connects the supergravity action (4.7) with correlation functions. We consider the resulting Witten diagrams, which are tree diagrams in the classical supergravity limit. In detail, we get three different Witten diagrams shown in Figs. 5.1 and 5.2. The six R -currents are inserted at the boundary of AdS_5 , represented by the circle. In the first diagram, see Fig. 5.1, the six bulk-to-boundary gauge boson propagators, the wavy lines, are connected by three bulk-to-bulk graviton propagators and a triple graviton vertex in the bulk. The double wavy lines symbolize as before the gravitons. The second type of diagrams is shown in Fig. 5.2. Here, the bulk-to-boundary gauge boson propagators are connected by two bulk-to-bulk graviton propagators, exchanged in the t -channels, and a bulk-to-bulk gauge boson propagator.

These diagrams in classical supergravity show a similar structure as the diagrams for the six point function at weak coupling in the large N_c -limit, presented in section 3.4.2. The triple graviton exchange diagram, Fig. 5.1, is in accordance with the two diagrams, which contain a triple vertex transition at weak coupling, shown in Figs. 3.17(a) and

3.17(b). The diagrams in Fig. 5.2 in classical supergravity correspond to the direct coupling diagram at weak coupling, Fig. 3.17(c). In the $\mathcal{N} = 4$ SYM diagram, two BFKL Pomerons are exchanged in the LLA and couple directly to the upper impact factor. In classical supergravity in lowest order, we have the exchange of two gravitons without any triple vertex transition. We observe this similarity of the diagrams for weak and strong coupling since $\mathcal{N} = 4$ SYM provides the new direct coupling. In QCD, the direct coupling is absent.

5.2 Graviton Exchange with the Triple Graviton Vertex

First, we consider the diagram in Fig. 5.1 with the triple graviton vertex in the bulk. We want to determine the high energy behavior of the amplitude (5.1) in the triple Regge limit. The diagram in Fig. 5.1 gives the contribution I^{TG} to the amplitude:

$$I^{\text{TG}} = \int d^4z dz_0 z_0 \int \frac{d^4v dv_0}{v_0} \int \frac{d^4w dw_0}{w_0} \int \frac{d^4y dy_0}{y_0} T_{(14)\nu_1\nu_4}(v) G_{\nu_1\nu_4;\mu_1\mu_2}(v, z) \\ \times T_{(25)\nu_2\nu_5}(w) G_{\nu_2\nu_5;\mu_3\mu_4}(w, z) T_{(36)\nu_3\nu_6}(y) G_{\nu_3\nu_6;\mu_5\mu_6}(y, z) V_{\mu_1\mu_2\mu_3\mu_4\mu_5\mu_6}(z). \quad (5.4)$$

I^{TG} contains the triple graviton vertex $V_{\mu_1\mu_2\mu_3\mu_4\mu_5\mu_6}$, the three graviton propagators $G_{\nu_i\nu_j\mu_k\mu_l}$, and three stress-energy tensors $T_{(ij)\nu_i\nu_j}$, which connect the external R -currents via bulk-to-boundary gauge boson propagators with the graviton propagators. Since we are interested in the triple Regge limit, Eq. (5.2), we have to transform the expression (5.4) to momentum space. From the computations in chapter 4 we know the stress-energy tensor and the graviton propagator in momentum space. To compute I^{TG} , we additionally need an expression for the triple graviton vertex $V_{\mu_1\mu_2\mu_3\mu_4\mu_5\mu_6}$ in an AdS_5 background in momentum space. We specify the vertex in the next section.

5.2.1 The Triple Graviton Vertex

The graviton field is identified as a small variation $h_{\mu\nu}$ from the metric of AdS_5 . The small deviation is defined as

$$\begin{aligned} \bar{g}_{\mu\nu} &= g_{\mu\nu} + \delta g_{\mu\nu} \\ &= g_{\mu\nu} + h_{\mu\nu} \end{aligned} \quad (5.5)$$

with the metric of AdS_5 given in Eq. (4.4). The triple graviton vertex contains terms in third order of $h_{\mu\nu}$. We derive the vertex from the Einstein-Hilbert action. The action is given by, see Eq. (4.7),

$$S = -\frac{1}{2\kappa^2} \int d^5z \sqrt{g} \mathcal{R}. \quad (5.6)$$

κ is the gravitational coupling, g is the determinant of the metric $g_{\mu\nu}$. \mathcal{R} is the scalar curvature with

$$\mathcal{R} = R_{\mu\nu} g^{\mu\nu} = R_{\rho\mu\sigma\nu} g^{\mu\nu} g^{\rho\sigma}. \quad (5.7)$$

$R_{\mu\nu}$ is the Ricci tensor and $R_{\rho\mu\sigma\nu}$ the Riemann tensor. The Riemann tensor is defined as

$$R_{\rho\mu\sigma\nu} = g_{\rho\lambda} R^{\lambda}_{\mu\sigma\nu} = g_{\rho\lambda} (\partial_{\sigma} \Gamma^{\lambda}_{\mu\nu} - \partial_{\nu} \Gamma^{\lambda}_{\mu\sigma} + \Gamma^{\lambda}_{\sigma\alpha} \Gamma^{\alpha}_{\mu\nu} - \Gamma^{\lambda}_{\nu\alpha} \Gamma^{\alpha}_{\mu\sigma}) \quad (5.8)$$

with the Christoffel symbols

$$\Gamma^{\alpha}_{\beta\gamma} = \frac{1}{2} g^{\alpha\rho} (\partial_{\beta} g_{\rho\gamma} + \partial_{\gamma} g_{\rho\beta} - \partial_{\rho} g_{\beta\gamma}). \quad (5.9)$$

To extract the triple graviton vertex, we vary the Einstein-Hilbert action (5.6) with respect to the metric $g_{\mu\nu}$ up to third order,

$$\frac{\delta^3 \mathcal{S}}{\delta g_{\mu\nu}^3} = -\frac{1}{2\kappa^2} \int d^5 z (3\delta^2 \sqrt{g} \delta \mathcal{R} + 3\delta \sqrt{g} \delta^2 \mathcal{R} + \delta^3 \sqrt{g} \mathcal{R} + \sqrt{g} \delta^3 \mathcal{R}). \quad (5.10)$$

As we see in Eq. (5.10), we have to variate the curvature \mathcal{R} and \sqrt{g} up to third order. We start with the first variation of the square root of g ,

$$\begin{aligned} \delta \sqrt{g} &= \frac{\partial \sqrt{g}}{\partial g_{\mu\nu}} \delta g_{\mu\nu} = \frac{1}{2} \frac{1}{\sqrt{g}} g g^{\mu\nu} \delta g_{\mu\nu} \\ &= \frac{1}{2} \sqrt{g} g^{\mu\nu} \delta g_{\mu\nu}, \end{aligned} \quad (5.11)$$

Here we have used $\delta g = g g^{\mu\nu} \delta g_{\mu\nu}$. We insert the metric $g^{\mu\nu} = z_0^2 \delta^{\mu\nu}$ as well as the square root of g , $\sqrt{g} = z_0^{-5}$, and get

$$\delta \sqrt{g} = \frac{1}{2} \frac{1}{z_0^3} h. \quad (5.12)$$

We have defined $\text{Tr}(h_{\alpha\beta}) = h_{\alpha}^{\alpha} = h$ here. We achieve in a similar way

$$\begin{aligned} \delta^2 \sqrt{g} &= \delta \left(\frac{1}{2} \sqrt{g} g^{\mu\nu} \delta g_{\mu\nu} \right) \\ &= \frac{1}{4} \sqrt{g} g^{\alpha\beta} g^{\mu\nu} h_{\alpha\beta} h_{\mu\nu} - \frac{1}{2} \sqrt{g} g^{\mu\rho} g^{\nu\sigma} h_{\rho\sigma} h_{\mu\nu} \\ &= \frac{1}{2} \frac{1}{z_0} \left(\frac{1}{2} h h - h_{\mu\nu} h_{\mu\nu} \right) \end{aligned} \quad (5.13)$$

and

$$\begin{aligned} \delta^3 \sqrt{g} &= \delta \left(\frac{1}{4} \sqrt{g} g^{\alpha\beta} g^{\mu\nu} h_{\alpha\beta} h_{\mu\nu} - \frac{1}{2} \sqrt{g} g^{\mu\rho} g^{\nu\sigma} h_{\rho\sigma} h_{\mu\nu} \right) \\ &= z_0 \left(\frac{1}{8} h h h - \frac{1}{8} h_{\mu\nu} h_{\mu\nu} h + h_{\mu\beta} h_{\beta\nu} h_{\mu\nu} \right). \end{aligned} \quad (5.14)$$

Next we vary the curvature \mathcal{R} . The first variation of \mathcal{R} is

$$\begin{aligned} \delta \mathcal{R} &= \delta (R_{\mu\nu} g^{\mu\nu}) = \delta R_{\mu\nu} g^{\mu\nu} + R_{\mu\nu} \delta g^{\mu\nu} \\ &= \delta R_{\mu\nu} g^{\mu\nu} - R_{\mu\nu} g^{\mu\alpha} g^{\nu\beta} \delta g_{\alpha\beta}. \end{aligned} \quad (5.15)$$

Here we have used $\delta g^{\mu\nu} = -g^{\mu\alpha}g^{\nu\beta}\delta g_{\alpha\beta}$. The variation of the Ricci tensor $R_{\mu\nu}$ reads

$$\begin{aligned}\delta R^\rho{}_{\mu\rho\nu} &= \partial_\rho\delta\Gamma^\rho{}_{\nu\mu} + \Gamma^\rho{}_{\rho\lambda}\delta\Gamma^\lambda{}_{\nu\mu} - \Gamma^\lambda{}_{\rho\mu}\delta\Gamma^\rho{}_{\nu\lambda} - \Gamma^\lambda{}_{\rho\nu}\Gamma^\rho{}_{\lambda\mu} \\ &\quad - \partial_\nu\delta\Gamma^\rho{}_{\rho\mu} + \Gamma^\lambda{}_{\nu\mu}\delta\Gamma^\rho{}_{\rho\lambda} - \Gamma^\rho{}_{\nu\lambda}\delta\Gamma^\lambda{}_{\rho\mu} + \Gamma^\lambda{}_{\rho\nu}\Gamma^\rho{}_{\lambda\mu} \\ &= \nabla_\rho(\delta\Gamma^\rho{}_{\nu\mu}) - \nabla_\nu(\delta\Gamma^\rho{}_{\rho\mu})\end{aligned}\quad (5.16)$$

with the covariant derivative ∇_μ of a tensor T defined as

$$\begin{aligned}\nabla_\mu T^{\mu_1\dots\mu_k}{}_{\nu_1\dots\nu_l} &= \partial_\mu T^{\mu_1\dots\mu_k}{}_{\nu_1\dots\nu_l} + \Gamma^\mu{}_{\mu\sigma}T^{\sigma\mu_2\dots\mu_k}{}_{\nu_1\dots\nu_l} + \dots + \Gamma^{\mu_k}{}_{\mu\sigma}T^{\mu_1\dots\mu_{k-1}\sigma}{}_{\nu_1\dots\nu_l} \\ &\quad - \Gamma^\sigma{}_{\mu\nu_1}T^{\mu_1\dots\mu_k}{}_{\sigma\nu_2\dots\nu_l} - \dots - \Gamma^\sigma{}_{\mu\nu_l}T^{\mu_1\dots\mu_l}{}_{\nu_1\dots\nu_{l-1}\sigma}.\end{aligned}\quad (5.17)$$

With the result for the variation of the Ricci tensor in Eq. (5.16) we get

$$\delta R_{\mu\nu}g^{\mu\nu} = g^{\mu\nu}(\nabla_\rho(\delta\Gamma^\rho{}_{\nu\mu}) - \nabla_\nu(\delta\Gamma^\rho{}_{\rho\mu}))\quad (5.18)$$

Since $\nabla_\rho g^{\mu\nu} = 0$, we arrive at

$$\delta R_{\mu\nu}g^{\mu\nu} = \nabla_\sigma(g^{\mu\nu}\delta\Gamma^\sigma{}_{\nu\mu} - g^{\mu\sigma}\delta\Gamma^\rho{}_{\rho\mu}).\quad (5.19)$$

Integration over this term in the action (5.6) only gives boundary terms, and we are allowed to neglect the term in the first variation of \mathcal{R} . Thus, we have

$$\delta\mathcal{R} = -R_{\mu\nu}g^{\mu\alpha}g^{\nu\beta}\delta g_{\alpha\beta}.\quad (5.20)$$

We insert the definition of the Ricci tensor, Eq. (5.7), and of the Riemann tensor, Eq. (5.8). Furthermore, we use the representation of the Christoffel symbols in Eq. (5.9), the variation of the metric, and the metric and arrive at

$$\delta\mathcal{R} = -R^{\mu\nu}\delta g_{\mu\nu} = 4z_0^2\delta_{\mu\nu}h_{\mu\nu} = 4z_0^2h.\quad (5.21)$$

From Eq. (5.21) we can read off the Ricci tensor that allows us to compute an explicit expression for the curvature \mathcal{R} , which is needed in the variation of S :

$$R_{\mu\nu} = -4z_0^2\delta_{\mu\nu}.\quad (5.22)$$

The resulting curvature \mathcal{R} is

$$\mathcal{R} = R^{\mu\nu}g_{\mu\nu} = -\frac{1}{z_0^2}4z_0^2\delta_{\mu\nu}\delta_{\mu\nu} = -20.\quad (5.23)$$

Now we have all necessary results to write down, as a first intermediate result, the first variation of the action:

$$\begin{aligned}\delta S &= -\frac{1}{2\kappa^2}\int d^5z\delta\sqrt{g}\mathcal{R} + \sqrt{g}\delta\mathcal{R} \\ &= \frac{1}{2\kappa^2}\int d^5z6\frac{1}{z_0^3}h.\end{aligned}\quad (5.24)$$

The second variation of the action S , computed in a similar way, gives the equation of motion for the graviton field $h_{\mu\nu}$ [57]. Since we do not need it in the future computations, we do not show the equation of motion here.

The result of the third variation, Eq. (5.10), reads

$$\begin{aligned}
\frac{\delta^3 S}{\delta g_{\mu\nu}^3} = & -\frac{1}{2\kappa^2} \int d^5 z z_0 (c_1 h h_{0\mu} h_{0\mu} - c_2 h_{\mu\nu} h_{0\mu} h_{0\nu} - c_3 h_{\mu\nu} h_{\mu\nu} h_{00} + c_4 h_{\mu\nu} h_{\mu\nu} h \\
& - c_5 h_{\mu\nu} h_{\nu\alpha} h_{\mu\alpha} + c_6 h h h_{00} - c_7 h h h) \\
& + z_0^2 (c_8 h_{0\mu} h_{\mu\nu} \partial_\alpha h_{\nu\alpha} + c_9 h_{0\mu} h_{\nu\alpha} \partial_\alpha h_{\mu\nu} + c_{10} h_{\mu\nu} h_{0\nu} \partial_\mu h + c_{11} h_{\mu\nu} h_{\mu\nu} \partial_\alpha h_{0\alpha} \\
& + c_{12} h_{\mu\nu} h_{0\alpha} \partial_\alpha h_{\mu\nu} - c_{13} h_{\mu\nu} h \partial_0 h_{\mu\nu} + c_{14} h_{\mu\alpha} h_{\mu\nu} \partial_0 h_{\nu\alpha} + c_{15} h h \partial_\mu h_{0\mu} \\
& - c_{16} h h_{\mu\nu} \partial_\mu h_{0\nu} + c_{17} h h_{0\nu} \partial_\mu h_{\mu\nu} + c_{18} h h \partial_0 h - c_{19} h_{\mu\nu} h_{\mu\nu} \partial_0 h) \\
& + z_0^3 (c_{20} \partial_\mu h \partial_\nu h h_{\mu\nu} + c_{21} \partial_\mu \partial_\nu h h h_{\mu\nu} + c_{22} \partial_\mu \partial_\nu h_{\mu\nu} h h + c_{23} \partial_\nu h_{\mu\nu} \partial_\mu h h \\
& - c_{24} \partial_\alpha \partial_\nu h h_{\mu\nu} h_{\mu\alpha} + c_{25} \partial_\alpha h \partial_\mu h_{\nu\alpha} h_{\mu\nu} - c_{26} \partial_\alpha h \partial_\nu h_{\mu\nu} h_{\mu\alpha} \\
& - c_{27} \partial_\mu \partial_\nu h_{\mu\alpha} h_{\nu\alpha} h + c_{28} \partial_\mu h_{\mu\nu} \partial_\alpha h_{\nu\alpha} h + c_{29} \partial_\mu h_{\nu\alpha} \partial_\alpha h_{\mu\nu} h - c_{30} \partial_\mu \partial_\mu h h h \\
& - c_{31} \partial_\mu h \partial_\mu h h - c_{32} \partial_\alpha \partial_\alpha h h_{\mu\nu} h_{\mu\nu} - c_{33} \partial_\alpha h \partial_\alpha h_{\mu\nu} h_{\mu\nu} - c_{34} h \partial_\mu h_{\nu\alpha} \partial_\mu h_{\nu\alpha} \\
& + c_{35} \partial_\alpha \partial_\alpha h_{\mu\nu} h_{\mu\nu} h - c_{36} \partial_\alpha \partial_\alpha h_{\nu\beta} h_{\mu\beta} h_{\mu\nu} + c_{37} \partial_\alpha h_{\mu\nu} \partial_\alpha h_{\nu\beta} h_{\mu\beta} \\
& + c_{38} \partial_\alpha \partial_\nu h_{\mu\beta} h_{\alpha\beta} h_{\mu\nu} + c_{39} \partial_\alpha h_{\mu\nu} \partial_\mu h_{\alpha\beta} h_{\nu\beta} - c_{40} \partial_\nu h_{\alpha\beta} \partial_\alpha h_{\mu\beta} h_{\mu\nu} \\
& - c_{41} \partial_\alpha h_{\mu\nu} \partial_\beta h_{\alpha\beta} h_{\mu\nu} + c_{42} h_{\mu\nu} h_{\alpha\beta} \partial_\alpha \partial_\beta h_{\mu\nu} - c_{43} h_{\mu\nu} \partial_\alpha \partial_\beta h_{\alpha\beta} h_{\mu\nu} \\
& + c_{44} \partial_\beta h_{\mu\nu} h_{\alpha\beta} \partial_\alpha h_{\mu\nu} + c_{45} h_{\mu\nu} \partial_\beta h_{\nu\beta} \partial_\alpha h_{\mu\alpha} + c_{46} h_{\mu\nu} \partial_\alpha \partial_\beta h_{\nu\beta} h_{\mu\alpha} \\
& - c_{47} \partial_\alpha h_{\mu\alpha} \partial_\nu h_{\mu\beta} h_{\nu\beta}). \tag{5.25}
\end{aligned}$$

The factors c_i are multiplicative numbers that are not relevant in determining the high energy behavior of the amplitude. ∂_λ is a derivative with respect to z_λ .

Now we extract the triple graviton vertex in momentum space from Eq. (5.25). To obtain a vertex from an action we use the usual rules. That is, we take three functional derivatives of the action with respect to the graviton field h and go to momentum space via Fourier transformation. The functional derivatives result in Kronecker symbols in the vertex. Due to the Fourier transformation every partial derivative acting on a graviton field $h_{\rho\sigma}$ in the action is replaced by $(-i)$ times the momentum of the field. Therefore, the derivative ∂_{k_λ} acting on one of the three fields $h_{\rho\sigma}$ in each term of the action is replaced by

$$\partial_{k_\lambda} \rightarrow \delta_{\lambda m} (-ip_k - ip_{k+3})_m + \delta_{\lambda 0} \partial_0 =: P_{k_\lambda} \tag{5.26}$$

with $k = 1, \dots, 3$ for the three graviton fields in each term of Eq. (5.25). p_k and p_{k+3} are the two incoming momenta of two connected bulk-to-boundary gauge boson propagator, and P_k is the graviton momentum.

Applying these rules the triple graviton vertex in momentum space reads

$$\begin{aligned}
& V_{\mu_1\mu_2\mu_3\mu_4\mu_5\mu_6}(P_1, P_2, P_3) \\
&= -z_0(c_1 \delta_{\mu_1\mu_2} \delta_{\mu_30} \delta_{\mu_50} \delta_{\mu_4\mu_6} - c_2 \delta_{\mu_1\mu_4} \delta_{\mu_2\mu_6} \delta_{\mu_30} \delta_{\mu_50} - c_3 \delta_{\mu_1\mu_3} \delta_{\mu_2\mu_4} \delta_{\mu_50} \delta_{\mu_60} \\
&\quad + c_4 \delta_{\mu_1\mu_3} \delta_{\mu_2\mu_4} \delta_{\mu_5\mu_6} - c_5 \delta_{\mu_1\mu_5} \delta_{\mu_2\mu_3} \delta_{\mu_4\mu_6} + c_6 \delta_{\mu_1\mu_2} \delta_{\mu_3\mu_4} \delta_{\mu_50} \delta_{\mu_60} \\
&\quad - c_7 \delta_{\mu_1\mu_2} \delta_{\mu_3\mu_4} \delta_{\mu_5\mu_6}) \\
&\quad - z_0^2(c_8 \delta_{\mu_10} \delta_{\mu_2\mu_3} \delta_{\mu_4\mu_5} P_{3\alpha} \delta_{\mu_6\alpha} + c_9 \delta_{\mu_10} \delta_{\mu_2\mu_5} \delta_{\mu_3\mu_6} P_{2\alpha} \delta_{\mu_4\alpha} \\
&\quad + c_{10} \delta_{\mu_1\alpha} \delta_{\mu_2\mu_4} \delta_{\mu_30} P_{3\alpha} \delta_{\mu_5\mu_6} + c_{11} \delta_{\mu_1\mu_3} \delta_{\mu_2\mu_4} P_{3\alpha} \delta_{\alpha\mu_6} \delta_{\mu_50} \\
&\quad + c_{12} \delta_{\mu_1\mu_5} \delta_{\mu_2\mu_6} \delta_{\mu_30} \delta_{\mu_4\alpha} P_{2\alpha} - c_{13} \delta_{\mu_1\mu_5} \delta_{\mu_2\mu_6} \delta_{\mu_3\mu_4} \delta_{\alpha0} P_{3\alpha} \\
&\quad + c_{14} \delta_{\mu_1\mu_3} \delta_{\mu_2\mu_6} \delta_{\mu_4\mu_5} \delta_{\alpha0} P_{3\alpha} + c_{15} \delta_{\mu_1\mu_2} \delta_{\mu_3\mu_4} \delta_{\alpha\mu_6} P_{3\alpha} \delta_{\mu_50} \\
&\quad - c_{16} \delta_{\mu_1\mu_2} \delta_{\mu_3\alpha} \delta_{\mu_4\mu_6} \delta_{\mu_50} P_{2\alpha} + c_{17} \delta_{\mu_1\mu_2} \delta_{\mu_30} \delta_{\mu_4\mu_6} P_{3\alpha} \delta_{\mu_5\alpha} \\
&\quad + c_{18} \delta_{\mu_1\mu_2} \delta_{\mu_3\mu_4} \delta_{\mu_5\mu_6} P_{3\alpha} \delta_{\alpha0} - c_{19} \delta_{\mu_1\mu_2} \delta_{\mu_3\mu_5} \delta_{\mu_4\mu_6} P_{1\alpha} \delta_{\alpha0}) \\
&\quad - z_0^3(c_{20} \delta_{\mu_1\mu_2} \delta_{\mu_3\mu_4} \delta_{\mu_5\alpha} \delta_{\mu_6\beta} P_{1\alpha} P_{2\beta} + c_{21} \delta_{\mu_1\mu_2} \delta_{\mu_3\mu_4} \delta_{\mu_5\alpha} \delta_{\mu_6\beta} P_{1\alpha} P_{1\beta} \\
&\quad + c_{22} \delta_{\mu_1\alpha} \delta_{\mu_2\beta} \delta_{\mu_3\mu_4} \delta_{\mu_5\mu_6} P_{1\alpha} P_{1\beta} + c_{23} \delta_{\mu_1\alpha} \delta_{\mu_2\beta} \delta_{\mu_3\mu_4} \delta_{\mu_5\mu_6} P_{1\alpha} P_{2\beta} \\
&\quad - c_{24} \delta_{\mu_1\mu_2} \delta_{\mu_3\mu_5} \delta_{\mu_4\alpha} \delta_{\mu_6\beta} P_{1\alpha} P_{1\beta} + c_{25} \delta_{\mu_1\mu_2} \delta_{\mu_3\mu_6} \delta_{\mu_4\alpha} \delta_{\mu_5\beta} P_{1\alpha} P_{2\beta} \\
&\quad - c_{26} \delta_{\mu_1\mu_2} \delta_{\mu_3\mu_5} \delta_{\mu_4\beta} \delta_{\mu_6\alpha} P_{1\alpha} P_{2\beta} - c_{27} \delta_{\mu_1\alpha} \delta_{\mu_2\mu_4} \delta_{\mu_3\beta} \delta_{\mu_5\mu_6} P_{1\alpha} P_{1\beta} \\
&\quad + c_{28} \delta_{\mu_1\alpha} \delta_{\mu_2\mu_3} \delta_{\mu_4\beta} \delta_{\mu_5\mu_6} P_{1\alpha} P_{2\beta} + c_{29} \delta_{\mu_1\mu_4} \delta_{\mu_2\beta} \delta_{\mu_3\alpha} \delta_{\mu_5\mu_6} P_{1\alpha} P_{2\beta} \\
&\quad - c_{30} \delta_{\mu_1\mu_2} \delta_{\mu_3\mu_4} \delta_{\mu_5\mu_6} P_{1\alpha} P_{1\alpha} - c_{31} \delta_{\mu_1\mu_2} \delta_{\mu_3\mu_4} \delta_{\mu_5\mu_6} P_{1\alpha} P_{2\alpha} \\
&\quad - c_{32} \delta_{\mu_1\mu_2} \delta_{\mu_3\mu_5} \delta_{\mu_4\mu_6} P_{1\alpha} P_{1\alpha} - c_{33} \delta_{\mu_1\mu_2} \delta_{\mu_3\mu_5} \delta_{\mu_4\mu_6} P_{1\alpha} P_{2\alpha} \\
&\quad - c_{34} \delta_{\mu_1\mu_2} \delta_{\mu_3\mu_5} \delta_{\mu_4\mu_6} P_{2\alpha} P_{3\alpha} + c_{35} \delta_{\mu_1\mu_2} \delta_{\mu_3\mu_5} \delta_{\mu_4\mu_6} P_{2\alpha} P_{2\alpha} \\
&\quad - c_{36} \delta_{\mu_1\mu_6} \delta_{\mu_2\mu_4} \delta_{\mu_3\mu_5} P_{1\alpha} P_{1\alpha} + c_{37} \delta_{\mu_1\mu_5} \delta_{\mu_2\mu_3} \delta_{\mu_4\mu_6} P_{1\alpha} P_{2\alpha} \\
&\quad - c_{38} \delta_{\mu_1\mu_5} \delta_{\mu_2\mu_4} \delta_{\mu_3\alpha} \delta_{\mu_6\beta} P_{1\alpha} P_{1\beta} - c_{39} \delta_{\mu_1\alpha} \delta_{\mu_2\mu_5} \delta_{\mu_3\beta} \delta_{\mu_4\mu_6} P_{1\beta} P_{2\alpha} \\
&\quad - c_{40} \delta_{\mu_1\alpha} \delta_{\mu_2\mu_3} \delta_{\mu_4\mu_5} \delta_{\mu_6\beta} P_{1\beta} P_{2\alpha} - c_{41} \delta_{\mu_1\mu_5} \delta_{\mu_2\mu_6} \delta_{\mu_3\alpha} \delta_{\mu_4\beta} P_{1\alpha} P_{2\beta} \\
&\quad + c_{42} \delta_{\mu_1\mu_5} \delta_{\mu_2\mu_6} \delta_{\mu_3\alpha} \delta_{\mu_4\beta} P_{3\alpha} P_{3\beta} - c_{43} \delta_{\mu_1\mu_5} \delta_{\mu_3\alpha} \delta_{\mu_4\beta} \delta_{\mu_2\mu_6} P_{2\alpha} P_{2\beta} \\
&\quad + c_{44} \delta_{\mu_1\mu_5} \delta_{\mu_2\mu_6} \delta_{\mu_3\alpha} \delta_{\mu_4\beta} P_{1\beta} P_{3\alpha} + c_{45} \delta_{\mu_1\mu_5} \delta_{\mu_2\mu_3} \delta_{\mu_4\alpha} \delta_{\mu_6\beta} P_{2\alpha} P_{3\beta} \\
&\quad + c_{46} \delta_{\mu_1\mu_5} \delta_{\mu_2\mu_3} \delta_{\mu_4\alpha} \delta_{\mu_6\beta} P_{2\alpha} P_{2\beta} - c_{47} \delta_{\mu_1\mu_3} \delta_{\mu_2\alpha} \delta_{\mu_4\mu_6} \delta_{\mu_5\beta} P_{1\alpha} P_{2\beta}) \\
&\quad + \text{symmetric terms.} \tag{5.27}
\end{aligned}$$

The symmetric terms are a result of taking the functional derivatives of the action. They can be identified from Eq. (5.27) performing the following substitutions:

$$(P_k, \mu_{2k-1}, \mu_{2k}) \leftrightarrow (P_j, \mu_{2j-1}, \mu_{2j}), \tag{5.28}$$

that is the exchange of the graviton momenta P_k in all possible ways and the corresponding indices with $k, j = 1, \dots, 3$ and subsequent, the second substitution

$$\mu_{2i-1} \leftrightarrow \mu_{2i} \tag{5.29}$$

with $i = 1, \dots, 3$, that is the exchange of indices of each graviton.

5.2.2 High Energy Behavior

We are interested in the high energy behavior of the diagram with the triple graviton vertex, shown in Fig. 5.1. According to Ref. [50] we expect in the triple Regge limit a high energy behavior of the amplitude proportional to

$$\left(\frac{s_1}{M^2}\right)^{j_1} \left(\frac{s_2}{M^2}\right)^{j_2} (M^2)^j \quad (5.30)$$

with the spins of the three gravitons: $j_1 = j_2 = j = 2$.

The stress-energy tensors $T_{(ij)\nu_i\nu_j}$ and the graviton propagators $G_{\nu_i\nu_j;\mu_k\mu_l}$ are contracted with the triple graviton vertex $V_{\mu_1\mu_2\mu_3\mu_4\mu_5\mu_6}$, see Eq. (5.4). From the computation of the four point function in chapter 4 we know the leading contribution of the stress-energy tensor, Eq. (4.64), and of the graviton propagator, Eq. (4.49), in the Regge limit. The contraction of the stress-energy tensors with the graviton propagators in the Regge limit gives

$$\begin{aligned} & T_{(14)\nu_1\nu_4} G_{\nu_1\nu_4;\mu_1\mu_2} T_{(25)\nu_2\nu_5} G_{\nu_2\nu_5;\mu_3\mu_4} T_{(36)\nu_3\nu_6} G_{\nu_3\nu_6;\mu_5\mu_6} \\ & \approx (2p_{1\mu_1}p_{4\mu_2} + 2p_{1\mu_2}p_{4\mu_1})(2p_{2\mu_3}p_{5\mu_4} + 2p_{2\mu_4}p_{5\mu_3})(2p_{3\mu_5}p_{6\mu_6} + 2p_{3\mu_6}p_{6\mu_5}). \end{aligned} \quad (5.31)$$

Here we suppress terms of the stress-energy tensor, which are contracted with the external polarization vectors of the R -currents since these terms do not contribute to the leading high energy behavior in the Regge limit.

The last step is to contract Eq. (5.31) with the triple graviton vertex $V_{\mu_1\mu_2\mu_3\mu_4\mu_5\mu_6}$. Contractions of the momenta p_1 or p_4 with p_2 or p_5 give terms proportional to s_1 , contractions of p_1 or p_4 with momenta p_3 or p_6 give terms proportional to s_2 . All other contractions of momenta provide subleading contributions. Consequently, in the triple Regge limit, the following part of the triple graviton vertex leads to the highest power of energies s_1 and s_2 in the amplitude:

$$\begin{aligned} & V_{\mu_1\mu_2\mu_3\mu_4\mu_5\mu_6}(P_1, P_2, P_3) \\ & \approx z_0(c_2 \delta_{\mu_1\mu_4} \delta_{\mu_2\mu_6} \delta_{\mu_30} \delta_{\mu_50} + c_3 \delta_{\mu_1\mu_3} \delta_{\mu_2\mu_4} \delta_{\mu_50} \delta_{\mu_60} \\ & \quad - c_4 \delta_{\mu_1\mu_3} \delta_{\mu_2\mu_4} \delta_{\mu_5\mu_6} + c_5 \delta_{\mu_1\mu_5} \delta_{\mu_2\mu_3} \delta_{\mu_4\mu_6}) \\ & + z_0^2(-c_{11} \delta_{\mu_1\mu_3} \delta_{\mu_2\mu_4} P_{3\alpha} \delta_{\alpha\mu_6} \delta_{\mu_50} - c_{12} \delta_{\mu_1\mu_5} \delta_{\mu_2\mu_6} \delta_{\mu_30} \delta_{\mu_4\alpha} P_{2\alpha} \\ & \quad + c_{13} \delta_{\mu_1\mu_5} \delta_{\mu_2\mu_6} \delta_{\mu_3\mu_4} \delta_{\alpha0} P_{3\alpha} - c_{14} \delta_{\mu_1\mu_3} \delta_{\mu_2\mu_6} \delta_{\mu_4\mu_5} \delta_{\alpha0} P_{3\alpha}) \\ & + z_0^3(c_{36} \delta_{\mu_1\mu_6} \delta_{\mu_2\mu_4} \delta_{\mu_3\mu_5} P_{1\alpha} P_{1\alpha} - c_{37} \delta_{\mu_1\mu_5} \delta_{\mu_2\mu_3} \delta_{\mu_4\mu_6} P_{1\alpha} P_{2\alpha} \\ & \quad + c_{38} \delta_{\mu_1\mu_5} \delta_{\mu_2\mu_4} \delta_{\mu_3\alpha} \delta_{\mu_6\beta} P_{1\alpha} P_{1\beta} + c_{41} \delta_{\mu_1\mu_5} \delta_{\mu_2\mu_6} \delta_{\mu_3\alpha} \delta_{\mu_4\beta} P_{1\alpha} P_{2\beta} \\ & \quad - c_{42} \delta_{\mu_1\mu_5} \delta_{\mu_2\mu_6} \delta_{\mu_3\alpha} \delta_{\mu_4\beta} P_{3\alpha} P_{3\beta} + c_{43} \delta_{\mu_1\mu_5} \delta_{\mu_3\alpha} \delta_{\mu_4\beta} \delta_{\mu_2\mu_6} P_{2\alpha} P_{2\beta} \\ & \quad - c_{44} \delta_{\mu_1\mu_5} \delta_{\mu_2\mu_6} \delta_{\mu_3\alpha} \delta_{\mu_4\beta} P_{1\beta} P_{3\alpha} - c_{45} \delta_{\mu_1\mu_5} \delta_{\mu_2\mu_3} \delta_{\mu_4\alpha} \delta_{\mu_6\beta} P_{2\alpha} P_{3\beta} \\ & \quad - c_{46} \delta_{\mu_1\mu_5} \delta_{\mu_2\mu_3} \delta_{\mu_4\alpha} \delta_{\mu_6\beta} P_{2\alpha} P_{2\beta}) \\ & + \text{contributions from symmetric terms.} \end{aligned} \quad (5.32)$$

The contributions from symmetric terms include all parts of the symmetrized terms in Eq. (5.27), which contribute in the triple Regge limit. The leading part of the

triple graviton vertex, Eq. (5.32), contracted with Eq. (5.31) provides terms with two connections between momenta, which give a contribution proportional to s_1 or s_2 .

Thus, we observe the following high energy behavior: The amplitude contains three terms proportional to $s_1 s_2$, s_1^2 , and s_2^2 . This result implies that the expected contribution of the amplitude in the triple Regge limit, see Eq. (5.30), vanishes. The diagram with the triple graviton vertex decouples in the high energy limit. The terms in Eq. (5.30) may contribute beyond the classical supergravity approximation where the graviton is expected to start to reggeize.

The diagrams in Fig. 5.2 contain the exchange of two gravitons in the t -channels. An explicit computation gives a high energy behavior proportional to $s_1^2 s_2^2$ in the triple Regge limit [45]. For large M^2 , the two graviton exchange diagrams fall with M^{-2} . They are the dominant ones compared to the triple graviton vertex diagram.

In case of the six point function of R -currents in $\mathcal{N} = 4$ SYM at weak coupling in chapter 3.4.2, the partial wave $F^{(\text{Dir})}$, which contains the direct coupling, is for large values of M^2 subleading compared to the partial waves $F^{(\text{P})}$ and $F^{(\text{NP})}$, which provide a triple vertex transition.

6 Summary

The elastic scattering of highly virtual photons in QCD is a reliable environment to study the BFKL Pomeron in a perturbative regime. However, the relation of the BFKL Pomeron to QCD at strong coupling is not clear.

The AdS/CFT-correspondence offers a new opportunity to investigate gauge theories at strong coupling. The correspondence is a duality between conformal field theories and string theories. The best understood example is the connection between $\mathcal{N} = 4$ SYM and IIB string theory on an $AdS_5 \times S_5$ background. In particular, the strong coupling limit of $\mathcal{N} = 4$ SYM in the large N_c -limit is related to weakly coupled type IIB supergravity. The duality connects the BFKL Pomeron in $\mathcal{N} = 4$ SYM with graviton exchange on the string theory side.

We have considered the scattering of conserved R -currents in $\mathcal{N} = 4$ SYM. R -current correlators are close analogs of electromagnetic current correlators. The supersymmetry of $\mathcal{N} = 4$ SYM does not influence the exchanged gluons in the scattering process at weak coupling, and as a consequence, in the LLA, the BFKL Pomeron is the same in QCD and $\mathcal{N} = 4$ SYM. In order to study R -current scattering at strong coupling, we have made use of the AdS/CFT-correspondence. The strong coupling limit of the R -current correlation functions has been addressed in the corresponding weakly coupled supergravity theory. Consequently, we have obtained analytic expressions for the four and six point correlation function at weak and strong coupling.

First, we have computed the four point function of R -currents at weak coupling in the Regge limit. We have shown the finiteness of the fermionic and scalar one-loop diagrams and have determined their high energy behavior. The leading diagrams are three-loop diagrams with two impact factors and two exchanged gluons in the t -channel. Their amplitude is proportional to s . We have given explicit results for the fermion and scalar impact factors with longitudinal and transverse polarization of the R -currents. A different result, compared with QCD, is the helicity conservation of R -currents even in the non-forward direction. In the LLA, we have pointed out that the Regge factorization of the amplitude in $\mathcal{N} = 4$ SYM stays the same as in QCD.

The investigation of the six point function of R -currents at weak coupling in the triple Regge limit has been the next step in our work since the function contains the most important unitarity corrections to the BFKL Pomeron. We have explained the connection between fermion impact factors in QCD and $\mathcal{N} = 4$ SYM and have written the new scalar impact factors with more than two gluons as a superposition of two gluon impact factors. One main result is a new coupling of the exchanged gluons to the R -currents, called direct coupling, which is absent in QCD. It can be traced back to the fact that the particles are in the adjoint representation of the gauge group in $\mathcal{N} = 4$ SYM. If we do not have s -channel gluons contributing to the M^2 -discontinuity,

the coupling of the gluons to the R -currents is mediated by the unintegrated impact factor. We have given its explicit expression for fermions and scalars. Besides the impact factors, the amplitude contains the BFKL and BKP equations as well as the triple Pomeron vertex. They are not influenced by the supersymmetry of $\mathcal{N} = 4$ SYM and are independent of the couplings to the external R -currents. As a result, the Regge factorization of the amplitude stays the same as in QCD. A further computation has been addressed to the large N_c -limit of the six point function of R -currents in a topological approach. This method has offered an additional understanding of the structure of the six point function. The different building blocks in the six point function are due to different topologies of the amplitude. Moreover, in the large N_c -limit, we have found a suppression of BKP states with more than two gluons in the six point function.

In the second part of this work, we have investigated the strong coupling limit of R -current correlators in $\mathcal{N} = 4$ SYM in the corresponding weakly coupled supergravity theory. In particular, we have computed Witten diagrams, which are similar to usual Feynman diagrams. However, Witten diagrams are given in a five-dimensional Anti-de Sitter background. Applying the classical supergravity limit, we only have had to consider tree Witten diagrams. The four point function of R -currents has led to Witten diagrams with one graviton and one gauge boson exchange, respectively. In the Regge limit, the graviton exchange diagram is proportional to s^2 , reflecting the spin of the graviton, and therefore gives the leading contribution. The gauge boson exchange diagram is only proportional to s . The graviton exchange diagram shows a familiar factorization of the amplitude. The amplitude can be written in terms of two impact factors and an exchange propagator, which are convoluted by a two-dimensional integration in the fifth dimension. The helicity of the R -currents is conserved in both amplitudes as it is the case for the four point function in $\mathcal{N} = 4$ SYM at weak coupling.

The six point function of R -currents in the weakly coupled supergravity theory corresponds to a Witten diagram with a triple graviton vertex and to two Witten diagrams with two graviton exchange. In order to determine the high energy behavior of the diagram with the triple graviton vertex, we have computed the vertex in an AdS_5 background. In the triple Regge limit, the amplitude is expected to be proportional to $(s_1/M^2)^2(s_2/M^2)^2(M^2)^2$. However, this contribution vanishes and the diagram with the triple graviton vertex consists of three terms proportional to s_1s_2 , s_1^2 , and s_2^2 . That is the triple graviton diagram decouples in the high energy limit, and the two graviton exchange diagrams are the leading ones.

Summarizing, we have studied the four and six point function of R -currents in $\mathcal{N} = 4$ SYM at weak and strong coupling and observed several similarities of the results. The amplitude of the four point function shows a factorization at weak and strong coupling. The leading diagrams can be written in terms of impact factors and exchange propagators convoluted by a two-dimensional integration. Nevertheless, a uniform description of the results for weak and strong coupling is still missing. In Ref. [38], the scattering of scalar primaries in $\mathcal{N} = 4$ SYM has been considered, and the BFKL Pomeron exchange at weak coupling has been analyzed directly in position

space. Using this method for the graviton exchange amplitude at strong coupling may provide a representation that interpolates between the weak and strong coupling limit.

The diagrams of the six point amplitude exhibit the same structure at weak and strong coupling. The amplitude at weak coupling leads to two different types of diagrams: diagrams with a triple vertex transition and one diagram containing a direct coupling of the gluons to the impact factor, which is a new coupling in $\mathcal{N} = 4$ SYM and absent in QCD. The same two structures appear in the six point function at strong coupling. We have one diagram with a triple vertex, the triple graviton vertex diagram, and diagrams with a direct exchange of two gravitons in the t -channels. This correspondence of diagrams is due to the occurrence of the new direct coupling in $\mathcal{N} = 4$ SYM.

In future work, several problems should be addressed: On the $\mathcal{N} = 4$ SYM side at weak coupling, the two gluon propagators in the leading diagrams of the four point function are replaced by the BFKL Green's function in the LLA. The reggeization of the gluons modifies the power behavior of the energy s from 1 to $1 + \omega_0$. On the string theory side, the graviton is expected to reggeize similarly as the gluon. The reggeization of the graviton would change the high energy behavior of the amplitude, that is s^2 at leading order, to $s^{2-\Delta}$. Δ symbolizes higher order corrections to the graviton trajectory with $\Delta = \mathcal{O}(1/\sqrt{\lambda})$. In order to determine these higher order corrections, computations beyond the classical supergravity limit are necessary. First corrections to the graviton trajectory have been deduced from the scattering of strings on an AdS_5 background in Ref. [33], see also Ref. [29].

Another line of interest is the analysis of integrable structures at strong coupling. In the large N_c -limit, BKP states are known to be integrable. Unfortunately, the BKP states are suppressed in the six point function of R -currents in the large N_c -limit at weak coupling. Therefore, higher order correlation functions have to be investigated in which the BKP states do not vanish in the large N_c -limit. The strong coupling limit of these correlation functions can be studied in the weakly coupled string theory as well.

Bibliography

- [1] H. D. Politzer, Phys. Rev. Lett. **30** (1973) 1346.
- [2] D. J. Gross and F. Wilczek, Phys. Rev. Lett. **30** (1973) 1343.
- [3] P. D. B. Collins, Cambridge 1977, 445p.
- [4] G. F. Chew and S. C. Frautschi, Phys. Rev. Lett. **7** (1961) 394.
- [5] G. Veneziano, Nuovo Cim. A **57** (1968) 190.
- [6] J. Bartels, A. De Roeck and H. Lotter, Phys. Lett. B **389** (1996) 742 [arXiv:hep-ph/9608401].
- [7] S. J. Brodsky, F. Hautmann and D. E. Soper, Phys. Rev. D **56** (1997) 6957 [arXiv:hep-ph/9706427].
- [8] E. A. Kuraev, L. N. Lipatov and V. S. Fadin, Sov. Phys. JETP **44** (1976) 443 [Zh. Eksp. Teor. Fiz. **71** (1976) 840].
- [9] E. A. Kuraev, L. N. Lipatov and V. S. Fadin, Sov. Phys. JETP **45** (1977) 199 [Zh. Eksp. Teor. Fiz. **72** (1977) 377].
- [10] I. I. Balitsky and L. N. Lipatov, Sov. J. Nucl. Phys. **28** (1978) 822 [Yad. Fiz. **28** (1978) 1597].
- [11] V. S. Fadin and L. N. Lipatov, Phys. Lett. B **429** (1998) 127 [arXiv:hep-ph/9802290].
- [12] M. Ciafaloni and G. Camici, Phys. Lett. B **430** (1998) 349 [arXiv:hep-ph/9803389].
- [13] J. Bartels, Nucl. Phys. B **175** (1980) 365.
- [14] J. Kwieciński and M. Praszalowicz, Phys. Lett. B **94** (1980) 413.
- [15] J. Bartels, Phys. Lett. B **298** (1993) 204.
- [16] J. Bartels, Z. Phys. C **60** (1993) 471.
- [17] J. Bartels and M. Wüsthoff, Z. Phys. C **66** (1995) 157.
- [18] J. Bartels and C. Ewerz, JHEP **9909** (1999) 026 [arXiv:hep-ph/9908454].

-
- [19] L. N. Lipatov, [arXiv:hep-th/9311037].
- [20] L. N. Lipatov, JETP Lett. **59** (1994) 596 [Pisma Zh. Eksp. Teor. Fiz. **59** (1994) 571].
- [21] L. D. Faddeev and G. P. Korchemsky, Phys. Lett. B **342** (1995) 311 [arXiv:hep-th/9404173].
- [22] L. N. Lipatov, Sov. Phys. JETP **63** (1986) 904 [Zh. Eksp. Teor. Fiz. **90** (1986) 1536].
- [23] J. Bartels, L. N. Lipatov and M. Wusthoff, Nucl. Phys. B **464** (1996) 298 [arXiv:hep-ph/9509303].
- [24] J. M. Maldacena, Adv. Theor. Math. Phys. **2** (1998) 231 [Int. J. Theor. Phys. **38** (1999) 1113] [arXiv:hep-th/9711200].
- [25] S. S. Gubser, I. R. Klebanov and A. M. Polyakov, Phys. Lett. B **428** (1998) 105 [arXiv:hep-th/9802109].
- [26] J. A. Minahan and K. Zarembo, JHEP **0303** (2003) 013 [arXiv:hep-th/0212208].
- [27] N. Beisert and M. Staudacher, Nucl. Phys. B **670** (2003) 439 [arXiv:hep-th/0307042].
- [28] A. V. Kotikov, L. N. Lipatov and V. N. Velizhanin, Phys. Lett. B **557** (2003) 114 [arXiv:hep-ph/0301021].
- [29] A. V. Kotikov, L. N. Lipatov, A. I. Onishchenko and V. N. Velizhanin, Phys. Lett. B **595** (2004) 521 [Erratum-ibid. B **632** (2006) 754] [arXiv:hep-th/0404092].
- [30] N. Beisert, B. Eden and M. Staudacher, J. Stat. Mech. **0701** (2007) P021 [arXiv:hep-th/0610251].
- [31] L. N. Lipatov, J. Phys. A **42** (2009) 304020 [arXiv:0902.1444 [hep-th]].
- [32] L. N. Lipatov, Phys. Lett. B **116** (1982) 411.
- [33] R. C. Brower, J. Polchinski, M. J. Strassler and C. I. Tan, JHEP **0712** (2007) 005 [arXiv:hep-th/0603115].
- [34] E. Witten, Adv. Theor. Math. Phys. **2** (1998) 253 [arXiv:hep-th/9802150].
- [35] S. Caron-Huot, P. Kovtun, G. D. Moore, A. Starinets and L. G. Yaffe, JHEP **0612** (2006) 015 [arXiv:hep-th/0607237].
- [36] Y. Hatta, E. Iancu and A. H. Mueller, JHEP **0801** (2008) 063 [arXiv:0710.5297 [hep-th]].

-
- [37] Y. Hatta, E. Iancu and A. H. Mueller, JHEP **0801** (2008) 026 [arXiv:0710.2148 [hep-th]].
- [38] L. Cornalba, M. S. Costa and J. Penedones, JHEP **0806** (2008) 048 [arXiv:0801.3002 [hep-th]].
- [39] L. Cornalba and M. S. Costa, Phys. Rev. D **78** (2008) 096010 [arXiv:0804.1562 [hep-ph]].
- [40] G. Chalmers, H. Nastase, K. Schalm and R. Siebelink, Nucl. Phys. B **540** (1999) 247 [arXiv:hep-th/9805105].
- [41] J. Bartels, A.-M. Mischler and M. Salvadore, Phys. Rev. D **78** (2008) 016004 [arXiv:0803.1423 [hep-ph]].
- [42] J. Bartels, C. Ewerz, M. Hentschinski, A.-M. Mischler, in preparation.
- [43] J. Bartels, M. Hentschinski and A.-M. Mischler, Phys. Lett. B **679** (2009) 460 [arXiv:0906.3640 [hep-ph]].
- [44] J. Bartels, J. Kotanski, A.-M. Mischler and V. Schomerus, [arXiv:0908.2301 [hep-th]].
- [45] J. Bartels, J. Kotanski, A.-M. Mischler and V. Schomerus, in preparation.
- [46] J. Bartels and M. Lublinsky, JHEP **0309** (2003) 076 [arXiv:hep-ph/0308181].
- [47] J. Bartels, K. J. Golec-Biernat and K. Peters, Acta Phys. Polon. B **34** (2003) 3051 [arXiv:hep-ph/0301192].
- [48] L. Brink, J. H. Schwarz and J. Scherk, Nucl. Phys. B **121** (1977) 77.
- [49] V. G. Gorshkov, V. N. Gribov, L. N. Lipatov and G. V. Frolov, Sov. J. Nucl. Phys. **6** (1968) 262 [Yad. Fiz. **6** (1967) 361].
- [50] R. C. Brower, C. E. DeTar and J. H. Weis, Phys. Rept. **14** (1974) 257.
- [51] G. 't Hooft, Nucl. Phys. B **72** (1974) 461.
- [52] J. Bartels and M. Hentschinski, [arXiv:0903.5464 [hep-ph]].
- [53] D. Z. Freedman, S. D. Mathur, A. Matusis and L. Rastelli, Nucl. Phys. B **546** (1999) 96 [arXiv:hep-th/9804058].
- [54] M. Cvetič *et al.*, Nucl. Phys. B **558** (1999) 96 [arXiv:hep-th/9903214].
- [55] E. D'Hoker and D. Z. Freedman, Nucl. Phys. B **544** (1999) 612 [arXiv:hep-th/9809179].

- [56] E. D'Hoker, D. Z. Freedman, S. D. Mathur, A. Matusis and L. Rastelli, Nucl. Phys. B **562** (1999) 330 [arXiv:hep-th/9902042].
- [57] H. Liu and A. A. Tseytlin, Phys. Rev. D **59** (1999) 086002 [arXiv:hep-th/9807097].

Danksagung

Zuallererst bedanke ich mich bei Herrn Prof. Dr. Bartels für das vielseitige, spannende Thema, für seine Betreuung, lehrreiche Gespräche und gute Ratschläge.

Bedanken möchte ich mich bei Herrn Prof. Dr. Schomerus für zahlreiche Gesprächsrunden und Diskussionen.

An Michele Salvatore geht auch großer Dank. Er hat mir den Anfang meiner Doktorandenzeit erleichtert. Die Arbeit mit ihm hat Spaß gemacht.

Bei Jan Kotanski bedanke ich mich für die hilfreiche und konstruktive Zusammenarbeit.

Dank sage ich nicht zuletzt meiner Familie, den Eltern, die mich auch in diesen drei Jahren der Hamburger Universitätszeit in jeglicher Hinsicht unterstützt haben, immer für mich da sind, - und meiner Schwester für alle anregenden Gespräche. Ein ausdrücklicher Dank geht an meine Oma.